Supplementary Materials

Appendix A Basic information of reviewed papers

Table A1 Basic information of reviewed papers

Citation	Geographical range[1]		Temporal range					Temperature indicator			UGS classification and identification		
	Location	**Climate zone**	**Year span**	**Sp[2]**	**Su[2]**	**Au[2]**	**Wi[2]**	**Type**	**Data Source**	**Spatial Range[3]**	**UGS definition**	**Data Source[4]**	**Detailed Classification[5]**
(Amani-Beni et al., 2019)	China - Beijing	Dwa	[M] 15y		√			LST	Landsat	Local neighborhood	LC	[F]SPOT	No
(An et al., 2022)	China - Beijing	Dwa	[S]		√			LST	Landsat	Central built-up area	LC	[F]GF	T/S/G
(Asgarian et al., 2014)	Iran - Isfahan	BWk	[S]	√				LST	Landsat	Central built-up area	LC	[C]Landsat	No
(Athukorala & Murayama, 2020)	Ghana - Accra	Aw	[M] 14y	√				LST	Landsat	Metropolitan area	LC	[C]Landsat	T/G
(Athukorala & Murayama, 2021)	Egypt - Cario	BWh	[M] 20y		√			LST	MODIS	Metropolitan area	LC	[C]Landsat	No
(Bao et al., 2016)	China - Baotou	BSk	[M] 15y		√			LST	Landsat	Central built-up area	LU	[C]Landsat	No
(Bartesaghi-Koc et al., 2020)	Australia - Sydney	Cfa	[S]		√		√	LST	Aerial Scanner	Local neighborhood	LC	[C]LiDAR	T/S/G
(Bera et al., 2022)	India - Kolkata	Aw	[S]	√	√	√	√	LST	Landsat	Central built-up area	LC	[F]GF	No
(Cai et al., 2022)	China - Fuzhou	Cfa	[M]10y		√			LST	Landsat	Central built-up area	LC	[C]Landsat	No
(Cao et al., 2010)	Japan - Nagoya	Cfa	[M] 5y	√	√	√		LST	ASTER	Central built-up area	LU	[F]IKONOS	T/S/G
(Chakraborti et al., 2019)	India - Hyderabad	BSh	[M] 13y			√		LST	Landsat	City boundary	LC	[C]Landsat	No
(Chen et al., 2014a)	China - Beijing	Dwa	[S]		√			LST	Landsat	Central built-up area	LC	[F]QuickBird	No
(Chen et al., 2014b)	China - Beijing	Dwa	[S]	√	√	√	√	LST	Landsat	Central built-up area	LC	[F]QuickBird	T/S/G
(D. Chen et al., 2022)	China - Urumqi	BWk	[S]		√			LST	Landsat	Central built-up area	LC	[F]PlanetScope	No
(J. Chen, P. Du, et al., 2022)	China – Nanjing	Cfa	[S]	√				LST	ASTER	Central built-up area	LC	[F]IKONOS	T only
(J. Chen, W. Zhan, et al., 2022)	China - Nanjing	Cfa	[S]	√	√	√	√	LST	Landsat	Central built-up area	LC	[F]IKONOS	T only
(Chen et al., 2020)	China - Nanjing	Cfa	[S]	√				LST	ASTER	Central built-up area	LC	[F]WorldView	T only
(J. Chen et al., 2021)	China - Nanjing	Cfa	[S]	√				LST	ASTER	Central built-up area	LC	[F]IKONOS, LiDAR	T/G
(X. Chen et al., 2022)	China - Guiyang	Cwa	[S]	√	√	√	√	LST	Landsat	Central built-up area	LC	[F]Google earth	No
(X. Chen et al., 2021)	China - Guiyang	Cwa	[S]		√			LST	Landsat	Central built-up area	LU	[F]Pleiades	No
(Cheng et al., 2015)	China - Shanghai	Cfa	[S]		√			LST	Landsat	Central built-up area	LU	[F]Aerial Image	No
(Connors et al., 2012)	US - Phoenix	BWh	[S]		√			LST	ASTER	City boundary	LC	[F]QuickBird	T/G
(Das et al., 2020)	India - Jaipur, Guwahati	BSh, Cwa	[M] 28y			√	√	LST	Landsat	City boundary	LC	[C]Landsat	No
(Du et al., 2022)	China - Xi'an	BSk	[S]		√			LST	Landsat	Central built-up area	LU	[F]Not specified	No
(Du et al., 2017)	China - Shanghai	Cfa	[S]		√			LST	Landsat	Central built-up area	LU	[F]Google earth	T/G
(Du et al., 2021)	China - Shanghai	Cfa	[S]		√			AT	Field Monitored	Central built-up area	LU	[F]Not specified	No
(Du et al., 2016)	China - Zhuhai	Cwa	[S]			√		LST	Landsat	Central built-up area	LC	[F]QuickBird	T/G
(Dugord et al., 2014)	Germany - Berlin	Dfb	[S]		√			LST	Landsat	City boundary	LU	[F]Governmental data	T/G
(Ekwe et al., 2020)	Nigeria - Port Harcourt	Am	[S]				√	LST	Landsat	Local neighborhood	LU	[F]Google earth	No
(Estoque et al., 2017)	Thailand - Bangkok, Indonesia - Jakarta, Philippines - Manila	Aw, Am, Aw	[S]	√		√		LST	Landsat	Metropolitan area	LC	[C]Landsat	No
(Fan et al., 2019)	India - Mumbai, China - Hong Kong, Kaohsiung, Tainan, Singapore, Malaysia - Kuala Lumpur, Indonesia - Jakarta	Am, Cwa, Aw, Aw, Af, Af, Am	[S]		√			LST	Landsat	City boundary	LC	[C]Landsat	T only
(Feng et al., 2020)	China - Nanjing	Cfa	[M] 8y	√	√		√	AT / LST	Landsat, Meteorology Station	City boundary	LC	[C]Landsat	No
(Feng & Myint, 2016)	China - Beijing	Dwa	[S]		√			LST	ASTER	Central built-up area	LC	[F]QuickBird	No

Citation	Geographical range[1]		Temporal range					Temperature indicator			UGS classification and identification		
	Location	Climate zone	Year span	Sp[2]	Su[2]	Au[2]	Wi[2]	Type	Data Source	Spatial Range[3]	UGS definition	Data Source[4]	Detailed Classification[5]
(Feyisa et al., 2014)	Ethiopia - Addis Ababa	Cwb	[S]			√		AT / LST	Landsat, Field Measured	Central built-up area	LU	[C]ASTER	T only
(Gage & Cooper, 2017)	US - Aurora	BSk	[S]		√			LST	Landsat		LC	[F]Publication: 1m	T/G
(Galletti et al., 2019)	US - Phoenix	BWh	[S]		√			LST	ASTER	Central built-up area	LC	[F]NAIP	T/G
(Gao et al., 2022)	US - Austin, Baltimore, Chicago, Los Angeles, Portland	Cfa, Cfa, Csa, Csb	[M]4y mean		√			LST	Landsat	Central built-up area	LU	[F]NA	No
(Greene & Kedron, 2018)	Canada - Toronto	Dfa	[S]		√			LST	Landsat	City boundary	LC	[F]QuickBird	T only
(A. Guo et al., 2020)	China - Dalian	Dwa	[M] 11y			√		LST	Landsat	Central built-up area	LU	[C]Landsat	No
(G. Guo et al., 2020)	China - Guangzhou	Cwa	[S]		√	√		LST	Landsat	Central built-up area	LC	[F]Aerial Image	No
(Guo et al., 2021)	China - Guangzhou, Shenzhen	Cwa	[S]		√			LST	Landsat	Central built-up area	LC	[F]Aerial Image	No
(Guo et al., 2019)	China - Guangzhou, Foshan, Dongguan, Shenzhen	Cwa, Cfa, Cwa, Cwa	[S]		√		√	LST	Landsat	Central built-up area	LC	[F]Aerial Image	No
(He et al., 2021)	US - Baltimore, Boston	Cfa, Dfa	[M] 5y		√			LST	MODIS	Metropolitan area	LC	[C]NLCD	T only
(Hou & Estoque, 2020)	China - Hangzhou	Cfa	[S]		√			LST	Landsat	Metropolitan area	LC	[C]Landsat	T/G
(Hu et al., 2021)	China - Beijing	Dwa	[S]		√			LST	Landsat	Local neighborhood	LC	[F]GF	T/G
(Huang et al., 2018)	China - Harbin	Dwa	[M] 9y		√			LST	Landsat	Central built-up area	LU	[C]Landsat	No
(Huang et al., 2022)	China – Xi'an	BSk	[M]20y		√			LST	Landsat	Central built-up area	LU	[F]NA	No
(Huang & Wang, 2019)	China - Wuhan	Cfa	[S]	√	√	√	√	LST	Landsat	Central built-up area	LC	[F]ZY-3	T/G
(Jaganmohan et al., 2016)	Germany - Lipzig	Cfb	[S]		√			AT	Field Measured	Central built-up area	LU	[F]Not specified	T only
(Kamarianakis et al., 2017)	US - Phoenix	Bwh	[S]		√			AT	Meteorology Station	Metropolitan area	LC	[F]NAIP	T/G
(Karunaratne et al., 2022)	Nepal - Kathmandu	Cwa	[M]20y					LST	Landsat	Metropolitan area	LC	[C]Landsat	T/G
(Ke et al., 2021)	China - Wuhan	Cfa	[M] 3y		√			LST	Landsat	Central built-up area	LC	[C]FROM-GLC10	No
(Kim et al., 2016)	US - Austin	Cfa	[S]		√			LST	Landsat	Central built-up area	LC	[F]Aerial Image	T/G
(Kong, Yin, James, et al., 2014)	China - Nanjing	Cfa	[S]		√			LST	Landsat	Central built-up area	LC	[F]IKONOS	T/G
(Kong, Yin, Wang, et al., 2014)	China - Nanjing	Cfa	[S]		√			LST	Landsat	Central built-up area	LC	[F]IKONOS	T/G
(Kowe et al., 2021)	Zimbabwe - Harare	Cwb	[M] 23y		√			LST	ASTER, Landsat	City boundary	LC	[C]ASTER, LANDSAT, Sentinel	No
(Lemoine-Rodríguez et al., 2022)	Mexico - Xalapa	Cfb	[S]	√				LST	Landsat	Central built-up area	LC	[F]SPOT	T/G
(Li et al., 2017)	US - Phoenix	BWh	[S]		√			LST	MASTER	Central built-up area	LC	[F]NAIP	T/G
(B. Li et al., 2020)	China - Zhengzhou	Cwa	[S]	√				LST	Landsat	Central built-up area	LU	[F]Google earth	No
(Li et al., 2018)	China - Xi'an	BSk	[M] 25y		√			LST	Landsat	Central built-up area	LC	[C]Landsat	No
(Li et al., 2022)	Bangladesh - Dhaka, India - Kolkata, Thailand - Bangkok	Aw	[M] 20y	√			√	LST	Landsat	Central built-up area	LC	[C]Landsat	No
(Li et al., 2011)	China - Shanghai	Cfa	[S]	√	√			LST	Landsat	Central built-up area	LU	[F]Aerial Image	No
(T. Li et al., 2020)	China - Beijing	Dwa	[S]		√			LST	Landsat	Central built-up area	LC	[F]IKONOS	T/G
(Li et al., 2013)	China - Beijing	Dwa	[S]			√		LST	Landsat	Central built-up area	LC	[F+C]QuickBird, SPOT, LANDSAT	No
(Li et al., 2012)	China - Beijing	Dwa	[S]			√		LST	Landsat	Central built-up area	LC	[F]SPOT	No
(T. Li et al., 2021)	China - Beijing	Dwa	[S]	√	√	√	√	LST	Landsat	Central built-up area	LC	[F]IKONOS	T/G
(Y. Li et al., 2020)	China - Beijing	Dwa	[S]		√		√	AT	Field Measured	Local neighborhood	LC	[F]GF	T/G
(Y. Li et al., 2021)	China - Beijing	Dwa	[S]		√			AT	Field Measured	Central built-up area	LU	[F]GF	No

Citation	Geographical range[1]		Temporal range					Temperature indicator			UGS classification and identification		
	Location	Climate zone	Year span	Sp[2]	Su[2]	Au[2]	Wi[2]	Type	Data Source	Spatial Range[3]	UGS definition	Data Source[4]	Detailed Classification[5]
(Li et al., 2019)	China - Shanghai	Cfa	[S]		√			LST	Landsat	Central built-up area	LC	[F]Governmental data	No
(W. Liu et al., 2022)	China - Beijing	Dwa	[S]			√		LST	Landsat	Central built-up area	LC	[C]FROM-GLC10	No
(Liu et al., 2021)	China - Xuchang	Cwa	[S]		√			LST	Landsat	Central built-up area	LU	[C]Landsat	No
(K. Liu et al., 2022)	China - Shijiazhuang	BSk	[S]		√			LST	Aerial Scanner, Landsat, MODIS	Central built-up area	LC	[F]Aerial Image	T/G
(Liu et al., 2016)	China - Beijing	Dwa	[S]	√	√	√	√	LST	Landsat	Central built-up area	LC	[F]GF	T/G
(H. Liu & Q. Weng, 2009)	US - Indianapolis	Dfa	[M] 6y	√	√	√	√	LST	Aster	Metropolitan area	LC	[C]ASTER	T/G
(S. Liu et al., 2022)	China - Fuzhou	Cfa	[M] 16y	√	√			LST	Landsat	Central built-up area	LC	[C]Landsat	No
(Wenrui Liu et al., 2022)	China - Beijing	Dwa	[S]			√		LST	Landsat	Central built-up area	LC	[C]Landsat + ESA	No
(Liu et al., 2018a)	China - Shenzhen	Cwa	[M] 28y		√	√	√	LST	Landsat	Central built-up area	LC	[C]Landsat	No
(Liu et al., 2018b)	China - Shenzhen	Cwa	[M] 28y		√	√	√	LST	Landsat	Central built-up area	LC	[C]Landsat	No
(Lu et al., 2012)	China - Chongqing	Cfa	[S]		√			AT	Field Measured	Local neighborhood	LU	[F]Not specified	No
(Lu et al., 2020)	China - Xi'an	BSk	[M] 25y	√				LST	Landsat	Central built-up area	LC	[C]Landsat	No
(Lyu et al., 2023)	China - Yinchuan	BWk	[S]		√			LST	Landsat	Central built-up area	LC	[C]Sentinel	No
(Ma & Peng, 2022)	China - Kunming	Cwb	[M] 28y	√				LST	Landsat	City boundary	LC	[C]Landsat	No
(Ma et al., 2021)	China - Xi'an	BSk	[M] 9y		√			LST	Landsat	Central built-up area	LC	[C]Landsat	T/G
(Maimaitiyiming et al., 2014)	China - Aksu	BWk	[S]		√			LST	Landsat	Central built-up area	LC	[C]Landsat	No
(Masoudi & Tan, 2019)	Singapore - Singapore	Af	[M] 42y					LST	Landsat	City boundary	LC	[C]Landsat	No
(Masoudi et al., 2021)	Singapore - Singapore	Af	[M] 10y				√	LST	Landsat	City boundary	LC	[C]Landsat, Governmental data	No
(Masoudi et al., 2019)	Malaysia - Kuala Lumpur, Indonesia - Jakarta, China - Hong Kong, Singapore - Singapore	Af, Am, Cwa, Af	[S]					LST	Landsat	City boundary	LC	[C]Landsat	No
(Naeem et al., 2018)	China - Beijing, Pakistan - Islamabad	Dwa, Cwa	[S]			√		LST	Landsat	Central built-up area	LC	[F]GF	No
(Pang et al., 2022)	China - Beijing, Tianjin, Xi'an, Zhengzhou	Dwa, Dwa, BSk, Cwa	[S]		√			LST	Landsat	Central built-up area	LU	[F]Google earth	No
(Park & Cho, 2016)	Koear - Ulsan	Cfa	[S]		√			LST	Landsat	Central built-up area	LU	[C]Landsat	No
(Peng et al., 2021)	China - Shenzhen	Cwa	[S]			√		LST	Landsat	Central built-up area	LU	[F]Governmental data	No
(Peng et al., 2018)	China - Shenzhen	Cwa	[S]	√				LST	Landsat	Central built-up area	LC	[F]Governmental data	T/G
(Peng et al., 2016)	China - Beijing	Dwa	[S]	√	√	√	√	LST	Landsat	City boundary	LC	[C]Landsat	No
(Pramanik & Punia, 2019)	India - Delhi	BSh	[S]	√				LST	Landsat	Central built-up area	LC	[C]Sentinel	T/G
(Qian et al., 2018)	China - Beijing	Dwa	[S]		√		√	AT	Field Monitored	Local neighborhood	LC	[F]Google earth	No
(Qiu & Jia, 2020)	China - Beijing	Dwa	[S]		√				Landsat	Central built-up area	LU	[F]Worldview	no
(Rahimi et al., 2021)	Iran - Tehran	BSk	[S]		√			LST	Landsat	Central built-up area	LC	[C]Landsat	No
(Rakoto et al., 2021)	Australia - Melbourne	Cfb	[S]		√			LST	Landsat	Central built-up area	LC	[F]LiDAR	DC
(Ren et al., 2013)	China - Changchun	Dwa	[S]		√	√		LST	Landsat	Central built-up area	LU	[F]SPOT	No
(Ren et al., 2014)	China - Changchun	Dwa	[S]		√			LST	Landsat	Central built-up area	LC	[F]SPOT	No
(Rhee et al., 2014)	US - Denver	BSk	[S]	√	√	√		LST	Landsat	Local neighborhood	LC	[F]LiDAR	T/G
(Rouhi et al., 2018)	Iran - Sari	Csa	[S]		√			LST	Landsat	Metropolitan area	LC	[C]Landsat	No
(Shah et al., 2021)	India - Berrrngaluru	Aw	[S]	√				LST	Landsat	Central built-up area	LU	[C]Landsat	No
(Shaker et al., 2019)	US - New York	Dfa	[S]			√		AT	Meteorology Station	Central built-up area	LC	[F]NYCPR: 0.914m	T/G
(Shi & Zhao, 2022)	China - Xi’an	BSk	[S]		√			LST	Landsat	Central built-up area		[C]Sentinel	T/G
(Shih, 2017)	China - Taipei	Cfa	[S]		√			LST	Landsat	Central built-up area	LC	[C]Landsat	No
(Shih, 2016)	China - Taipei	Cfa	[S]		√			LST	Landsat	Central built-up area	LC	[C]Landsat	No

Citation	Geographical range[1]		Temporal range					Temperature indicator			UGS classification and identification		
	Location	Climate zone	Year span	Sp[2]	Su[2]	Au[2]	Wi[2]	Type	Data Source	Spatial Range[3]	UGS definition	Data Source[4]	Detailed Classification[5]
(Simwanda et al., 2019)	Nigeria - Lagos, Kenya - Nairobi, Ethiopia - Addis Ababa, Zambia - Lusaka	Aw, Cfb, Cwb, Cwa	[S]		√		√	LST	Landsat	Metropolitan area	LC	[C]Landsat	No
(Song et al., 2020)	China - Hangzhou	Cfa	[S]	√	√	√	√	LST	Landsat	Metropolitan area	LC	[F]SPOT	T/G
(Xiang Sun et al., 2020)	China - Nanjing	Cfa	[M] 8y		√			LST	Landsat	Central built-up area	LU	[F]Google earth	No
(Sun et al., 2021)	China – Shanghai	Cfa	[S]		√		√	LST	Landsat	Central built-up area	LU	[F]Google earth	T/G
(Sun et al., 2022)	China - Chengdu	Cfa	[M]29y	√				LST	Landsat	Central built-up area	LC	[C]Landsat	T/G
(Tan & Li, 2013)	China - Beijing	Dwa	[S]		√			LST	Landsat	Central built-up area	LC	[C]Landsat	No
(X. Tan et al., 2021)	China - Nanning	Cfa	[M] 4y			√		LST	Landsat	Central built-up area	LC	[C]Landsat	No
(Tang et al., 2023)	China - Wuhan	Cfa	[S]		√			LST	Landsat	Central built-up area	LC	[C]FROM-GLC10 10m, EULUC land use	No
(Terfa et al., 2020)	Ethiopia - Addis Ababa	Cwb	[M]22y				√	LST	Landsat	City boundary	LC	[C]Landsat	No
(Vaz Monteiro et al., 2016)	UK - London	Cfb	[S]		√	√		AT	Field Monitored	Local neighborhood	LU	[F]Not specified	T/G
(Wang & Zhou, 2022)	China - Beijing	Dwa	[M] 5y		√			LST	MODIS	Central built-up area	LC	[F]SPOT, ALOS	T/G
(Wang et al., 2023)	China - Beijing, Shenzhen, US - Sacramento, Baltimore	Dwa, Cwa, Csa, Cfa	[S]		√			LST	Landsat	Central built-up area	LC	[F]Publication: 1m	T only
(Wang et al., 2020)	China - Nanjing, Wuhan, Chongqing	Cfa	[M]19y		√			LST	Landsat	Metropolitan area	LC	[F]Landsat	T/G
(Wang et al., 2022)	China - Shanghai	Cfa	[S]		√			LST	Landsat	Central built-up area	LU	[F]Amap	No
(Wang et al., 2018)	China - Changzhou	Cfa	[S]	√				LST	Landsat	Central built-up area	LU	[F]NA	No
(X. Wang et al., 2021)	China - Beijing	Dwa	[S]		√			LST	Landsat	Central built-up area	LC	[F]SPOT	T/G
(Y. Wang et al., 2021)	China - Taiyuan	BSk	[S]		√			LST	Landsat	Central built-up area	LU	[C]Governmental data	T/G
(Weber et al., 2014)	Germany - Lipzig	Cfb	[S]			√		LST	Aerial Scanner	City boundary	land use*land use	[F]Governmental data	No
(Wen et al., 2011)	China - Guangzhou	Cwa	[S]			√		AT	Meteorology Station	City boundary	LC	[C]CBERS	No
(Wesley & A. Brunsell, 2019)	US - Kansas City	Dfa	[M] 3y		√			LST	Landsat	Metropolitan area	LC	[C]NRI	No
(Wu et al., 2021)	China - Shanghai	Cfa	[S]		√			LST	Landsat	Central built-up area	LU	[C]Landsat	No
(Wu et al., 2014)	China - Wuhan	Cfa	[S]		√			LST	HJ-1B	City boundary	LC	[C]HJ-1B	No
(Q. Wu et al., 2022)	China - Beijing	Dwa	[S]		√			LST	Landsat	Central built-up area	LC	[C]FROM-GLC10	T/G
(Y. Wu et al., 2022)	China - Hangzhou	Cfa	[M] 20y		√			LST	Landsat	Metropolitan area	LC	[C]Landsat	T/G
(Wu & Zhang, 2018)	China - Suzhou	Cfa	[S]	√				LST	Landsat	Central built-up area	LC	[C]Landsat	No
(Xie et al., 2020)	China - Shenzhen	Cwa	[M] 10y		√			LST	Landsat	City boundary	LC	[C]Landsat	T/G
(Xie et al., 2013)	China - Shenzhen	Cwa	[S]			√		LST	Landsat	City boundary	LC	[C]Landsat	T/G
(Xu et al., 2017)	China - Beijing	Dwa	[S]		√			LST	Landsat	Central built-up area	LU	[F]QuickBird	T/G
(Yan et al., 2019)	US - Phoenix	BWh	[S]		√			LST	MASTER	Local neighborhood	LC	[F]NAIP	T/G
(Yan et al., 2021)	China - Beijing	Dwa	[S]		√			LST	Landsat	Central built-up area	LC	[F]SPOT	No
(Yang, He, Wang, et al., 2017)	China - Changchun	Dwa	[S]	√	√	√	√	LST	Landsat	Central built-up area	LC	[F]GF	No
(Yang, He, Yu, et al., 2017)	China - Changchun	Dwa	[S]	√	√	√		LST	Landsat	Central built-up area	LU	[F]GF	T/G
(C. Yang et al., 2021)	China - Changchun	Dwa	[S]		√			AT / LST	Landsat, Field Measured	Central built-up area	LC	[F]GF	No
(Yang et al., 2020)	Denmark - Copenhagen	Dfb	[S]	√	√	√	√	LST	Landsat	Central built-up area	LC	[F]Governmental data	T/G
(Yang et al., 2022)	China - Fuzhou	Cfa	[M]3y		√			LST	Landsat	Central built-up area	LC	[F]GF	T/G
(L. Yang et al., 2021)	China - Fuzhou	Cfa	[S]	√	√		√	LST	Landsat	City boundary	LC	[F]GF	No
(Yao et al., 2020)	China - Beijing	Dwa	[S]	√	√	√	√	LST	Landsat	Central built-up area	LC	[F]IKONOS	No

Citation	Geographical range[1]		Temporal range					Temperature indicator			UGS classification and identification		
	Location	Climate zone	Year span	Sp[2]	Su[2]	Au[2]	Wi[2]	Type	Data Source	Spatial Range[3]	UGS definition	Data Source[4]	Detailed Classification[5]
(Ye et al., 2021)	China-Beijing, Tianjin, Shanghai,Guangzhou, Shenzhen	Dwa, Dwa, Cwa, Cwa	[M]27y		√			LST	Landsat	Central built-up area	LC	[F]IKONOS	No
(Yin et al., 2019)	China - Beijing	Dwa	[S]			√		LST	Landsat	Central built-up area	LC	[F]SPOT	T/G
(Yu et al., 2020)	China - Shanghai	Cfa	[S]		√			LST	Landsat	Central built-up area	LC	[F]ZY-3	No
(Yu et al., 2017)	China - Fuzhou	Cfa	[M] 13y		√			LST	Landsat	Central built-up area	LC	[F]SPOT	T/G
(Yuan et al., 2021)	China - Xi'an	BSk	[S]		√			LST	Landsat	Central built-up area	LC	[F]GF2	T/G
(Zawadzka et al., 2020)	UK - Milton keynes, bedford, luton/dunstable	Cfb	[S]		√			LST	Landsat	Central built-up area	LC	[F]Governmental data	T/G
(Zawadzka et al., 2021)	UK - Milton keynes, bedford, luton/dunstable	Cfb	[S]		√			LST	Landsat	Central built-up area	LC	[F]LiDAR	T/G
(Zeng et al., 2022)	China - Shanghai	Cfa	[S]		√			LST	Landsat	Central built-up area	LC	[F]GF2	T/G
(H. Zhang et al., 2022)	China - Shanghai	Cfa	[M]7y		√			LST	Landsat	Local neighborhood	LC	[F]Governmental data: 1m	T/G
(L. Zhang et al., 2022)	China - Beijing	Dwa	[S]			√		LST	Landsat	Central built-up area	LC	[F]WorldView	No
(M. Zhang et al., 2022)	China - Urumqi	BWk	[S]		√			LST	Landsat	Central built-up area	LC	[F]GF	No
(Zhang et al., 2009)	China - Nanjing	Cfa	[S]		√			LST	Landsat	Central built-up area	LC	[F]IKONOS	T/S/G
(Y. Zhang et al., 2022)	China - Xuzhou	Cfa	[M]6y	√				LST	Landsat	Central built-up area	LC	[F]GF	No
(Zhao et al., 2020)	China - Zhengzhou	Cwa	[M] 15y					LST	Landsat	City boundary	LC	[C]Landsat	T/G
(W. Zhou et al., 2022)	China - Beijing, Tianjin, Shanghai	Dwa, Dwa, Cfa	[S]		√			LST	Landsat	Central built-up area	LC	[C]Landsat	T/G
(G. Zhou et al., 2019)	US - Washington DC	Cfa	[S]	√				LST	Landsat	City boundary	OC	[C]ASTER	No
(L. Zhou et al., 2022)	China - Xi'an	BSk	[S]		√			LST	Landsat	Metropolitan area	LC	[C]Sentinel	No
(Zhou & Cao, 2020)	China - Shanghai	Cfa	[S]	√	√	√	√	LST	Landsat	Central built-up area	LC	[F]SPOT	T/G
(W. Zhou, F. Cao, et al., 2019)	China - Shanghai	Cfa	[S]		√			LST	Landsat	Central built-up area	LC	[F]SPOT	T/G
(W. Zhou, X. Shen, et al., 2019)	China - Nanjing	Cfa	[S]	√				LST	Landsat	Central built-up area	LC	[C]Landsat	No
(Zhou et al., 2011)	US - Baltimore	Cfa	[S]		√			LST	Landsat	Central built-up area	LC	[F]LiDAR	T/G
(Zhou et al., 2017)	US - Sacramento, Baltimore	Csa, Cfa	[S]		√			LST	Landsat	City boundary	LC	[F]NAIP	T only
(Zhu et al., 2021)	China - Jinan	Dwa	[M]3y mean		√			LST	Landsat	Central built-up area	LU	[F]GF2	No

Note: 1 Climate zone classified following world's current Köppen climate classification. **2** Sp=spring, Su=summer, Au=autumn, Wi=winter. [M] refers to that multiple years' data were used. [S] refers to that single year data was used. **3** Classified into 4 types, i.e., metropolitan area, city boundary, central built-up area, and local neighborhood, by the spatial range taken into consideration of analysis. **4** [C] Coarse resolution data used, [F] Fine resolution data used. **5** T only=tree canopy specified only, T/G=specified tree canopy and grassland/cropland coverage, T/S/G=specified tree canopy, shrub coverage, and grassland/cropland coverage, DC=detailed classification.

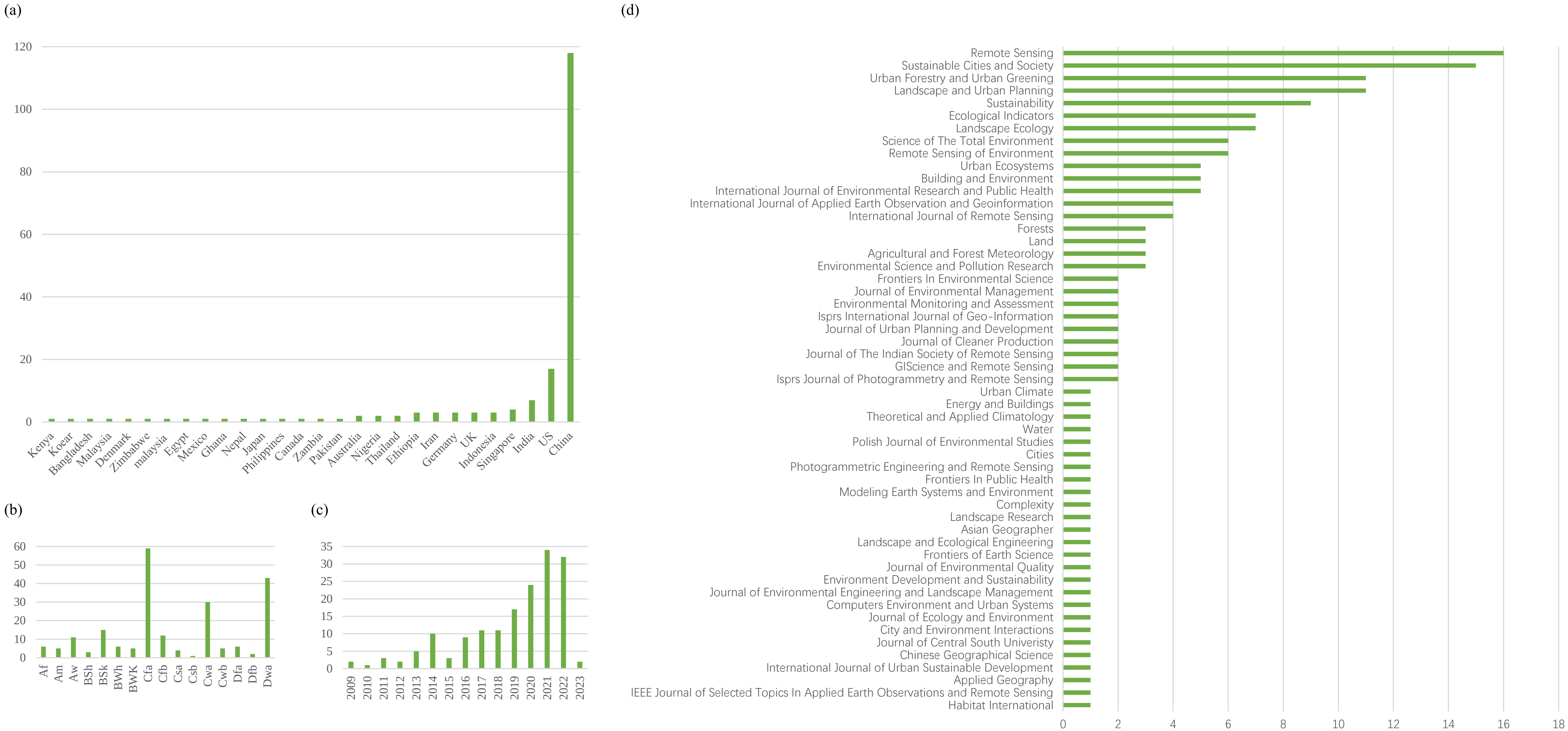

Fig. A1 Reviewed paper amount by (a)country, and (b) Köppen climate zone, (c) published year, and (d) published journals.

Appendix B Frequency of landscape metrics used in reviewed papers

Table B1 2D patch level LMs used in reviewed papers

Metric category	Landscape metric	Calculation#	Description#	Range	Frequency in reviewed papers
Shape metrics	Perimeter-area ratio (PARA)	$PARA = \frac{p_{ij}}{A_{ij}}$	It describes the patch complexity in a straightforward way. However, because it is not standardized to a certain shape (e.g., a square), it is not scale independent, meaning that increasing the patch size while not changing the patch form will change the ratio.	PARA > 0 Increases, without limit, as the shape complexity increases.	**15** (Asgarian et al., 2014; Bao et al., 2016; Du et al., 2021; Ekwe et al., 2020; Huang et al., 2018; Huang et al., 2022; W. Liu et al., 2022; Qiu & Jia, 2020; Ren et al., 2013; Shih, 2016; Vaz Monteiro et al., 2016; Wang et al., 2022; Wang et al., 2018; Yang, He, Wang, et al., 2017; Zhang et al., 2009)
	Shape index (SHAPE)	$SHAPE = \frac{p_{ij}}{2\sqrt{\pi A_{ij}}}$ (a) $SHAPE = \frac{p_{ij}}{4\sqrt{A_{ij}}}$ (b)	It describes the patch complexity by comparing the shape to a circle (a) or a square (b). It corrects the size problems of PARA and offers a simple and straightforward way of describing shape complexity.	SHAPE≥1 Increases, without limit, as the shape complexity increases. SHAPE = 1 when the patch is circle (a) or square (b).	**34** 16 papers used equation (a) (Cao et al., 2010; Chen et al., 2014b; Du et al., 2017; Fan et al., 2019; Li et al., 2022; Park & Cho, 2016; Shah et al., 2021; Shih, 2017; X. Sun et al., 2020; Tan & Li, 2013; X. Y. Tan et al., 2021; Yan et al., 2021; Yang, He, Yu, et al., 2017; Yang et al., 2020; Yu et al., 2017; W. Zhou, X. Shen, et al., 2019) 10 papers used equation (b) (X. Chen et al., 2021; Y. Li et al., 2021; Wenrui Liu et al., 2022; Lu et al., 2012; Pang et al., 2022; Xu et al., 2017; Yang, He, Wang, et al., 2017; Zhang et al., 2009; W. Zhou et al., 2022; Zhu et al., 2021) 7 papers didn't specify (Asgarian et al., 2014; Cai et al., 2022; Feyisa et al., 2014; Gao et al., 2022; Lemoine-Rodríguez et al., 2022; Pramanik & Punia, 2019; W. Zhou, F. Cao, et al., 2019)
	Fractal dimension index (FRAC)	$FRAC = \frac{2 * \ln\ (0.25 * p_{ij})}{\ln A_{ij}}$	The index is based on the patch perimeter and the patch area and describes the patch complexity. Because it is standardized, it is scale independent, meaning that increasing the patch size while not changing the patch form will not change the ratio.	1≤FRAC≤2 Approaches FRAC = 1 for a squared patch shape form and FRAC = 2 for an irregular patch shape.	**5** (Cai et al., 2022; Chen et al., 2014b; Fan et al., 2019; Pang et al., 2022; Wang et al., 2022; Yu et al., 2017)
Core area metrics	Core area index (CAI)	$CAI = \left(\frac{a_{ij}^{core}}{a_{ij}}\right) * 100$	It equals the percentage of a patch that is core area. A cell is defined as core area if the cell has no neighbor with a different value than itself (rook's case). It describes patch area and shape simultaneously (more core area when the patch is large and the shape is rather compact, i.e., a square). Because the index is relative, it is comparable among patches with different area.	0≤CAI≤100 CAI = 0 when the patch has no core area and approaches CAI = 100 with increasing percentage of core area within a patch.	**1** (Asgarian et al., 2014)
Self-defined metrics	Mean shape index (MSI)	$MSI = \frac{p_{ij}}{\sqrt{A_{ij}}}$	*NA*	Increases, without limit, as the shape complexity increases.	(Jaganmohan et al., 2016)
	Mean span (MS)	$MS = \frac{L_w + L_l}{2}$	where L_w is the park width, and L_l is the park length.	*NA*	(Vaz Monteiro et al., 2016)
	Park vegetation and shape index (PVSI)	$PVSI = log_{10}\left(\frac{A_{tree} + A_{shrub}}{SHAPE}\right)$	where A_{tree} and A_{shrub} refer to the areas of tree and shrub cover (m2). Designed to interpret PCI.	*NA*	(Cao et al., 2010)
	Length-width ratio	$SI = \frac{L_l}{L_w}$	where L_w is the park width, and L_l is the park length.	*NA*	(Sun et al., 2021)

Self-defined shape factor	$SI = \frac{A_{ij}}{p_{ij}}$	NA	SI > 0 Increases, without limit, as the shape complexity decreases.	(Peng et al., 2021)*

* Confirmed by personal correspondence with the corresponding authors.

Calculation formulas and descriptions are adopted from McGarigal et al. (2012) and https://r-spatialecology.github.io/landscapemetrics/index.html (accessed Oct. 2022). ***A*** area, ***p*** perimeter.

Table B2 2D class level LMs used in reviewed papers

Metric category	Landscape metric	Calculation#	Description	Range	Frequency in reviewed papers
Area and edge metrics	Largest patch index (LPI)	$LPI = \frac{max_{j=1}^{n}(a_{ij})}{A} * 100$	It is the percentage of the landscape covered by the corresponding largest patch of each class i. It is a simple measure of dominance.	0 < LPI <= 100 Approaches LPI = 0 when the largest patch is becoming small and equals LPI = 100 when only one patch is present	**51** (Amani-Beni et al., 2019; Athukorala & Murayama, 2020, 2021; D. Chen et al., 2022; J. Chen, P. Du, et al., 2022; J. Chen, W. Zhan, et al., 2022; J. Chen et al., 2021; Cheng et al., 2015; Feng & Myint, 2016; Gage & Cooper, 2017; G. Guo et al., 2020; Guo et al., 2019; He et al., 2021; Hou & Estoque, 2020; Hu et al., 2021; Karunaratne et al., 2022; Kong, Yin, James, et al., 2014; B. Li et al., 2020; Li et al., 2018; Liu et al., 2021; K. Liu et al., 2022; S. Liu et al., 2022; Liu et al., 2018a, 2018b; Lu et al., 2020; Ma & Peng, 2022; Ma et al., 2021; Masoudi & Tan, 2019; Masoudi et al., 2019; Qian et al., 2018; Ren et al., 2014; Shaker et al., 2019; Song et al., 2020; Wang et al., 2020; X. Wang et al., 2021; Wesley & A. Brunsell, 2019; Q. Wu et al., 2022; Y. Wu et al., 2022; Xie et al., 2020; Yao et al., 2020; Yuan et al., 2021; H. Zhang et al., 2022; L. Zhang et al., 2022; M. Zhang et al., 2022; Y. Zhang et al., 2022; L. Zhou et al., 2022; Zhou & Cao, 2020; W. Zhou, F. Cao, et al., 2019; Zhou et al., 2011; Zhou et al., 2017; W. Zhou et al., 2022)
	Total edge (TE)	$TE = E$	It measures the configuration of the landscape because a highly fragmented landscape will have many edges. However, total edge is an absolute measure, making comparisons among landscapes with different total areas difficult.	TE >= 0 Equals TE = 0 if all cells are edge cells. Increases, without limit, as landscape becomes more fragmented	**2** (Liu et al., 2018a; M. Zhang et al., 2022)
	Edge density (ED)	$ED = \frac{\sum_{k=1}^{m} e_{ik}}{A} * 10000$	It describes the configuration of the landscape, e.g. because an aggregation of the same class will result in a low edge density. The metric is standardized to the total landscape area, and therefore comparisons among landscapes with different total areas are possible.	ED >= 0 Equals ED = 0 if only one patch is present (and the landscape boundary is not included) and increases, without limit, as the landscapes becomes more patchy	**59** (An et al., 2022; J. Chen, P. Du, et al., 2022; Chen et al., 2020; J. Chen, W. Zhan, et al., 2022; J. Chen et al., 2021; Cheng et al., 2015; Connors et al., 2012; Dugord et al., 2014; Feng & Myint, 2016; Gage & Cooper, 2017; G. Guo et al., 2020; Guo et al., 2021; Guo et al., 2019; He et al., 2021; Hu et al., 2021; Huang & Wang, 2019; Kamarianakis et al., 2017; Kowe et al., 2021; B. Li et al., 2020; Li et al., 2011; T. Li et al., 2021; Li et al., 2017; Li et al., 2013; Li et al., 2012; Liu et al., 2016; Liu et al., 2018a; Lu et al., 2020; Lyu et al., 2023; Maimaitiyiming et al., 2014; Masoudi & Tan, 2019; Masoudi et al., 2019; Naeem et al., 2018; Peng et al., 2018; Qian et al., 2018; Rakoto et al., 2021; Shi & Zhao, 2022; Song et al., 2020; Terfa et al., 2020; Wang & Zhou, 2022; Wang et al., 2023; X. Wang et al., 2021; Wen et al., 2011; Wesley & A. Brunsell, 2019; Wu et al., 2021; Wu et al., 2014; Q. Wu et al., 2022; Yan et al., 2019; C. Yang et al., 2021; L. Yang et al., 2021; Yao et al., 2020; Ye et al., 2021; Yu et al., 2020; Yuan et al., 2021; M. Zhang et al., 2022; Zhao et al., 2020; G. Zhou et al., 2019; L. Zhou et al., 2022; Zhou et al., 2011; Zhou et al., 2017)

Metric category	Landscape metric	Calculation[#]	Description	Range	Frequency in reviewed papers
	Patch area distribution (AREA_)	$AREA\_MN = mean(AREA[patch_{ij}])$ $AREA\_AM = am(AREA[patch_{ij}])$ $AREA\_SD = sd(AREA[patch_{ij}])$ $AREA\_CV = cv(AREA[patch_{ij}])$	The metric summarizes each class as the mean / area weighted mean / standard deviation / coefficient of variation of all patch areas belonging to class i.	≥ 0 AREA_MN/AM=0 if all patches are small. AREA_SD/CV = 0 if all patches are identical in size.	**56** AREA_MN (Athukorala & Murayama, 2020, 2021; Chakraborti et al., 2019; J. Chen, W. Zhan, et al., 2022; Cheng et al., 2015; Estoque et al., 2017; Feng & Myint, 2016; Gage & Cooper, 2017; G. Guo et al., 2020; Guo et al., 2019; He et al., 2021; Hou & Estoque, 2020; Hu et al., 2021; Karunaratne et al., 2022; Ke et al., 2021; Kim et al., 2016; Kong, Yin, James, et al., 2014; Kowe et al., 2021; Li et al., 2013; Li et al., 2012; Li et al., 2019; Liu et al., 2021; K. Liu et al., 2022; S. Liu et al., 2022; Liu et al., 2018a, 2018b; Lu et al., 2020; Ma & Peng, 2022; Ma et al., 2021; Masoudi & Tan, 2019; Masoudi et al., 2019; Qian et al., 2018; Rakoto et al., 2021; Rouhi et al., 2018; Simwanda et al., 2019; Song et al., 2020; Tang et al., 2023; Wang & Zhou, 2022; Wang et al., 2023; Wang et al., 2020; Y. Wu et al., 2022; Wu & Zhang, 2018; L. Yang et al., 2021; Ye et al., 2021; Yuan et al., 2021; H. Zhang et al., 2022; L. Zhang et al., 2022; M. Zhang et al., 2022; L. Zhou et al., 2022; Zhou & Cao, 2020; W. Zhou, F. Cao, et al., 2019; Zhou et al., 2011; Zhou et al., 2017; W. Zhou et al., 2022) AREA_AM (Liu et al., 2018a, 2018b; Masoudi & Tan, 2019; Masoudi et al., 2021; Masoudi et al., 2019; Shaker et al., 2019; M. Zhang et al., 2022) AREA_SD (Feng & Myint, 2016; Qian et al., 2018; Ye et al., 2021; Zhou et al., 2011) AREA_CV (Li et al., 2019) AREA_MD (M. Zhang et al., 2022)
	Radius of gyration distribution (GYRATE_)	$\text{GYRATE\_}MN = mean(\text{GYRATE}[patch_{ij}])$ $\text{GYRATE\_}AM = am(\text{GYRATE}[patch_{ij}])$ where, $GYRATE = \sum_{r=1}^{z} \frac{h_{ijr}}{z}$	The metric summarizes each class as the mean / area weighted mean of the radius of gyration of all patches belonging to class i. GYRATE measures the distance from each cell to the patch centroid and is based on cell center-to-cell center distances. The metrics characterizes both the patch area and compactness.	≥ 0 = 0 if every patch is a single cell. Increases, without limit, when only one patch is present.	**5** GYRATE_MN, GYRATE_AM (Gage & Cooper, 2017; Kong, Yin, James, et al., 2014; Liu et al., 2018a, 2018b; M. Zhang et al., 2022)

Metric category	Landscape metric	Calculation[#]	Description	Range	Frequency in reviewed papers
Shape metrics	Perimeter-area fractal dimension (PAFRAC)	$PAFRARC = \frac{2}{\beta}$ where β is the slope of the regression of the area against the perimeter (logarithm) $n_i \sum_{j=1}^{n} \ln a_{ij}$ $= a + \beta n_i \sum_{j=1}^{n} \ln p_{ij}$	It describes the patch complexity of class i while being scale independent. This means that increasing the patch size while not changing the patch form will not change the metric. However, it is only meaningful if the relationship between the area and perimeter is linear on a logarithmic scale. Furthermore, if there are less than 10 patches in class i, the metric returns NA because of the small-sample issue.	1 <= PAFRAC <= 2 Approaches PAFRAC = 1 for patches with simple shapes and approaches PAFRAC = 2 for irregular shapes	**2** (Y. Wang et al., 2021)
	Perimeter-area ratio distribution (PARA_)	PARA_MN $= mean$(PARA[$patch_{ij}$]) PARA_AM $= am$(PARA[$patch_{ij}$])	It summarizes each class as the mean / area weighted mean of each patch belonging to class i. The perimeter-area ratio describes the patch complexity in a straightforward way.	>0 Increases, without limit, as PARA increases, i.e. patches become more complex.	**7** **PARA_AM** (Kong, Yin, James, et al., 2014; Liu et al., 2021; Song et al., 2020; M. Zhang et al., 2022; Zhou & Cao, 2020) **PARA_MN** (Song et al., 2020) **Not specified** (B. Li et al., 2020) **Special use** (Peng et al., 2016)
	Shape index distribution (SHAPE_)	$SHAPE\_MN$ $= mean(SHAPE[patch_{ij}])$ $SHAPE\_AM$ $= am(SHAPE[patch_{ij}])$ $SHAPE\_SD$ $= sd(SHAPE[patch_{ij}])$	Each class is summarized as the mean / area weighted mean / standard deviation of each patch belonging to class i.	SHAPE_MN/AM = 0 if all patches are squares. Increases, without limit, as the shapes of patches become more complex. SHAPE_SD = 0 if all patches have an identical shape index. Increases, without limit, as the variation of the shape index increases.	**48** **SHAPE_MN** (Athukorala & Murayama, 2020; J. Chen, P. Du, et al., 2022; Chen et al., 2020; J. Chen, W. Zhan, et al., 2022; J. Chen et al., 2021; Estoque et al., 2017; Hou & Estoque, 2020; Hu et al., 2021; Kim et al., 2016; Kong, Yin, James, et al., 2014; Li et al., 2013; Li et al., 2012; Li et al., 2019; Liu et al., 2018a; Lu et al., 2020; Lyu et al., 2023; Ma et al., 2021; Peng et al., 2018; Qian et al., 2018; Rakoto et al., 2021; Rouhi et al., 2018; Simwanda et al., 2019; Song et al., 2020; Wang et al., 2023; Wang et al., 2020; Wesley & A. Brunsell, 2019; Y. Wu et al., 2022; L. Yang et al., 2021; Ye et al., 2021; M. Zhang et al., 2022; Zhao et al., 2020; L. Zhou et al., 2022; Zhou & Cao, 2020; W. Zhou, F. Cao, et al., 2019; Zhou et al., 2011; Zhou et al., 2017) **SHAPE _AM** (Galletti et al., 2019; Ke et al., 2021; Kowe et al., 2021; Y. Li et al., 2020; Liu et al., 2018a; Ma & Peng, 2022; Masoudi & Tan, 2019; Masoudi et al., 2021; Masoudi et al., 2019; Shaker et al., 2019; Song et al., 2020; Tang et al., 2023) **SHAPE _SD** (Wesley & A. Brunsell, 2019; Ye et al., 2021; Zhou et al., 2011) **Different use** (X. Chen et al., 2022) **Not specified** (B. Li et al., 2020; Wu & Zhang, 2018)

Metric category	Landscape metric	Calculation#	Description	Range	Frequency in reviewed papers
	Fractal index distribution (FRAC_)	$FRAC\_AM = am(FRAC[patch_{ij}])$ $FRAC\_MN = mean(FRAC[patch_{ij}])$	The metric summarizes each class as the mean / area weighted mean of the fractal dimension index of all patches belonging to class i.	1≤FRAC_MN≤2 Approaches 1 for a squared patch shape form and 2 for an irregular patch shape.	**22** **FRAC_MN** (Liu et al., 2018a, 2018b; Lyu et al., 2023; Simwanda et al., 2019; Song et al., 2020; M. Zhang et al., 2022; Zhao et al., 2020) **FRAC_AM** (An et al., 2022; Connors et al., 2012; Feng & Myint, 2016; Galletti et al., 2019; Kowe et al., 2021; Liu et al., 2018a, 2018b; Masoudi & Tan, 2019; Masoudi et al., 2019; Shaker et al., 2019; Song et al., 2020; X. Wang et al., 2021; Wen et al., 2011; Xie et al., 2020; L. Zhang et al., 2022) **Not specified** (Dugord et al., 2014; Kamarianakis et al., 2017; Li et al., 2017)
	Related circumscribing circle distribution (CIRCLE_)	$CIRCLE\_AM = am(CIRCLE[patch_{ij}])$ $CIRCLE\_MN = mean(CIRCLE[patch_{ij}])$ where, $CIRCLE = 1 - \frac{a_{ij}}{a_{ij}^{circle}}$	It summarizes each class as the mean / area weighted mean of the related circumscribing circle of all patches belonging to class i.	>0 = 0 if the related circumscribing circle of all patches is small. Increases as the related circumscribing circles increase.	**4** CIRCLE_AM (Bartesaghi-Koc et al., 2020; Liu et al., 2018a; M. Zhang et al., 2022) CIRCLE_MN (Guo et al., 2021; Liu et al., 2018a)
	Contiguity index distribution (CONTIG_)	$CONTIG\_AM = am(CONTIG[patch_{ij}])$ $CONTIG\_MN = mean(CONTIG[patch_{ij}])$ where, $CONTIG = \frac{\left[\frac{\sum_{r=1}^{z} c_{ijr}}{a_{ij}}\right] - 1}{v - 1}$	It summarizes each class as the mean of each patch belonging to class i. It assesses the spatial connectedness (contiguity) of cells in patches.	0≤CONTIG≤1 Equals 0 for one-pixel patches and increases to a limit of 1 (fully connected patch).	**7** CONTIG_AM (Galletti et al., 2019; Guo et al., 2021; Liu et al., 2018a; Song et al., 2020; M. Zhang et al., 2022) CONTIG_MN (Chakraborti et al., 2019; Liu et al., 2018a; Song et al., 2020) Not specified (Dugord et al., 2014)
Aggregation metrics	Interspersion and juxtaposition index (IJI)	$IJI = \frac{-\sum_{k=1}^{m}\left[\left(\frac{e_{ik}}{\sum_{k=1}^{m} e_{ik}}\right)\ln\left(\frac{e_{ik}}{\sum_{k=1}^{m}}\right.\right.}{\ln(m-1)} * 100$	It describes the intermixing of classes (i.e. without considering like adjacencies - the diagonal of the adjacency table). The number of classes to calculate IJI must be >= than 3.	0 < IJI <= 100 Approaches 0 if a class is only adjacent to a single other class and equals 100 when a class is equally adjacent to all other classes.	**8** (An et al., 2022; Chakraborti et al., 2019; Feng & Myint, 2016; Gage & Cooper, 2017; Galletti et al., 2019; B. Li et al., 2020; Song et al., 2020; M. Zhang et al., 2022)
	Percentage of like adjacencies (PLADJ)	$PLADJ = \left(\frac{g_{ij}}{\sum_{k=1}^{m} g_{ik}}\right) * 100$	It calculates the frequency how often patches of different classes i (focal class) and k are next to each other, and following is a measure of class aggregation. The adjacencies are counted using the double-count method.	0 <= PLADJ <= 100 Equals PLADJ = 0 if class i is maximal disaggregated, i.e. every cell is a different patch. Equals PLADJ = 100 when the only one patch is present.	**8** (D. Chen et al., 2022; Dugord et al., 2014; Lyu et al., 2023; Shaker et al., 2019; Song et al., 2020; Wesley & A. Brunsell, 2019; Zawadzka et al., 2021; M. Zhang et al., 2022)

Metric category	Landscape metric	Calculation[#]	Description	Range	Frequency in reviewed papers
	Aggregation index (AI)	$AI = \left[\frac{g_{ii}}{max - g_{ii}}\right](100)$	It equals the number of like adjacencies divided by the theoretical maximum possible number of like adjacencies for that class. The metric is based on he adjacency matrix and the the single-count method.	0 <= AI <= 100 Equals 0 for maximally disaggregated and 100 for maximally aggregated classes.	**39** (Amani-Beni et al., 2019; An et al., 2022; Athukorala & Murayama, 2020, 2021; D. Chen et al., 2022; Estoque et al., 2017; Feng et al., 2020; Hou & Estoque, 2020; Kong, Yin, James, et al., 2014; B. Li et al., 2020; Liu et al., 2021; S. Liu et al., 2022; Liu et al., 2018a, 2018b; Lu et al., 2020; Lyu et al., 2023; Ma & Peng, 2022; Ma et al., 2021; Masoudi & Tan, 2019; Masoudi et al., 2019; Ren et al., 2014; Shaker et al., 2019; Simwanda et al., 2019; Song et al., 2020; Wang et al., 2020; X. Wang et al., 2021; Wu et al., 2021; Y. Wu et al., 2022; Wu & Zhang, 2018; Xie et al., 2020; L. Yang et al., 2021; Yao et al., 2020; Yuan et al., 2021; L. Zhang et al., 2022; M. Zhang et al., 2022; Y. Zhang et al., 2022; L. Zhou et al., 2022; Zhou & Cao, 2020; W. Zhou, F. Cao, et al., 2019)
	Clumpiness index (CLUMPY)	$Give\ G_i = \left(\frac{g_{ii}}{\sum_{k=1}^{m} g_{ik}}\right)$ $CLUMPY = \begin{cases} \frac{G_i - P_i}{1 - P_i}\ for\ G_i \geq P_i \\ \frac{G_i - P_i}{1 - P_i}\ for\ G_i < P_i, P_i \geq 0.5 \\ \frac{G_i - P_i}{-P_i}\ for\ G_i < P_i, P_i < 0.5 \end{cases}$	It equals the proportional deviation of the proportion of like adjacencies involving the corresponding class from that expected under a spatially random distribution. The metric is based on the adjacency matrix and the the double-count method.	-1 <= CLUMPY <= 1 Equals -1 for maximally disaggregated, 0 for randomly distributed and 1 for maximally aggregated classes.	**9** (Gage & Cooper, 2017; B. Li et al., 2020; Li et al., 2011; Liu et al., 2018a; Shaker et al., 2019; Song et al., 2020; Wu et al., 2021; M. Zhang et al., 2022; G. Zhou et al., 2019)
	Landscape shape index (LSI)	$LSI = \frac{p_{ij}}{\min p_{ij}}$	LSI is an 'Aggregation metric'. It is the ratio between the actual edge length of class i and the hypothetical minimum edge length of class i. The minimum edge length equals the edge length if class i would be maximally aggregated.	LSI >= 1 Increases, without limit, as the length of the actual edges increases, i.e. the patches become less compact.	**44** (Amani-Beni et al., 2019; Chakraborti et al., 2019; D. Chen et al., 2022; Cheng et al., 2015; Connors et al., 2012; Gage & Cooper, 2017; Guo et al., 2021; Huang & Wang, 2019; Kamarianakis et al., 2017; Li et al., 2018; Li et al., 2011; T. Li et al., 2020; T. Li et al., 2021; Li et al., 2017; Li et al., 2013; Li et al., 2012; H. Liu & Q. Weng, 2009; Liu et al., 2016; Liu et al., 2018a, 2018b; Lyu et al., 2023; Ma & Peng, 2022; Masoudi & Tan, 2019; Masoudi et al., 2019; Naeem et al., 2018; Peng et al., 2018; Rakoto et al., 2021; Ren et al., 2014; Shi & Zhao, 2022; Song et al., 2020; Tang et al., 2023; Wang & Zhou, 2022; X. Wang et al., 2021; Wu et al., 2021; Wu et al., 2014; Yan et al., 2019; Yin et al., 2019; Zawadzka et al., 2021; H. Zhang et al., 2022; L. Zhang et al., 2022; M. Zhang et al., 2022; Y. Zhang et al., 2022; Zhao et al., 2020)
	Normalized landscape shape index (nLSI)	$nLSI = \frac{e_i - \min e_i}{\max e_i - \min e_i}$	It describes the ratio of the actual edge length of class i in relation to the hypothetical range of possible edge lengths of class i (min/max). It ignores all background cells when calculating the minimum and maximum total edge length.	0 <= nlsi <= 1 Equals nLSI = 0 when only one squared patch is present. nLSI increases the more disaggregated patches are and equals nLSI = 1 for a maximal disaggregated (i.e. a "checkerboard pattern").	**4** (Bartesaghi-Koc et al., 2020; Gage & Cooper, 2017; Liu et al., 2018a; M. Zhang et al., 2022)

Metric category	Landscape metric	Calculation[#]	Description	Range	Frequency in reviewed papers
	Patch cohesion index (COHESION)	$COHESION = 1 - \left(\frac{\sum_{j=1}^{n} p_{ij}}{\sum_{j=1}^{n} p_{ij}\sqrt{a_{ij}}}\right) * \left(1 - \frac{1}{\sqrt{Z}}\right)^{-1} * 100$	It characterizes the connectedness of patches belonging to class i. It can be used to assess if patches of the same class are located aggregated or rather isolated and thereby COHESION gives information about the configuration of the landscape.	0 < COHESION < 100 Approaches COHESION = 0 if patches of class i become more isolated. Increases if patches of class i become more aggregated.	**29** (D. Chen et al., 2022; J. Chen, P. Du, et al., 2022; Chen et al., 2020; J. Chen et al., 2021; Feng et al., 2020; Gage & Cooper, 2017; Huang & Wang, 2019; Karunaratne et al., 2022; Kim et al., 2016; Kowe et al., 2021; B. Li et al., 2020; Liu et al., 2018a; Ma & Peng, 2022; Ren et al., 2014; Shaker et al., 2019; Song et al., 2020; Sun et al., 2022; Wesley & A. Brunsell, 2019; Q. Wu et al., 2022; Ye et al., 2021; Yu et al., 2020; Zawadzka et al., 2021; M. Zhang et al., 2022; Y. Zhang et al., 2022; Zhou & Cao, 2020; Zhou et al., 2011)
	Number of patches (NP)	$NP = n_i$	It describes the fragmentation of a class, however, does not necessarily contain information about the configuration or composition of the class.	NP >= 1 Equals NP = 1 when only one patch is present and increases, without limit, as the number of patches increases	**15** (Amani-Beni et al., 2019; D. Chen et al., 2022; Gage & Cooper, 2017; Karunaratne et al., 2022; Kim et al., 2016; Kong, Yin, James, et al., 2014; Masoudi & Tan, 2019; Masoudi et al., 2019; Song et al., 2020; Q. Wu et al., 2022; Yin et al., 2019; L. Zhang et al., 2022; M. Zhang et al., 2022; W. Zhou, F. Cao, et al., 2019; W. Zhou et al., 2022)
	Patch density (PD)	$PD = \frac{n_i}{A} * 10000 * 100$	It describes the fragmentation of a class, however, does not necessarily contain information about the configuration or composition of the class.	PD > 0 Increases as the landscape gets more patchy. Reaches its maximum if every cell is a different patch.	**66** (Amani-Beni et al., 2019; Chakraborti et al., 2019; D. Chen et al., 2022; J. Chen, P. Du, et al., 2022; Chen et al., 2020; J. Chen et al., 2021; Cheng et al., 2015; Connors et al., 2012; Dugord et al., 2014; Gage & Cooper, 2017; Galletti et al., 2019; Guo et al., 2021; Huang & Wang, 2019; Kamarianakis et al., 2017; Ke et al., 2021; Kong, Yin, James, et al., 2014; B. Li et al., 2020; Li et al., 2011; Li et al., 2017; Li et al., 2013; Li et al., 2012; Li et al., 2019; H. Liu & Q. Weng, 2009; H. Liu & Q. H. Weng, 2009; Liu et al., 2021; K. Liu et al., 2022; Liu et al., 2016; Liu et al., 2018a, 2018b; Lyu et al., 2023; Ma & Peng, 2022; Maimaitiyiming et al., 2014; Masoudi & Tan, 2019; Masoudi et al., 2021; Masoudi et al., 2019; Naeem et al., 2018; Peng et al., 2018; Peng et al., 2016; Qian et al., 2018; Rakoto et al., 2021; Ren et al., 2014; Shaker et al., 2019; Shi & Zhao, 2022; Simwanda et al., 2019; Song et al., 2020; Tang et al., 2023; Terfa et al., 2020; X. Wang et al., 2021; Y. Wang et al., 2021; Wesley & A. Brunsell, 2019; Wu et al., 2021; Wu et al., 2014; Xie et al., 2020; Yan et al., 2019; C. Yang et al., 2021; L. Yang et al., 2021; Yao et al., 2020; Ye et al., 2021; Yin et al., 2019; Yu et al., 2020; Yuan et al., 2021; M. Zhang et al., 2022; G. Zhou et al., 2019; L. Zhou et al., 2022; Zhou & Cao, 2020; Zhou et al., 2011)
	Landscape division index (DIVISION)	$DIVISION = \left(1 - \sum_{j=1}^{n}\left(\frac{a_{ij}}{A}\right)^2\right)$	It can be in as the probability that two randomly selected cells are not located in the same patch of class i. The landscape division index is negatively correlated with the effective mesh size (MESH).	0 <= Division < 1 Equals DIVISION = 0 if only one patch is present. Approaches DIVISION = 1 if all patches of class i are single cells.	**12** (D. Chen et al., 2022; Feng et al., 2020; B. Li et al., 2020; T. Li et al., 2021; Liu et al., 2018a, 2018b; Shaker et al., 2019; Song et al., 2020; Y. Wang et al., 2021; Q. Wu et al., 2022; M. Zhang et al., 2022; Zhao et al., 2020)
	Splitting index (SPLIT)	$SPLIT = \frac{A^2}{\sum_{j=1}^{n} a_{ij}^2}$	It describes the number of patches if all patches of class i would be divided into equally sized patches.	1 <= SPLIT <= Number of cells squared Equals SPLIT = 1 if only one patch is present. Increases as the number of patches of class i increases and is limited if all cells are a patch	**9** (D. Chen et al., 2022; B. Li et al., 2020; Liu et al., 2018a; Ren et al., 2014; Shi & Zhao, 2022; Sun et al., 2022; X. Wang et al., 2021; H. Zhang et al., 2022; M. Zhang et al., 2022)

Metric category	Landscape metric	Calculation[#]	Description	Range	Frequency in reviewed papers
	Effective mesh size (MESH)	$MESH = \frac{\sum_{j=1}^{n} a_{ij}^2}{A} * \frac{1}{10000}$	Because each patch is squared before the sums for each group i are calculated and the sum is standardized by the total landscape area, MESH is a relative measure of patch structure.	cell size / total area <= MESH <= total area Equals cell size/total area if class covers only one cell and equals total area if only one patch is present.	**5** (D. Chen et al., 2022; Liu et al., 2018a; Shaker et al., 2019; Q. Wu et al., 2022; M. Zhang et al., 2022)
	Euclidean nearest neighbor distance distribution (ENN_)	$ENN\_AM = am(ENN[patch_{ij}])$ $ENN\_MN = mean(ENN[patch_{ij}])$ $ENN\_SD = sd(ENN[patch_{ij}])$ where, $ENN = h_{ij}$	It summarizes each class as the mean / area weighted mean / standard deviation of each patch belonging to class i.	ENN_MN/_AM> 0 = 0 as the distance to the nearest neighbor decreases, i.e. patches of the same class i are more aggregated. ENN_SD > 0 = 0 if the nearest-neighbor distance is identical for all patches.	**19** ENN_MN (Cheng et al., 2015; Ke et al., 2021; Kim et al., 2016; Li et al., 2013; Li et al., 2012; Li et al., 2019; Masoudi & Tan, 2019; Masoudi et al., 2019; Rakoto et al., 2021; Rouhi et al., 2018; Terfa et al., 2020; Wu et al., 2021; Q. Wu et al., 2022; Ye et al., 2021; Yu et al., 2020; M. Zhang et al., 2022; Zhou et al., 2011) ENN_AM (Masoudi & Tan, 2019; Masoudi et al., 2021; Masoudi et al., 2019; L. Zhang et al., 2022) ENN_SD (Ye et al., 2021; Zhou et al., 2011)
	Proximity index distribution (PROX_)	$PROX\_AM = am(PROX[patch_{ij}])$ $PROX\_MN = mean(PROX[patch_{ij}])$ where, $PROX = \sum_{s=1}^{n} \frac{a_{ijs}}{h_{ijs}^2}$	It summarizes each class as the mean / area weighted mean of each patch belonging to class i.	PROX_≥0 = 0 if all patches of the corresponding patch type have no neighbors of the same type within the specified search radius. It increases as patches of the corresponding patch type become less isolated and the patch type becomes less fragmented in distribution.	**4** PROX_MN (Feng & Myint, 2016; Li et al., 2019) PROX_AM (Shaker et al., 2019) Not specified (Yu et al., 2020)
	Connectance (CONNECT)	$CONNECT = \left[\frac{\sum_{j \neq k}^{n} c_{ijk}}{\frac{n_i(n_i - 1)}{2}}\right]$	It equals the number of functional joinings between all patches of the corresponding patch type, divided by the number of possible joinings.	0<CONNECT≤100 =0 when either the focal class consists of a single patch or none of the patches of the focal class are connected. =100 when every patch of the focal class is connected.	**2** (Amani-Beni et al., 2019; Shaker et al., 2019)
Core area metrics	Core area distribution (CORE_)	$CORE\_AM = am(CORE[patch_{ij}])$ where, $CORE = n_{ij}^{core}$	The metric summarizes each class as the area weighted mean of the core area of all patches belonging to class i.	CORE_AM ≥0 = 0 if CORE = 0 for all patches. Increases, without limit, as the core area indices increase.	**1** CORE_AM (Shaker et al., 2019)
	Core area index distribution (CAI_)	$CAI\_AM = am(CAI[patch_{ij}])$ $CAI\_MN = mean(CAI[patch_{ij}])$	The metric summarizes each class as the mean / area weighted mean of the core area index of all patches belonging to class i.	0≤CAI_MN/AM≤100 = 0 when all patches have no core area, and = 100 with increasing percentage of core area within patches.	**1** CAI_AM (Shaker et al., 2019)

Metric category	Landscape metric	Calculation#	Description	Range	Frequency in reviewed papers
Contrast metrics	Contrast-weighted edge density (CWED)	$CWED = \frac{\sum_{k=1}^{m}(e_{ik} \times d_{ik})}{A}$	It equals the sum of lengths of each edge segment involving the corresponding patch type multiplied by the corresponding contrast weight, divided by the sum of the lengths of all edge segments involving the same type.	CWED ≥0 =0 when there is no class edge in the landscape. It increases as the amount of class edge in the landscape increases and / or as the contrast in edges involving the corresponding patch type increase.	**1** (Du et al., 2016)
Others	FD	$FD = \frac{n}{A_i}$	It measures the fragmentation of patches of the same class.	FD>0 It increases as the patch type is increasingly fragmented.	**1** (Wu & Zhang, 2018)

* Confirmed by personal correspondence with the corresponding authors.

Calculation formulas are

Table B3 2D landscape level LMs used in reviewed papers

Metric category	Landscape metric	Calculation[#]	Description	Range	Frequency in reviewed papers
Area and edge metrics	Largest patch index (LPI)	$LPI = \frac{\max a_{ij}}{A} * 100$	It is the percentage of the landscape covered by the largest patch in the landscape. It is a simple measure of dominance.	0 < LPI <= 100 Approaches LPI = 0 when the largest patch is becoming small and equals LPI = 100 when only one patch is present	**10** (Cheng et al., 2015; Das et al., 2020; Du et al., 2016; Gage & Cooper, 2017; A. Guo et al., 2020; B. Li et al., 2020; X. Wang et al., 2021; Weber et al., 2014; Yang et al., 2022; Zhao et al., 2020)
	Total edge (TE)	$TE = \sum_{k=1}^{m} e_{ik}$	Total edge includes all edges. It measures the configuration of the landscape because a highly fragmented landscape will have many edges. However, total edge is an absolute measure, making comparisons among landscapes with different total areas difficult.	TE >= 0 Equals TE = 0 if all cells are edge cells. Increases, without limit, as landscape becomes more fragmented	1 (Weber et al., 2014)
	Edge density (ED)	$ED = \frac{E}{A} * 10000$	The edge density equals all edges in the landscape in relation to the landscape area. The metric describes the configuration of the landscape, e.g. because an overall aggregation of classes will result in a low edge density. The metric is standardized to the total landscape area, and therefore comparisons among landscapes with different total areas are possible.	ED >= 0 Equals ED = 0 if only one patch is present (and the landscape boundary is not included) and increases, without limit, as the landscapes becomes more patchy	**8** (Bera et al., 2022; Cheng et al., 2015; Connors et al., 2012; Li et al., 2017; Rakoto et al., 2021; X. Wang et al., 2021; Weber et al., 2014; Wu et al., 2021)
	Patch area distribution (AREA_)	$AREA\_MN = mean(AREA[patch_{ij}])$ $AREA\_AM = am(AREA[patch_{ij}])$ $AREA\_SD = sd(AREA[patch_{ij}])$ $AREA\_CV = cv(AREA[patch_{ij}])$	The metric summarizes the total landscape as the mean / area weighted mean / standard deviation / coefficient of variation of all patch areas belonging to class i.	≥ 0 AREA_MN/AM=0 if all patches are small. AREA_SD/CV = 0 if all patches are identical in size.	**7** AREA_MN (Cheng et al., 2015; Das et al., 2020; Ma & Peng, 2022; Rakoto et al., 2021) AREA_SD (Du et al., 2016; Weber et al., 2014) AREA_AM (Liu et al., 2018b) AREA_CV (Weber et al., 2014)
	Radius of gyration distribution (GYRATE_)	$\text{GYRATE}\_AM = am(\text{GYRATE}[patch_{ij}])$ where, $GYRATE = \sum_{r=1}^{z} \frac{h_{ijr}}{z}$	The metric summarizes the whole landscape as the area weighted mean of the radius of gyration of all patches in the total landscape. GYRATE measures the distance from each cell to the patch centroid and is based on cell center-to-cell center distances. The metrics characterizes both the patch area and compactness.	≥ 0 = 0 if every patch is a single cell. Increases, without limit, when only one patch is present.	**1** GYRATE_AM (Liu et al., 2018b)

Metric category	Landscape metric	Calculation[#]	Description	Range	Frequency in reviewed papers
Shape metrics	Perimeter-area fractal dimension (PAFRAC)	$PAFRARC = \frac{2}{\beta}$ where β is the slope of the regression of the area against the perimeter (logarithm) $N \sum_{i=1}^{m} \sum_{j=1}^{n} \ln a_{ij} = a + N \sum_{i=1}^{m} \sum_{j=1}^{n} \ln p_{ij}$	It describes the patch complexity of the landscape while being scale independent. This means that increasing the patch size while not changing the patch form will not change the metric.	1≤PAFRAC≤2 Approaches 1 for shapes with very simple perimeters and approaches 2 for shapes with highly convoluted, plane-filling perimeters.	**1** (H. Liu & Q. H. Weng, 2009)
	Shape index distribution (SHAPE_)	$SHAPE\_MN = mean(SHAPE[patch_{ij}])$ $SHAPE\_AM = am(SHAPE[patch_{ij}])$ $SHAPE\_SD = sd(SHAPE[patch_{ij}])$	The total landscape is summarized as the mean / area weighted mean / standard deviation of each patch belonging to the total landscape.	SHAPE_MN/AM = 0 if all patches are squares. Increases, without limit, as the shapes of patches become more complex. SHAPE_SD = 0 if all patches have an identical shape index. Increases, without limit, as the variation of the shape index increases.	**7** SHAPE_AM (Galletti et al., 2019; Ma & Peng, 2022; Weber et al., 2014) SHAPE_MN (Bera et al., 2022; Rakoto et al., 2021; Weber et al., 2014) SHAPE_SD (J. Chen, P. Du, et al., 2022; Du et al., 2016)
	Fractal index distribution (FRAC_)	$FRAC\_AM = am(FRAC[patch_{ij}])$ $FRAC\_MN = mean(FRAC[patch_{ij}])$	The metric summarizes the landscape as the mean / area weighted mean of the fractal dimension index of all patches belonging to class i.	1≤FRAC_MN≤2 Approaches 1 for a squared patch shape form and 2 for an irregular patch shape.	**9** (Connors et al., 2012; Galletti et al., 2019; Li et al., 2017; H. Liu & Q. H. Weng, 2009; Liu et al., 2018b; X. Wang et al., 2021; Y. Wang et al., 2021; Weber et al., 2014; Yu et al., 2020)
Aggregation metrics	Contagion (CONTAG)	$CONTAG = 1 + \frac{\sum_{q=1}^{n_a} p_q \ln(p_q)}{2\ln(t)}$	It is based on cell adjacencies and describes the probability of two random cells belonging to the same class. It is affected by both the dispersion and interspersion of classes. E.g., low class dispersion (= high proportion of like adjacencies) and low interspersion (= uneven distribution of pairwise adjacencies) lead to a high contagion value.	0 < Contag <=100 Approaches CONTAG = 0 if all cells are unevenly distributed and 100 indicates that all cells are equally adjacent to all other classes.	**14** (J. Chen, P. Du, et al., 2022; Connors et al., 2012; Das et al., 2020; Du et al., 2016; Gage & Cooper, 2017; Galletti et al., 2019; Kamarianakis et al., 2017; Li et al., 2017; H. Liu & Q. H. Weng, 2009; Wu et al., 2021; Wu et al., 2014; Wu et al., 2019; Y. Zhang et al., 2022; Zhao et al., 2020)
	Interspersion and juxtaposition index (IJI)	$IJI = \frac{-\sum_{i=1}^{m}\sum_{k=i+1}^{m}\left[\left(\frac{e_{ik}}{E}\right)\ln\left(\frac{e_{ik}}{E}\right)\right]}{\ln(0.5[m(m-1)])} * 100$	It describes the intermixing of classes (i.e. without considering like adjacencies - the diagonal of the adjacency table).	0<IJI≤100 Approaches 0 if a class is only adjacent to a single other class and equals 100 when a class is equally adjacent to all other classes.	**4** (Das et al., 2020; Du et al., 2016; Gage & Cooper, 2017; Galletti et al., 2019)
	Aggregation index (AI)	$AI = \left[\sum_{i=1}^{m}\left(\frac{g_{ii}}{max - g_{ii}}\right)P_i\right](100)$	It equals the number of like adjacencies divided by the theoretical maximum possible number of like adjacencies for that class summed over each class for the entire landscape. The metric is based on he adjacency matrix and the single-count method.	0 <= AI <= 100 Equals 0 for maximally disaggregated and 100 for maximally aggregated classes.	**8** (Gage & Cooper, 2017; A. Guo et al., 2020; Ma & Peng, 2022; X. Wang et al., 2021; Wu et al., 2021; Yang et al., 2022; Zhao et al., 2020)
	Splitting index (SPLIT)	$SPLIT = \frac{A^2}{\sum_{i=1}^{m}\sum_{j=1}^{n} a_{ij}^2}$	It describes the number of patches if all patches the landscape would be divided into equally sized patches.	1 <= SPLIT <= Number of cells squared Equals SPLIT = 1 if only one patch is present. Increases as the number of patches of class i increases and is limited if all cells are a patch	**1** (X. Wang et al., 2021)

Metric category	Landscape metric	Calculation#	Description	Range	Frequency in reviewed papers
	Landscape shape index (LSI)	$LSI = \frac{E}{\min E}$	It is the ratio between the actual landscape edge length and the hypothetical minimum edge length. The minimum edge length equals the edge length if only one patch would be present.	LSI≥1 = 1 when only one squared patch is present. Increases, without limit, as the length of the actual edges increases, i.e. the patches become less compact.	**15** (Bera et al., 2022; Cheng et al., 2015; Connors et al., 2012; Das et al., 2020; Gage & Cooper, 2017; T. Li et al., 2020; Li et al., 2017; H. Liu & Q. H. Weng, 2009; Rakoto et al., 2021; X. Wang et al., 2021; Weber et al., 2014; Wu et al., 2021; Wu et al., 2019; Yang et al., 2022; Yu et al., 2020)
	Patch cohesion index (COHESION)	$COHESION = 1 - \left(\frac{\sum_{i=1}^{m}\sum_{j=1}^{n} p_{ij}}{\sum_{i=1}^{m}\sum_{j=1}^{n} p_{ij}\sqrt{a_{ij}}}\right) * \left(1 - \frac{1}{\sqrt{Z}}\right)^{-1} * 100$	It characterizes the connectedness of patches in the total landscape. It can be used to assess if patches are located aggregated or rather isolated and thereby COHESION gives information about the configuration of the landscape.	0 < COHESION < 100 Approaches COHESION = 0 if patches become more isolated. Increases if patches become more aggregated.	**1** (H. Liu & Q. H. Weng, 2009; Sun et al., 2022)
	Number of patches (NP)	$NP = N$	It describes the fragmentation of the landscape, however, does not necessarily contain information about the configuration or composition of the landscape.	Equals NP = 1 when only one patch is present and increases, without limit, as the number of patches increases	**4** (Das et al., 2020; Gage & Cooper, 2017; Ma & Peng, 2022; Yang, He, Wang, et al., 2017)
	Patch density (PD)	$PD = \frac{N}{A} * 10000 * 100$	It describes the fragmentation the landscape, however, does not necessarily contain information about the configuration or composition of the landscape. It is standardized to the area and comparisons among landscapes with different total area are possible.	PD > 0 Increases as the landscape gets patchier. Reaches its maximum if every cell is a different patch.	**19** (Bera et al., 2022; Cheng et al., 2015; Connors et al., 2012; Das et al., 2020; Du et al., 2016; Gage & Cooper, 2017; Galletti et al., 2019; A. Guo et al., 2020; B. Li et al., 2020; Li et al., 2017; Ma & Peng, 2022; Rakoto et al., 2021; X. Wang et al., 2021; Y. Wang et al., 2021; Weber et al., 2014; Wu et al., 2021; Yu et al., 2020; Y. Zhang et al., 2022; Zhao et al., 2020)
	Landscape division index (DIVISION)	$DIVISION = \left(1 - \sum_{i=1}^{m}\sum_{j=1}^{n}\left(\frac{a_{ij}}{A}\right)^2\right)$	It can be in as the probability that two randomly selected cells are not located in the same patch.	0 <= Division < 1 Equals DIVISION = 0 if only one patch is present. Approaches DIVISION = 1 if all patches of class i are single cells.	**3** (Gage & Cooper, 2017; Y. Wang et al., 2021; Wu et al., 2019)
	Effective mesh size (MESH)	$MESH = \frac{\sum_{i=1}^{m}\sum_{j=1}^{n} a_{ij}^2}{A} * \frac{1}{10000}$	Because each patch is squared before the sum is calculated and the sum is standardized by the total landscape area, MESH is a relative measure of patch structure.	cell size / total area <= MESH <= total area Equals cell size/total area if class covers only one cell and equals total area if only one patch is present.	**1** (Yang et al., 2022)
	Euclidean nearest neighbor distance distribution (ENN__MN)	$ENN\_MN = mean(ENN[patch_{ij}])$ where, $ENN = h_{ij}$	It summarizes the total landscape as the mean of each patch.	ENN_MN> 0 = 0 as the distance to the nearest neighbor decreases, i.e. patches in the total landscape are more aggregated.	**4** (Cheng et al., 2015; Rakoto et al., 2021; Weber et al., 2014; Wu et al., 2021)
	Proximity index distribution (PROX)	$PROX = \sum_{s=1}^{n}\frac{a_{ijs}}{h_{ijs}}$	It summarizes the total landscape as the mean of each patch belonging.	PROX_≥0 = 0 if all patches within the specified search radius. It increases as patches of the corresponding patch type become less isolated and the patch type becomes less fragmented in distribution.	**1** (H. Liu & Q. H. Weng, 2009)

* Confirmed by personal correspondence with the corresponding authors. # Calculation formulas and descriptions are adopted from McGarigal et al. (2012) and https://r-spatialecology.github.io/landscapemetrics/index.html (accessed Oct. 2022). $\boldsymbol{A}$ area, $\boldsymbol{p}$ perimeter, $\boldsymbol{n_{ij}^{core}}$ core area of patch ij based on specified edge depths, $\boldsymbol{g_{ii}}$ number of like adjacencies between pixels of class type i based on the double-count method, $\boldsymbol{e_{ik}}$ total length of edge in landscape between patch types i and k, $\boldsymbol{d_{ik}}$ dissimilarity between patch types i and k, $\boldsymbol{c_{ijk}}$ joining between patch j and k of the corresponding patch type based on a user specified threshold distance, $\boldsymbol{\min e_i}$ minimum total length of edge of class i in terms of number of cell surfaces, $\boldsymbol{h_{ijs}}$ distance between patch ijs and patch ijs, based on patch edge-to-edge distance computed from cell center to cell center.

Table B4 Studies that have included 3D metrics and their key findings

Citation	3D metrics		Key findings
	Quantify buildings	Quantify UGS	
(C. Yang et al., 2021)	Mean building height, building height index, mean building volume, building volume index, floor area ratio, building height variance	NA	2D metrics were found contributing more than 3D metrics to LST.
(Q. Wu et al., 2022)	Root mean square deviation of a surface, skewness of surface height distribution, mean height, maximum height, sky view factor	NA	Results of multiple regression and random forest models reveal that 3D metrics better explain LST variance than 2D metrics.
(Chen et al., 2020)	NA	Mean tree height, maximum height of tree canopy, variance of tree canopy height, amplitude of tree canopy height, normalized tree canopy height variance	2D composition metrics and 3D metrics jointly may best explain LST variance both during daytime and nighttime.
(Yuan et al., 2021)	Building coverage ratio, mean building height, floor area ratio, sky view factor, low-rise buildings area ratio, mid-rise buildings area ratio, high-rise building area ratio	NA	Building metrics were found contributing more than UGS metrics. Building coverage ratio was found contributing the most, followed by high-rise building area ratio and low-rise building area ratio.
(J. Chen et al., 2021)	Mean/maximum/variance height of buildings, normalized of building height, sky view factor achieved by buildings, building height value at 10th percentile, building height value at 90th percentile	Mean/maximum/variance of tree canopy height, normalized tree canopy height variance, 10th percentile tree height value, 90th percentile tree height value	During daytime, 2D metrics were found contributing more than 3D metrics. Opposite for nighttime. During daytime, 3D metrics of trees have better performance than those of buildings. Opposite for nighttime.
(Gage & Cooper, 2017)	Building height	Tree height	Contribution of 3D metrics varies among land cover clusters.
(Huang & Wang, 2019)	Shape coefficient, mean height, height variance, normalized height variance, sky view factor	NA	2D metrics were found contributing more than 3D metrics. Among 3D metrics, mean height and sky view factor were found the most prominent. Contribution of 3D landscape metrics of building varied among urban function zones and seasons, with the strongest in winter.
(W.-B. Wu et al., 2022)	Mean building height, volume of building	Mean tree height, volume of tree	3D metrics effectively improve the interpretation of SRHII. Landscape metrics' significance to SRHII varies across climate zones, seasons and day and night.
(Yu et al., 2020)	Class level: volume, ED, PROX, CO, PD, ten-point average height, summit curvature of a surface, density of summit Landscape level: diversity, LSI, FRAC, PD, mean of height, root mean square of height, ten-point average height, root-mean-square slope of a surface, skewness of surface height distribution, kurtosis of surface height distribution, developed interfacial area ratio, summit curvature of a surface, density of summit		3D metrics may well explain LST without including 2D metrics. For vegetation coverage, 3D metrics can be treated as 2D metrics.
(Zeng et al., 2022)	Mean height, mean height standard deviation, high ratio, SHDI		Building metrics demonstrate greater influence. Varies by building and vegetation coverage.
(J. Chen, W. Zhan, et al., 2022)SEM model	SVFbuilding, mean height, variance of building height, maximum height of buildings	Variance of tree height, mean tree canopy height, maximum height of tree canopy	2D and 3D building structures showed much stronger indirect impacts on LST through horizontal and vertical tree structures
(H. Zhang et al., 2022)	Mean building height, mean aspect ratio	Green volume	Interactions of 3D green volume and 2D LMs were significant. (PLSR interaction)
(X. Chen et al., 2022)	mean height, mean volume, floor area ratio	NA	2D landscape metrics explained more of the variation in LST than 3D landscape metrics in spring, summer, and autumn, while 3D landscape metrics had a stronger effect on LST in winter.
(J. Chen, P. Du, et al., 2022)	Maximum building height, mean building height, normalized variance of building height, $10/90^{th}$ percentile of building height	Maximum tree height, mean tree height, normalized variance of tree height, $10/90^{th}$ percentile of tree height	2D and 3D factors jointly demonstrated the best performaces. Multilevel model for better performance than OLS model.
(Lyu et al., 2023)	Building height	Green volume, LAI	3D green volume demonstrates high relative importance.

Appendix C Summary of meta-analysis results of Pearson correlation between patch, class level landscape metrics and temperature indicators

Table C1 and C2 are summaries of meta-analysis results of Pearson correlation between patch and class level landscape metrics (LMs) and temperature indicators respectively. Detailed results of each combination of landscape metric and temperature indicator are shown in Appendix D.

The studies used for meta-analysis are identical to those demonstrated in Fig. 6 and Fig. 8. To ensure homogeneity among synthesized studies, all extracted Pearson correlations were calculated by using temperature indicators based on daytime LST. Their full information can be referred to in Appendix A.

Table C1 Meta-analysis results of Pearson correlation between patch-level LMs and temperature indicators

LMs	Temperature indicators	Sub-group (Climate Zone)	Studies included	Total sample size	Random effects model	Heterogeneity
PARA	CE	C	3	342	[-0.83,0.88]	p<0.01
		D	1	300	N/A	N/A
		Overall	4	642	[-0.77,0.69]	p<0.01
	CI	A	1	4	N/A	N/A
		C	4	382	[-0.80,0.14]	p<0.01
		D	2	333	[-0.71,-0.59]	p=0.52
		Overall	7	719	[-0.76,-0.21]	p<0.01
	LST statistics	C	3	82	[0.17,0.63]	p=0.21
		D	1	300	N/A	N/A
		Overall	4	382	[0.30,0.47]	p=0.35
SHAPE	CE	A	4	532	[-0.01,0.28]	p=0.05
		B	1	15	N/A	N/A
		C	3	391	[-0.10,0.56]	p<0.01
		Overall	8	938	[-0.01,0.30]	p<0.01
	CI	A	3	270	[-0.13,0.11]	p=0.95
		B	1	15	N/A	N/A
		C	5	466	[0.05.0.49]	p<0.01
		Overall	9	751	[-0.07,0.30]	p<0.01
	LST statistics	C	3	668	[-0.45,-0.04]	p<0.01
		D	4	966	[-0.33,-0.21]	p=0.80
		Overall	7	1634	[-0.32,-0.18]	p=0.03

Note: Results marked in yellow are constantly positive or negative pooled Pearson correlation with 95% confidence interval, and homogenous groups. Same below.

Table C2 Meta-analysis of Pearson correlation of class-level LMs and mean LST

LMs	UGS type	Sub-group (Climate Zone)	Studies included	Total sample size	Random effects model	Heterogeneity
AREA_MN	Vegetation	A	4	280	[-0.57,-0.29]	p=0.11
		B	2	1025	[-0.72,0.58]	p<0.01
		C	4	7869	[-0.30,-0.26]	p=0.91
		D	4	7608	[-0.02,0.90]	p<0.01
		Overall	14	16782	[-0.35,0.31]	p<0.01
	Tree	A	1	40	N/A	N/A
		C	1	25	N/A	N/A
		Overall	2	65	[-0.79,0.08]	p=0.03
	Grass	A	1	40	N/A	N/A
		C	1	25	N/A	N/A
		Overall	2	65	[-0.20,0.30]	p=0.36
LPI	Vegetation	B	3	1132	[-0.51,0.44]	p<0.01
		C	2	7629	[-0.47,-0.44]	p=0.39
		D	3	7599	[-0.61,-0.39]	p=0.01
		Overall	8	16360	[-0.56,-0.11]	p<0.01
	Tree	A	1	40	N/A	N/A
		B	1	66	N/A	N/A
		C	2	2275	[-0.73,-0.27]	p=0.10
		D	1	235	N/A	N/A
		Overall	5	2616	[-0.61,-0.19]	p<0.01
	Grass	A	1	40	N/A	N/A
		C	2	2275	[-0.26,-0.18]	p=0.35
		D	1	235	N/A	N/A
		Overall	4	2550	[-0.24,0.09]	p<0.01
ED	Vegetation	B	1	1000	N/A	N/A
		C	4	7835	[-0.49,-0.46]	p=0.76
		D	4	7608	[-0.54,0.67]	p<0.01
		Overall	9	16443	[-0.55,0.11]	p<0.01
	Tree	B	3	634	[-0.60,-0.49]	p=0.92
		C	2	2275	[-0.53,0.38]	p=0.02
		D	1	235	N/A	N/A
		Overall	6	3144	[-0.53,-0.13]	p<0.01
	Grass	B	1	500	N/A	N/A
		C	1	2250	N/A	N/A
		D	1	235	N/A	N/A
		Overall	3	2985	[-0.43,0.07]	p<0.01
SHAPE_MN	Vegetation	A	4	280	[-0.65,-0.33]	p=0.02

LMs	UGS type	Sub-group (Climate Zone)	Studies included	Total sample size	Random effects model	Heterogeneity
		B	1	1000	N/A	N/A
		C	5	410	[-0.53,-0.30]	p=0.08
		D	3	327	[0.03,0.85]	p<0.01
		Overall	13	2017	[-0.48,0.09]	p<0.01
	Tree	A	1	40	N/A	N/A
		C	1	2250	N/A	N/A
		Overall	2	2290	[-0.34,-0.26]	p=0.50
	Grass	A	1	40	N/A	N/A
		C	1	2250	N/A	N/A
		Overall	2	2290	[-0.57,0.78]	p<0.01
LSI	Vegetation	B	1	107	N/A	N/A
		C	1	25	N/A	N/A
		D	5	645	[-0.06,0.52]	p<0.01
		Overall	7	777	[-0.25,0.39]	p<0.01
	Tree	B	1	500	N/A	N/A
		C	1	25	N/A	N/A
		D	1	58	N/A	N/A
		Overall	3	583	[-0.48,0.11]	p=0.02
	Grass	B	1	500	N/A	N/A
		D	1	58	N/A	N/A
		Overall	2	558	[-0.27,-0.11]	p=0.47
AI	Vegetation	A	4	280	[-0.77,-0.33]	p<0.01
		B	2	1025	[-0.45,0.08]	p=0.14
		C	5	410	[-0.61,-0.09]	p<0.01
		D	2	318	[-0.77,-0.10]	p<0.01
		Overall	13	2033	[-0.58,-0.30]	p<0.01
	Tree	A	1	40	N/A	N/A
		B	1	66	N/A	N/A
		D	1	235	N/A	N/A
		Overall	3	341	[-0.58,-0.03]	p<0.01
	Grass	A	1	40	N/A	N/A
		D	1	235	N/A	N/A
		Overall	2	275	[-0.19,0.21]	p=0.19
COHESION	Vegetation	C	1	60	N/A	N/A
		D	1	158	N/A	N/A
		Overall	2	218	[-0.69,-0.08]	p=0.01
	Tree	B	1	66	N/A	N/A
		C	1	25	N/A	N/A
		Overall	2	91	[-0.94,-0.40]	p<0.01

LMs	UGS type	Sub-group (Climate Zone)	Studies included	Total sample size	Random effects model	Heterogeneity
PD	Vegetation	A	1	100	N/A	N/A
		C	6	566	[-0.37,-0.11]	p=0.03
		D	5	645	[-0.54,0.24]	p<0.01
		Overall	12	1311	[-0.40,-0.05]	p<0.01
	Tree	B	1	500	N/A	N/A
		C	3	2300	[-0.77,0.35]	p<0.01
		D	2	293	[0.04,0.33]	p=0.25
		Overall	6	3093	[-0.46,0.23]	p<0.01
	Grass	B	1	500	N/A	N/A
		C	2	2275	[-0.31,0.41]	p=0.06
		D	2	293	[-0.53,0.28]	p<0.01
		Overall	5	3069	[-0.31,0.13]	p<0.01

Appendix D Meta-analysis of Pearson correlation patch, class level landscape metrics and temperature indicators

Fig. D1 Forest plot of Pearson correlation between patch-level SHAPE and cooling intensity

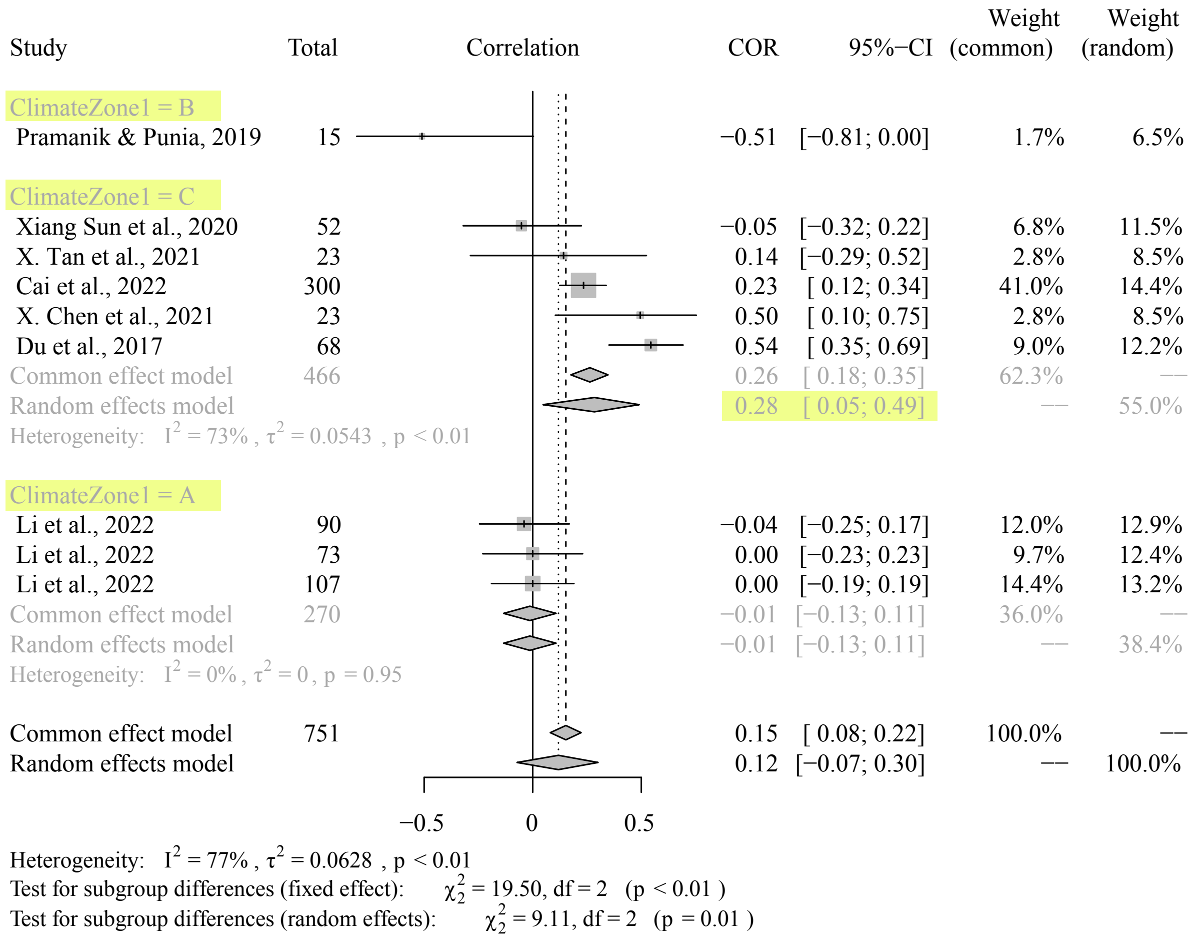

Fig. D2 Forest plot of Pearson correlation between patch-level SHAPE and cooling extent

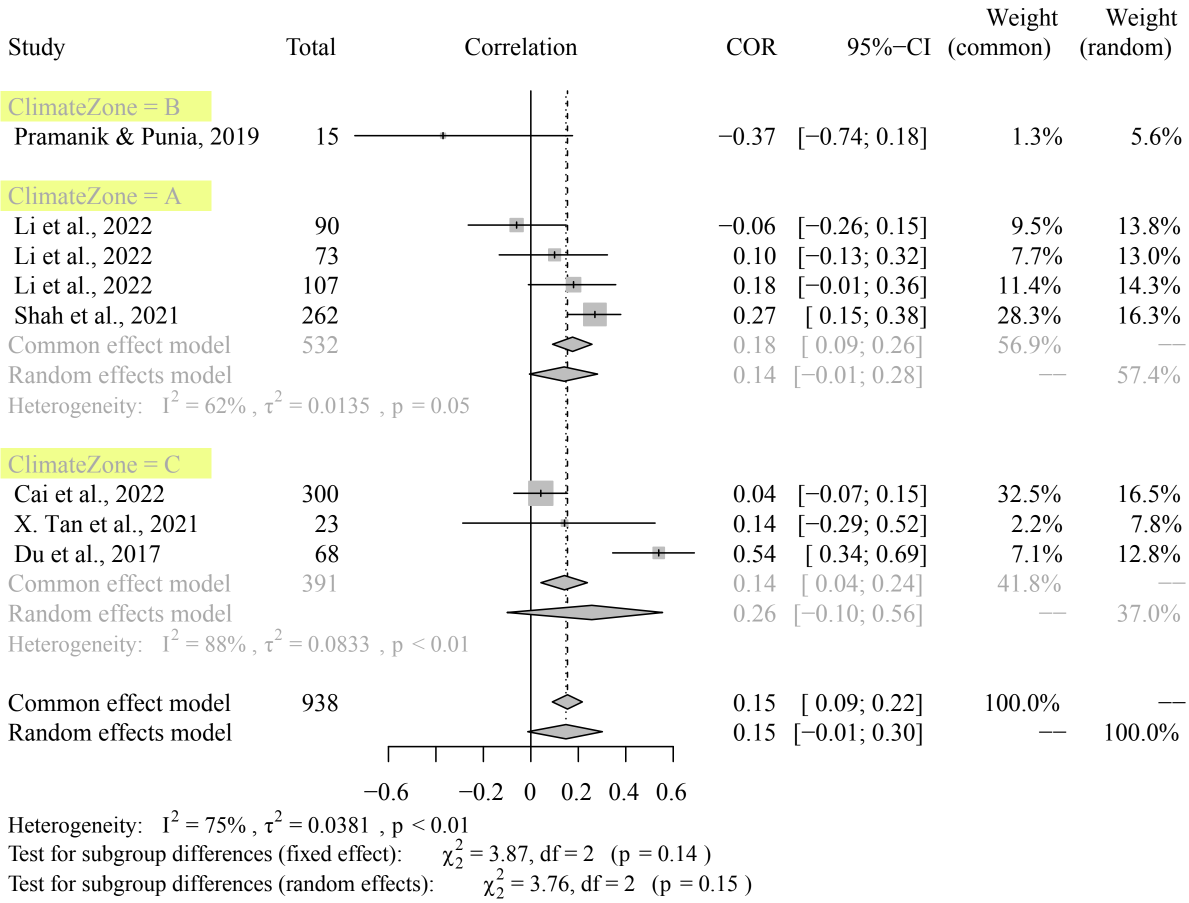

Fig. D3 Forest plot of Pearson correlation between patch-level SHAPE and LST statistics

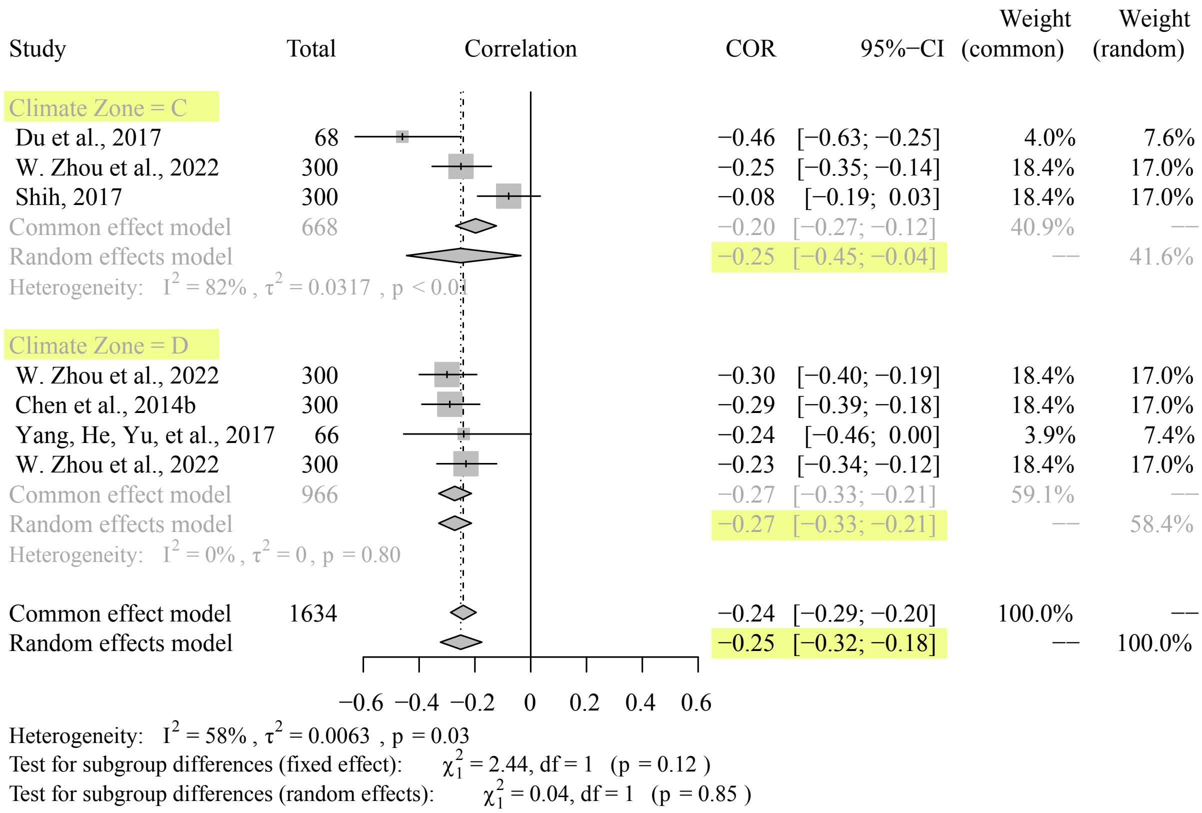

Fig. D4 Forest plot of Pearson correlation between patch-level PARA and cooling intensity

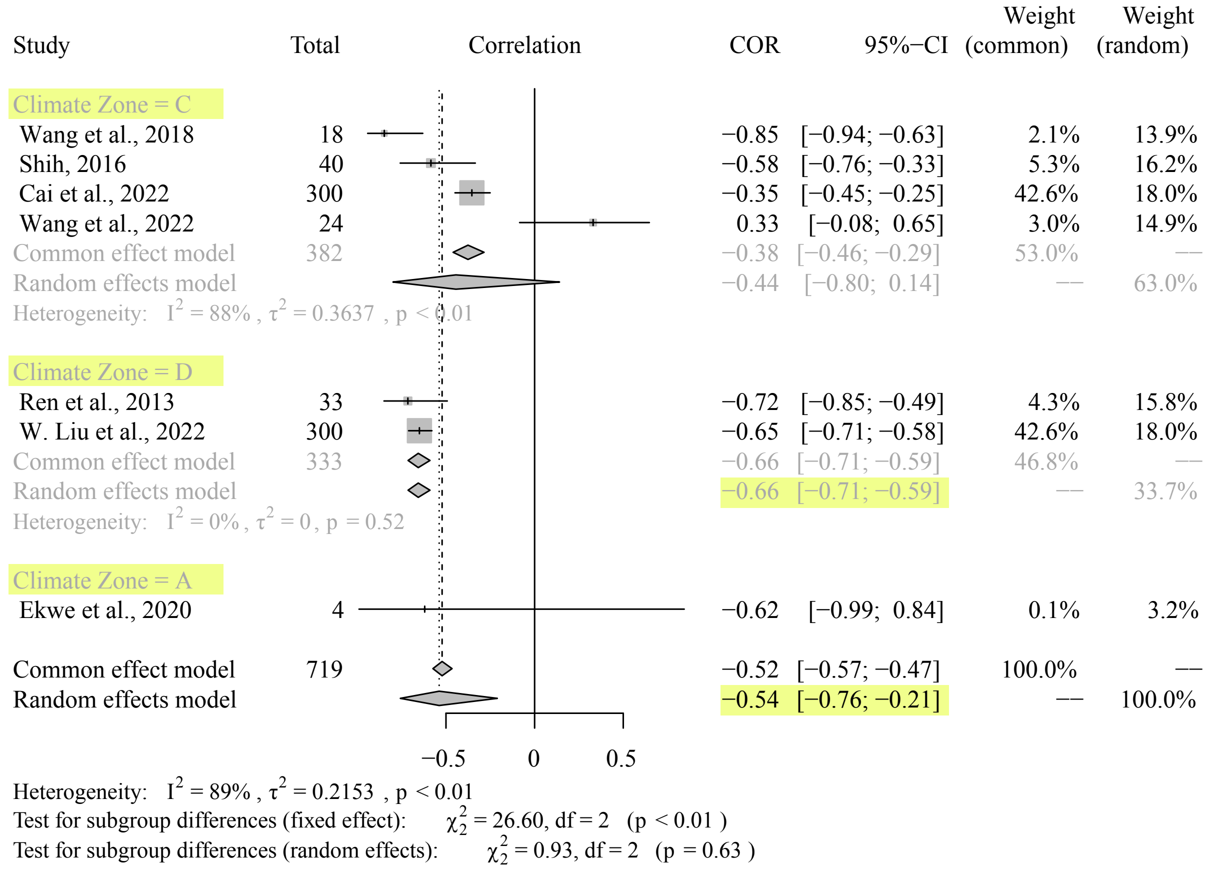

Fig. D5 Forest plot of Pearson correlation between patch-level PARA and cooling extent

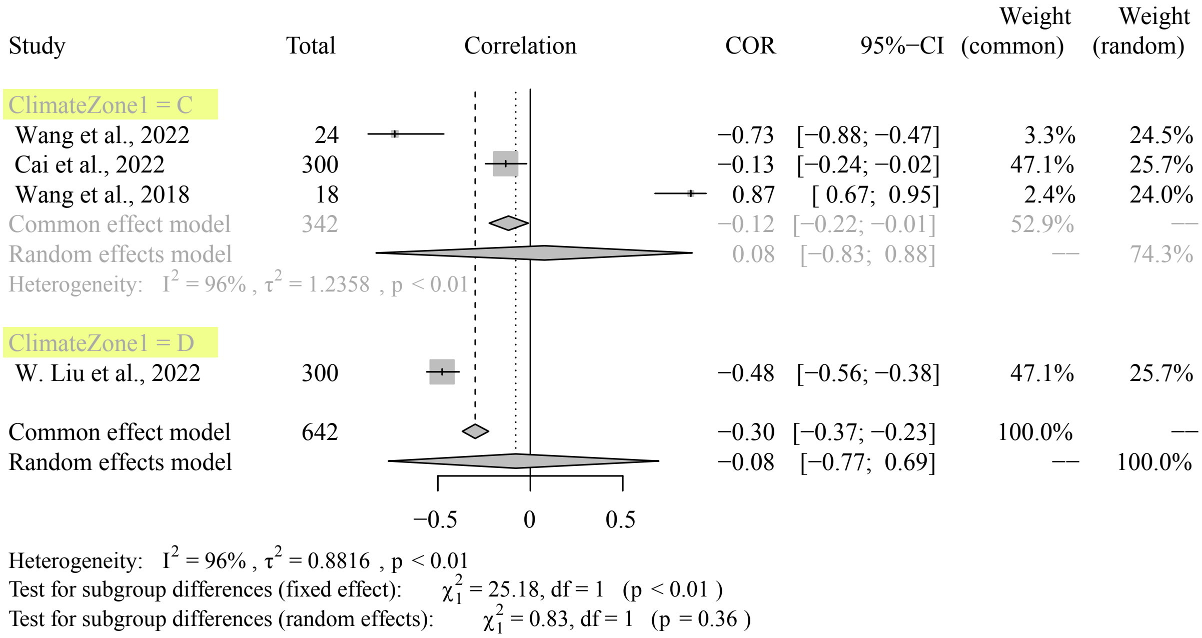

Fig. D6 Forest plot of Pearson correlation between patch-level PARA and LST statistics

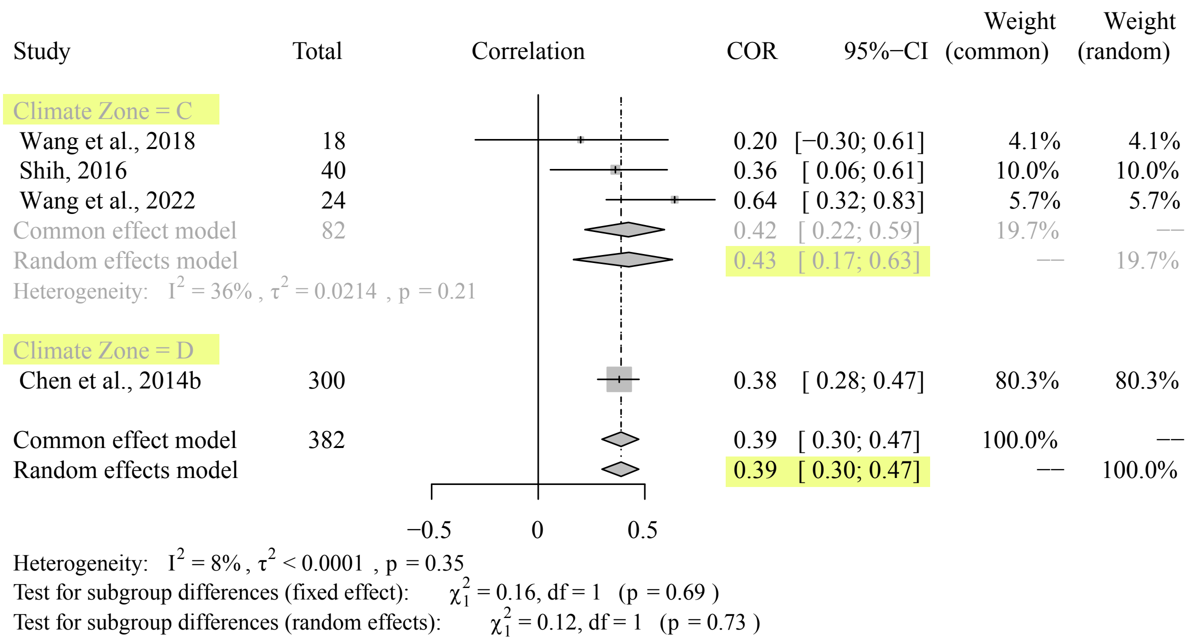

Fig. D7 Forest plot of Pearson correlation between class-level AREA_MN of urban vegetation coverage and mean LST

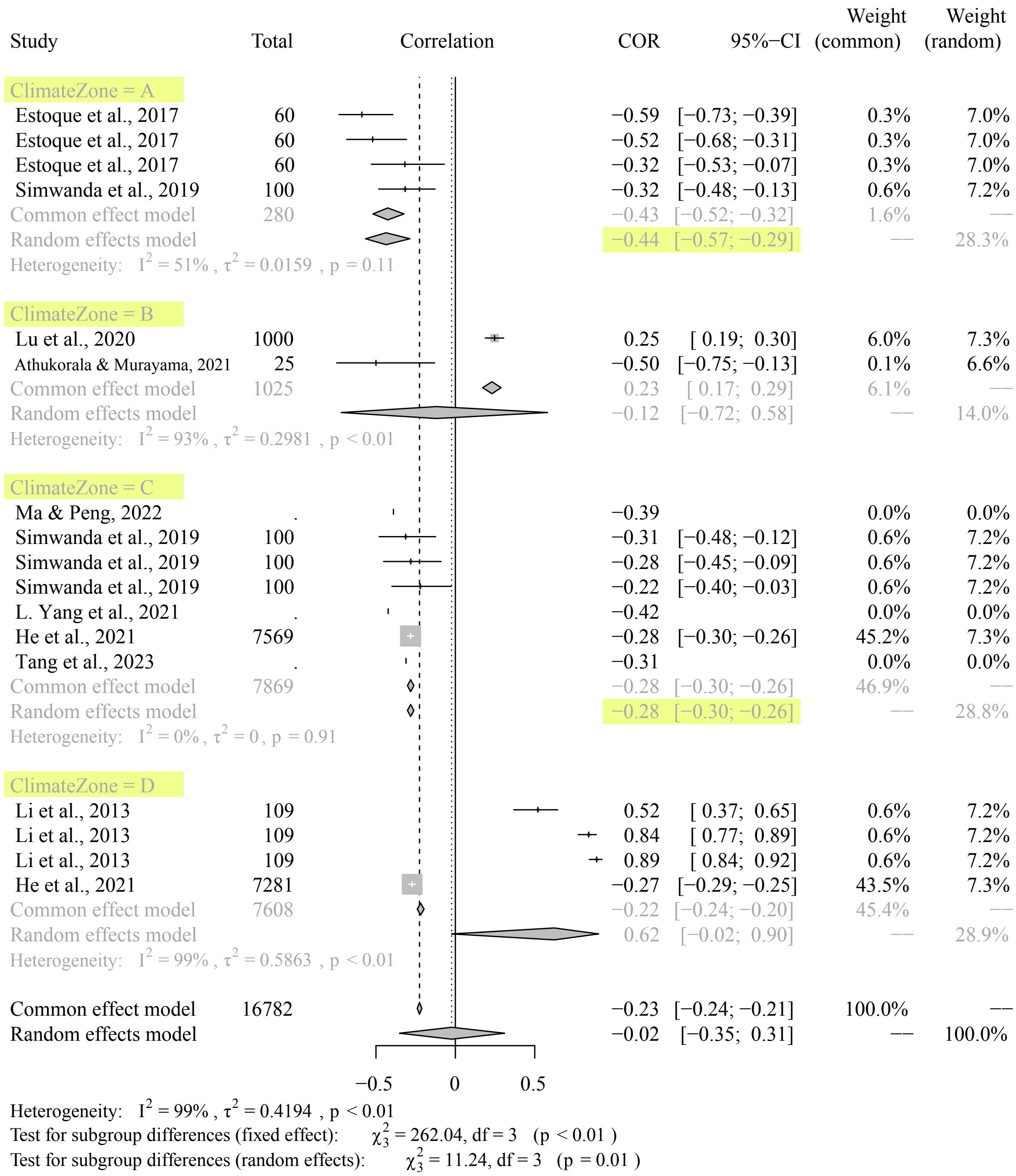

Fig. D8 Forest plot of Pearson correlation between class-level AREA_MN of tree canopy coverage and mean LST

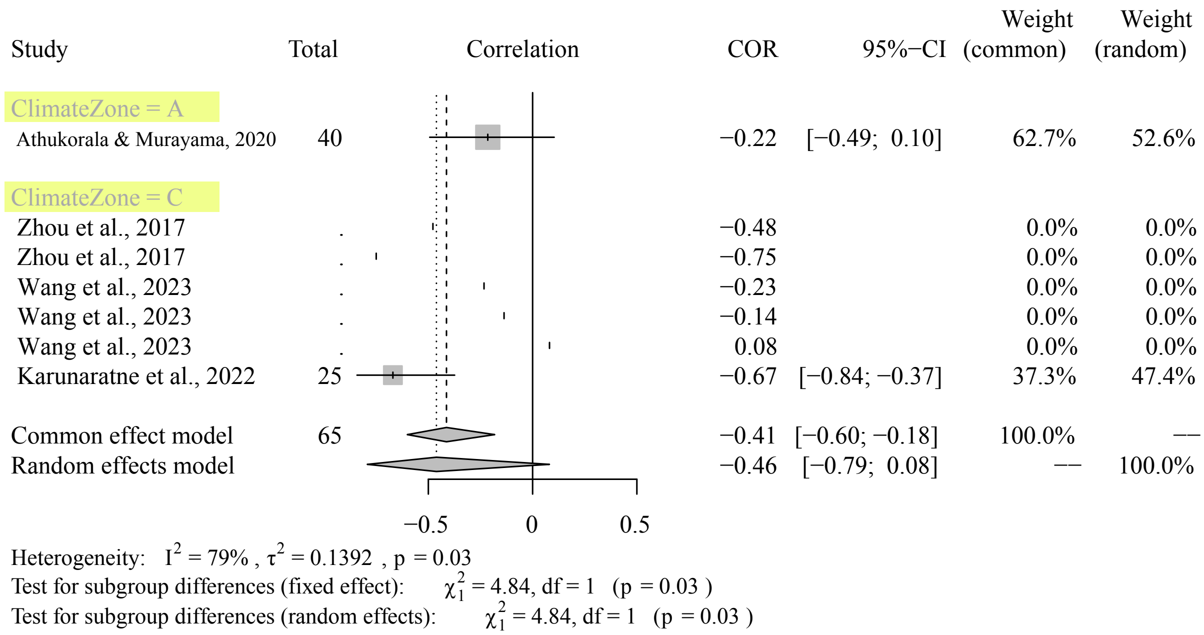

Fig. D9 Forest plot of Pearson correlation between class-level AREA_MN of grassland coverage and mean LST

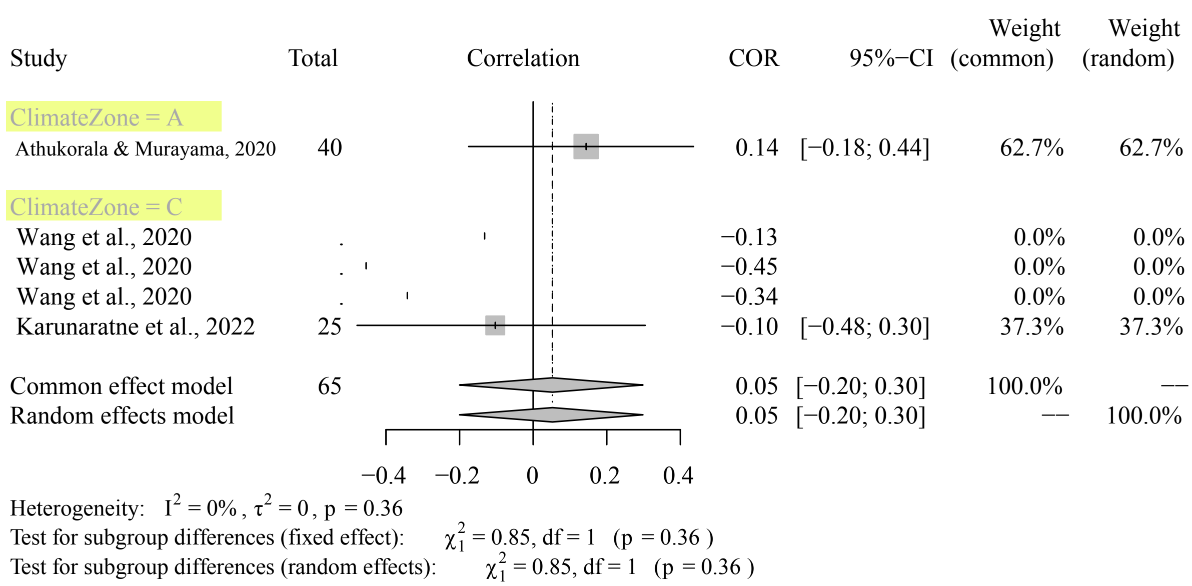

Fig. D10 Forest plot of Pearson correlation between class-level LPI of urban vegetation coverage and mean LST

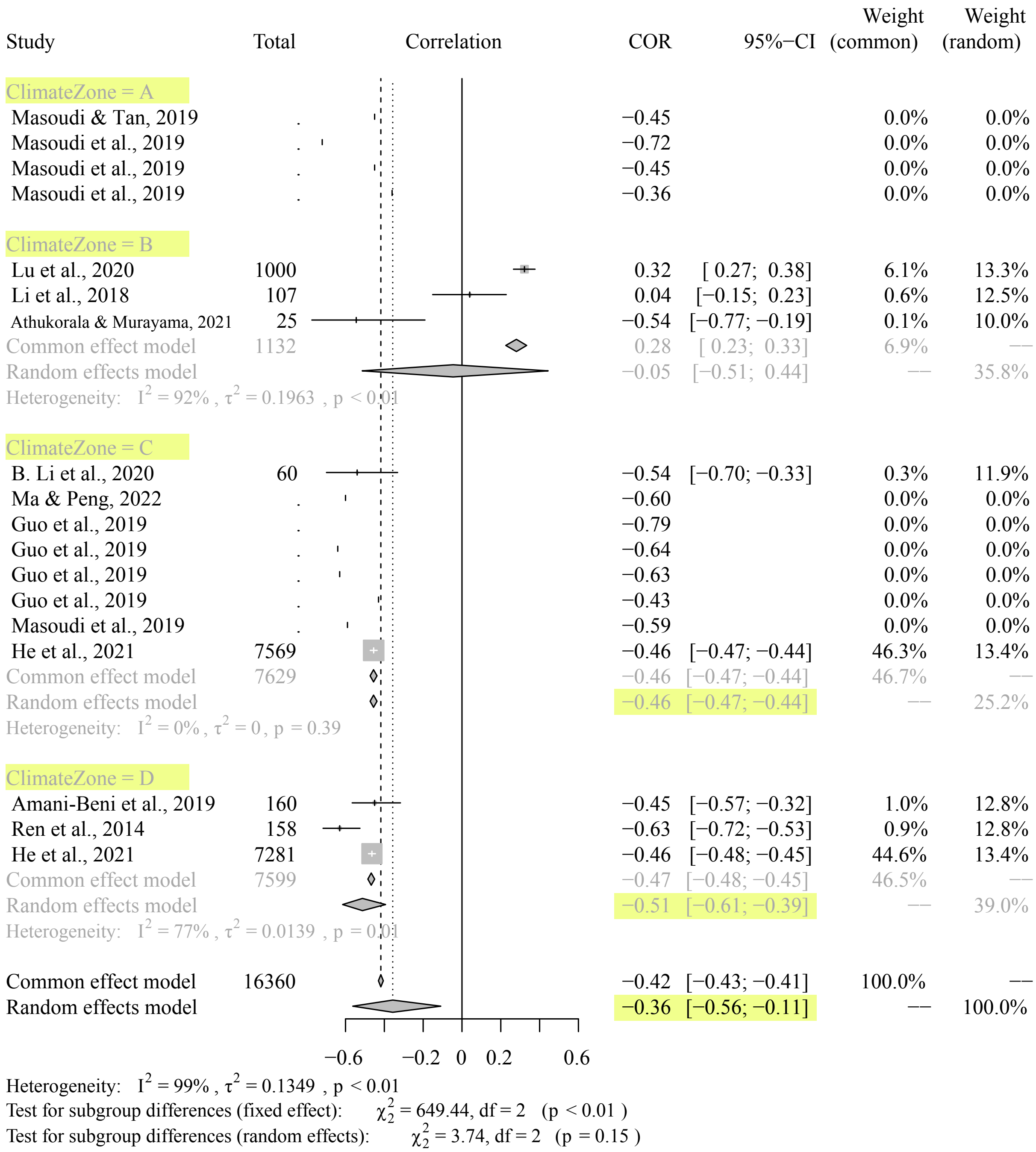

Fig. D11 Forest plot of Pearson correlation between class-level LPI of tree canopy coverage and mean LST

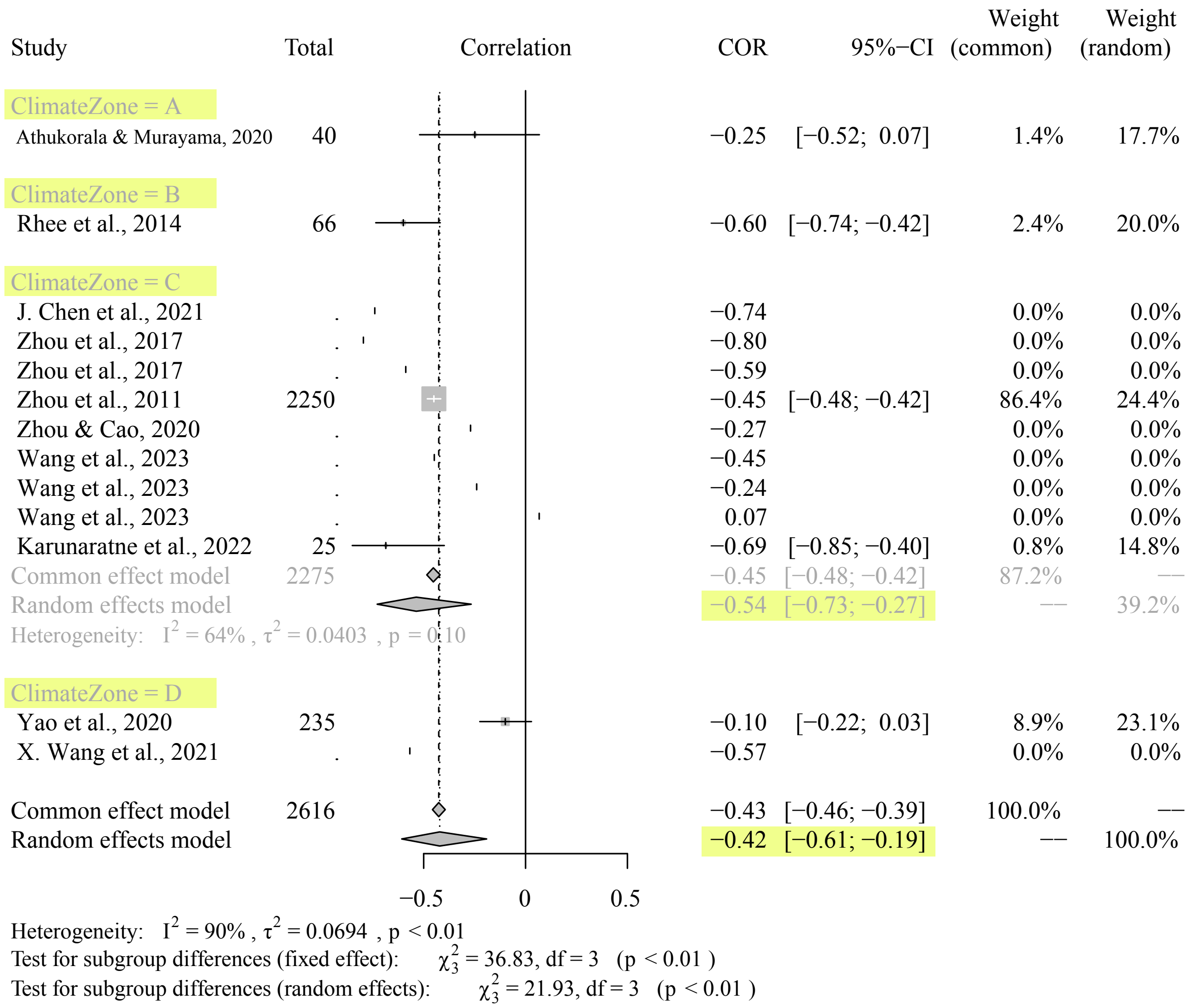

Fig. D12 Forest plot of Pearson correlation between class-level LPI of grassland coverage and mean LST

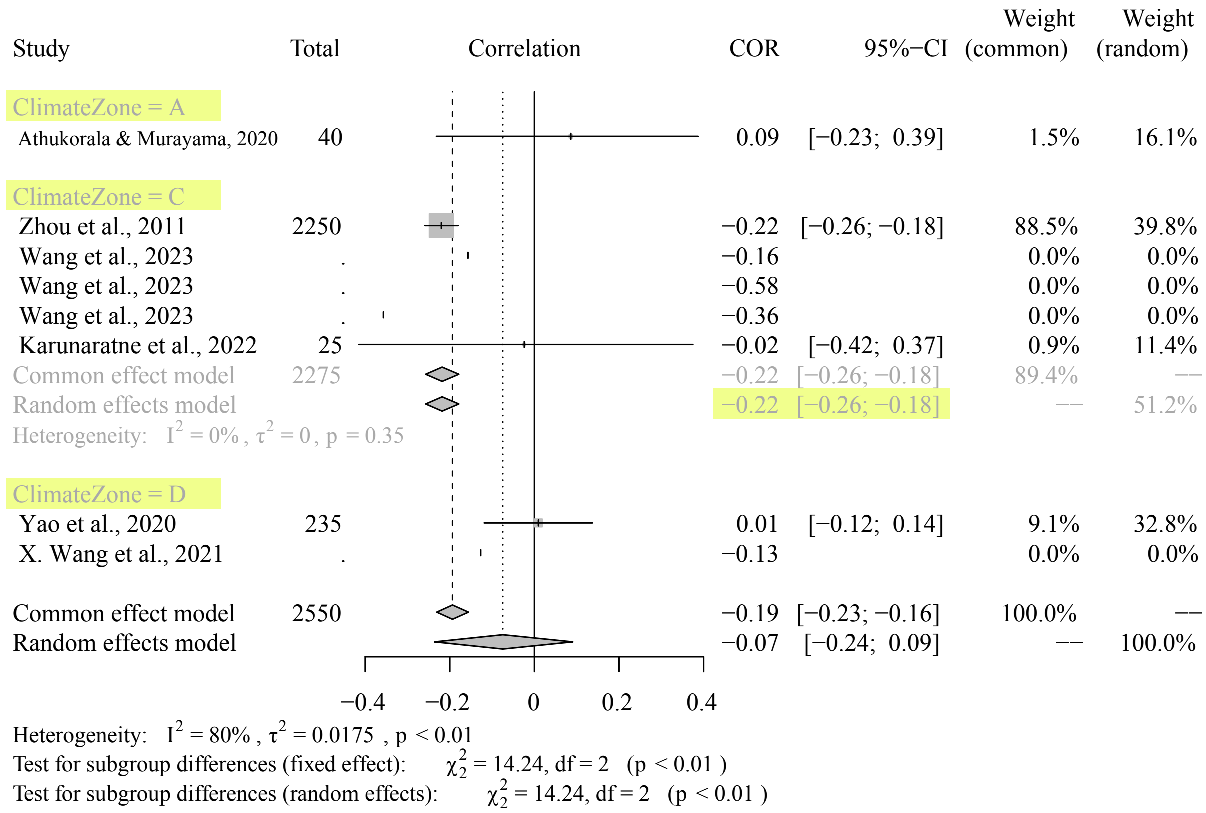

Fig. D13 Forest plot of Pearson correlation between class-level ED of urban vegetation coverage and mean LST

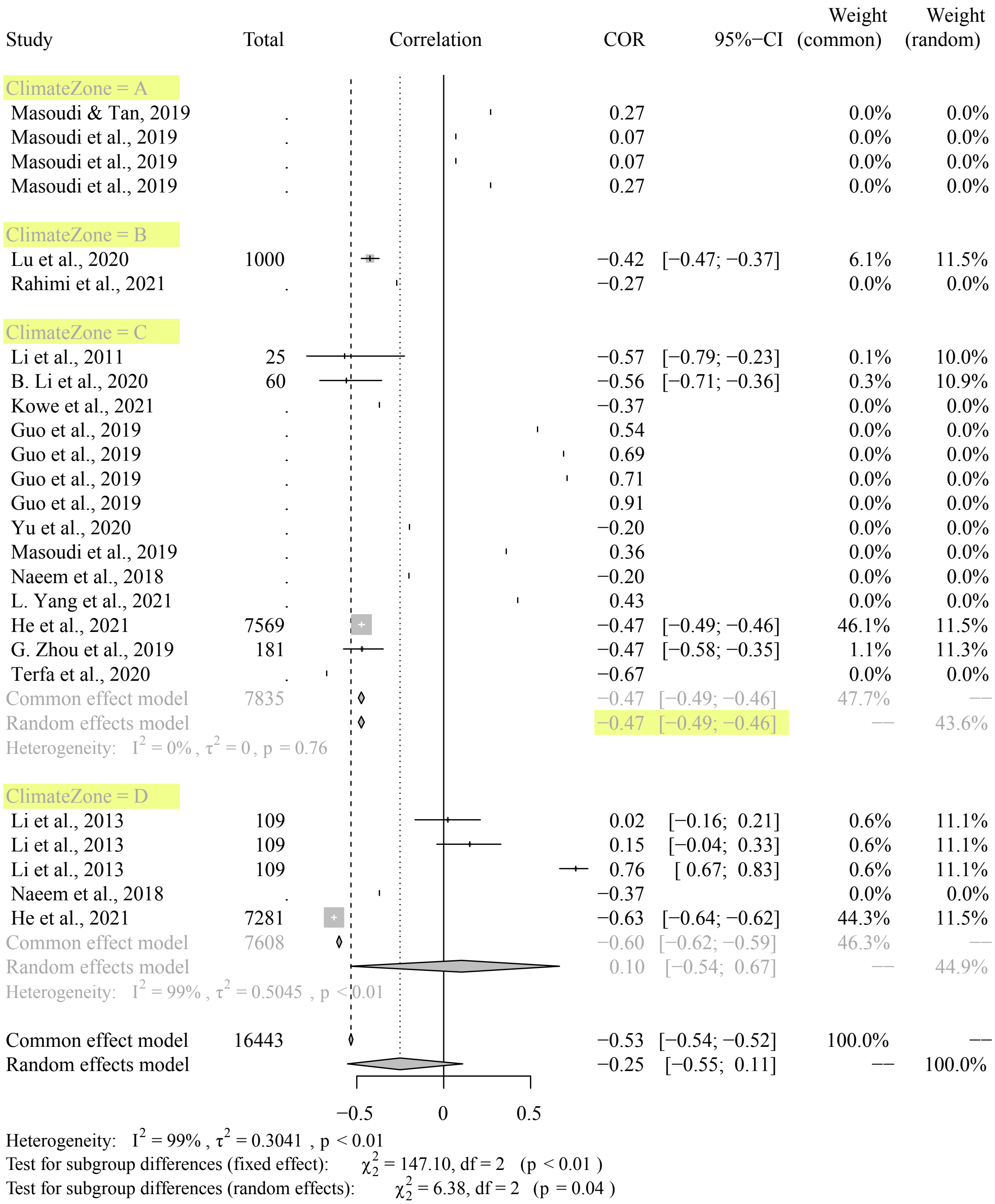

Fig. D14 Forest plot of Pearson correlation between class-level ED of tree canopy coverage and mean LST

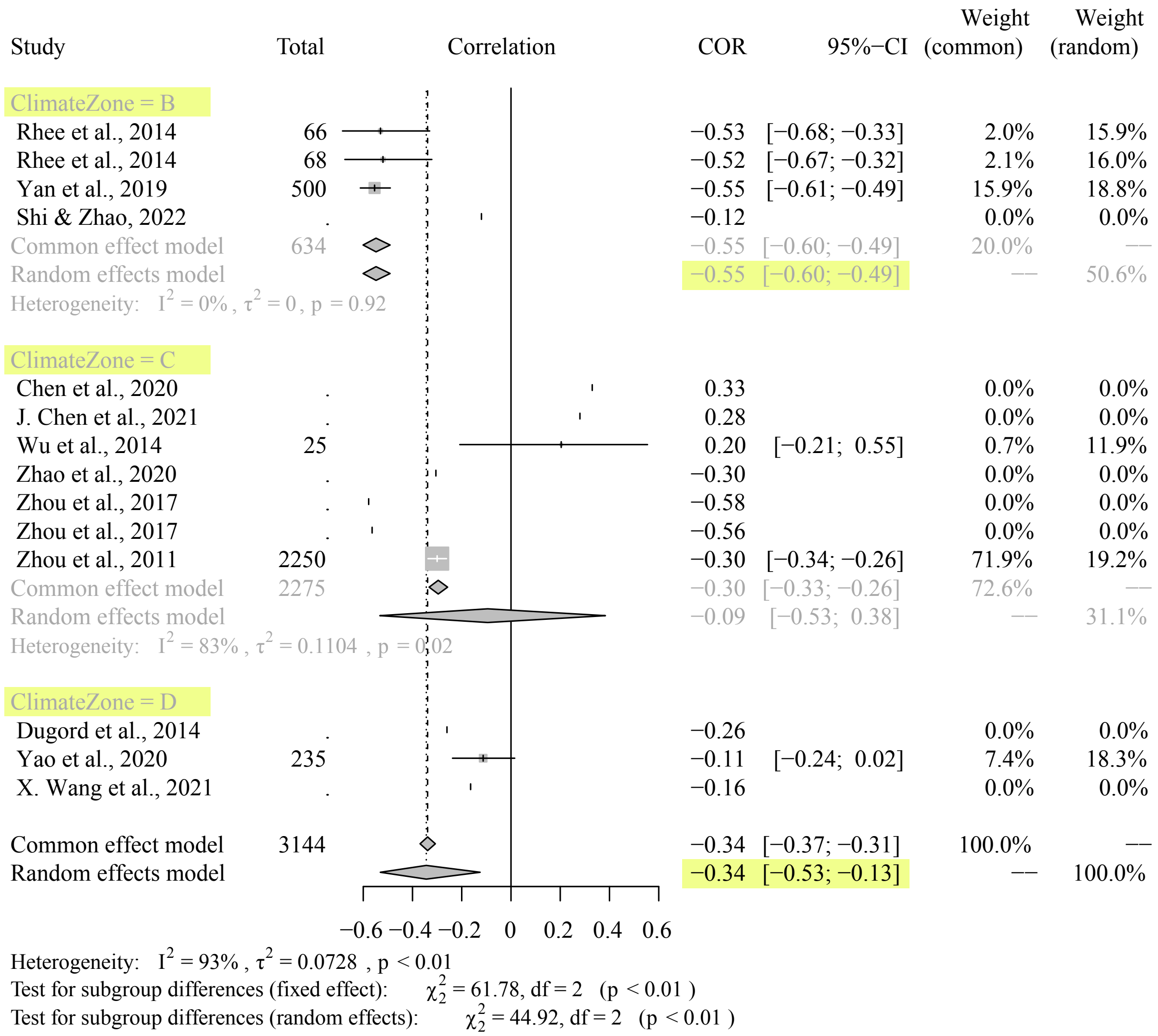

Fig. D15 Forest plot of Pearson correlation between class-level ED of grassland coverage and mean LST

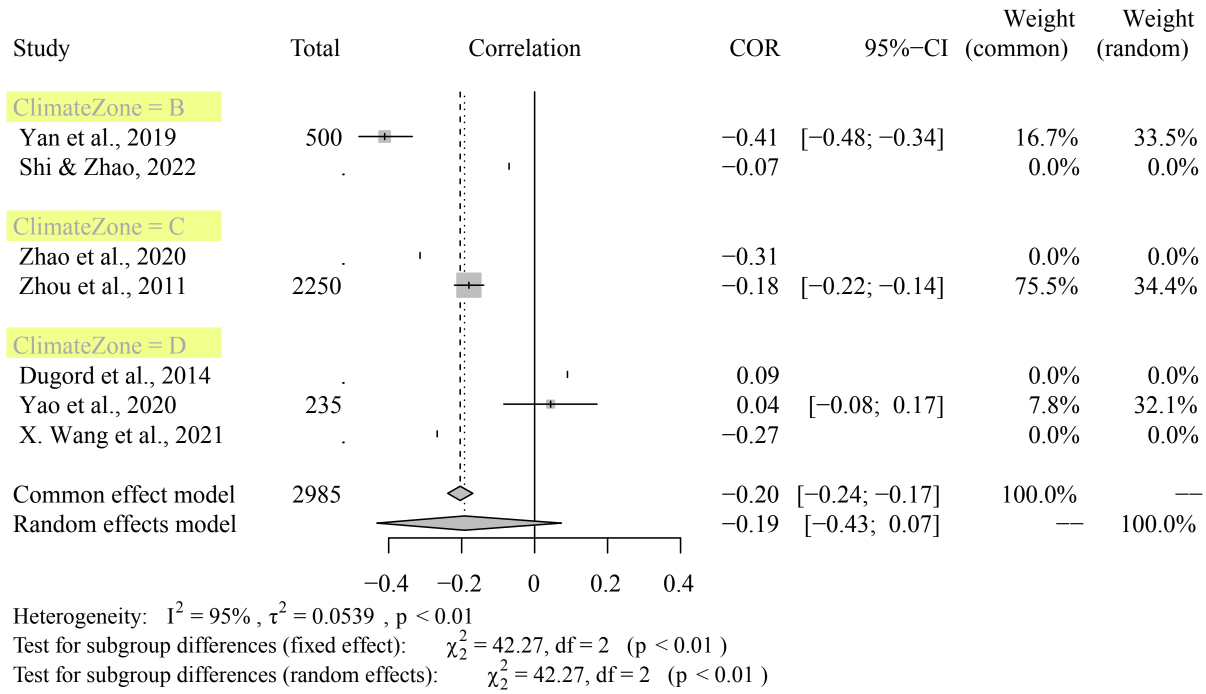

Fig. D16 Forest plot of Pearson correlation between class-level SHAPE_MN of urban vegetation coverage and mean LST

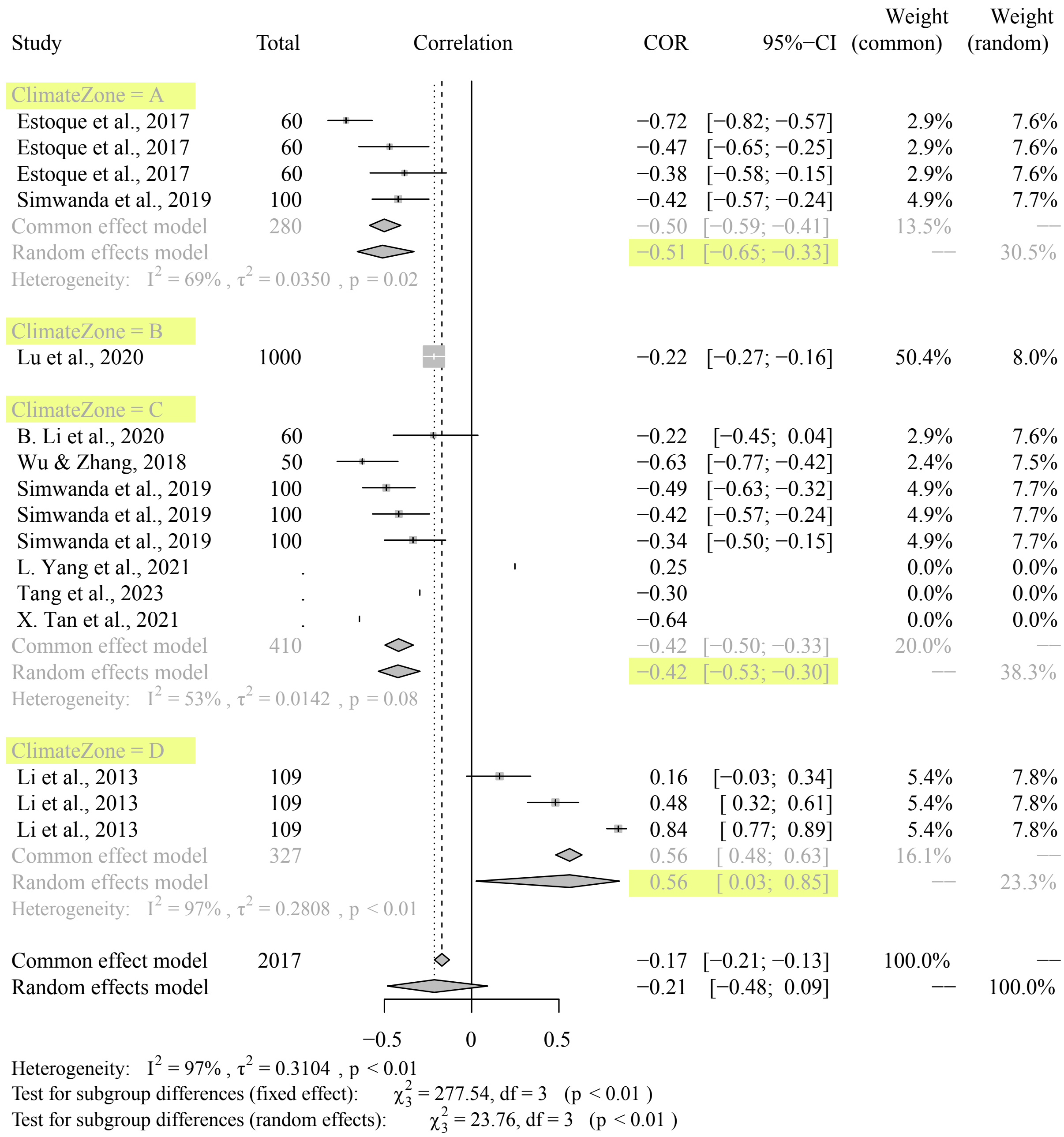

Fig. D17 Forest plot of Pearson correlation between class-level SHAPE_MN of tree canopy coverage and mean LST

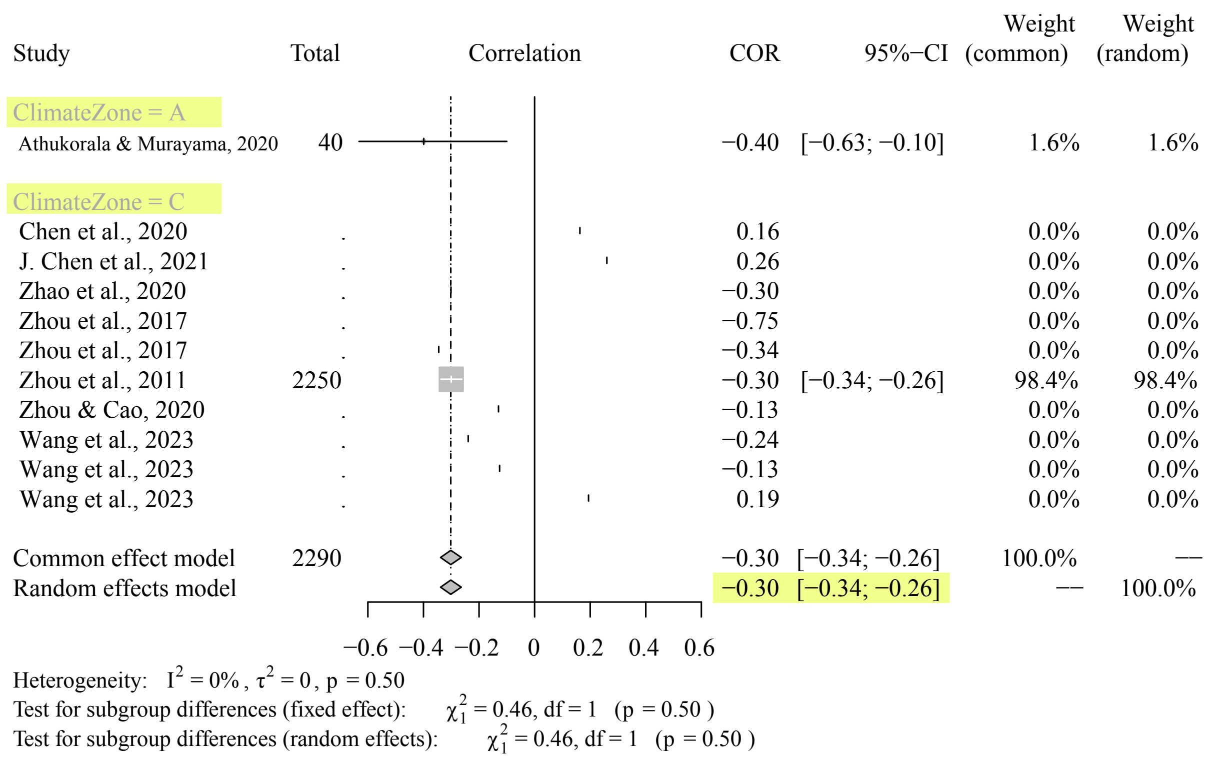

Fig. D18 Forest plot of Pearson correlation between class-level SHAPE_MN of grassland coverage and mean LST

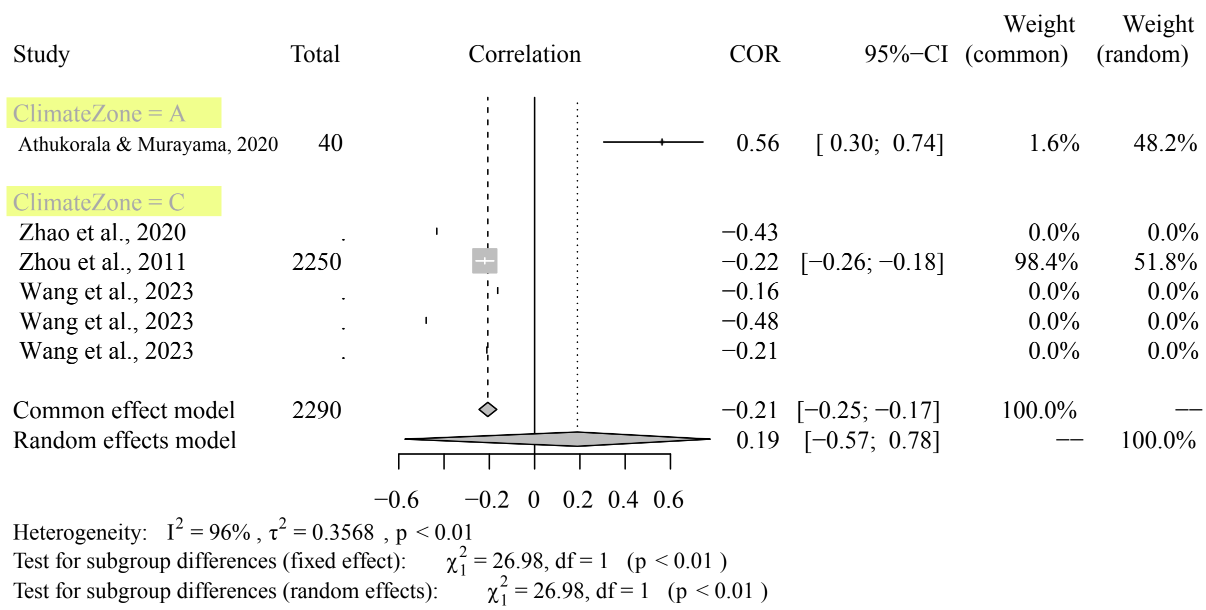

Fig. D19 Forest plot of Pearson correlation between class-level LSI of urban vegetation coverage and mean LST

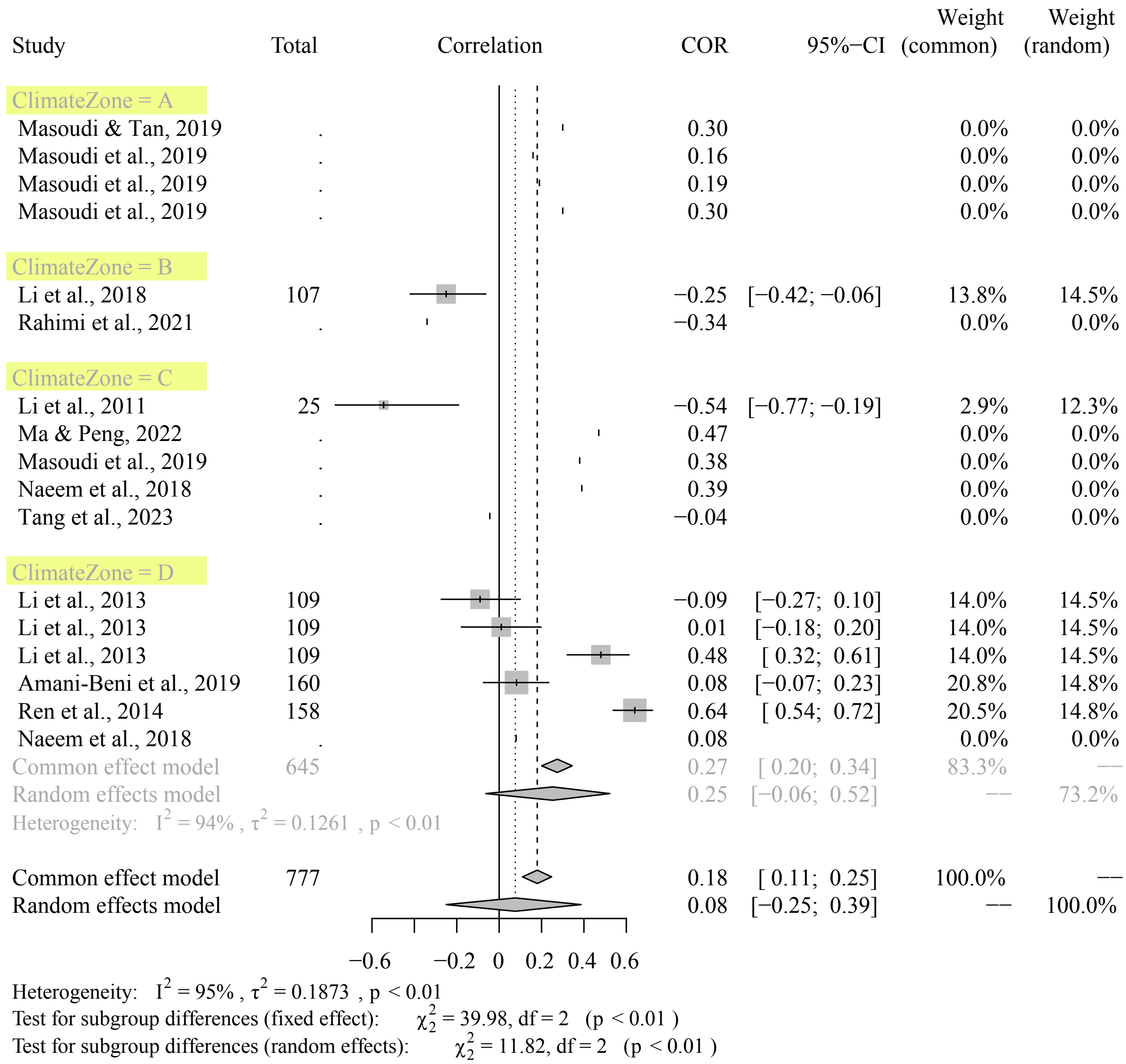

Fig. D20 Forest plot of Pearson correlation between class-level LSI of tree canopy coverage and mean LST

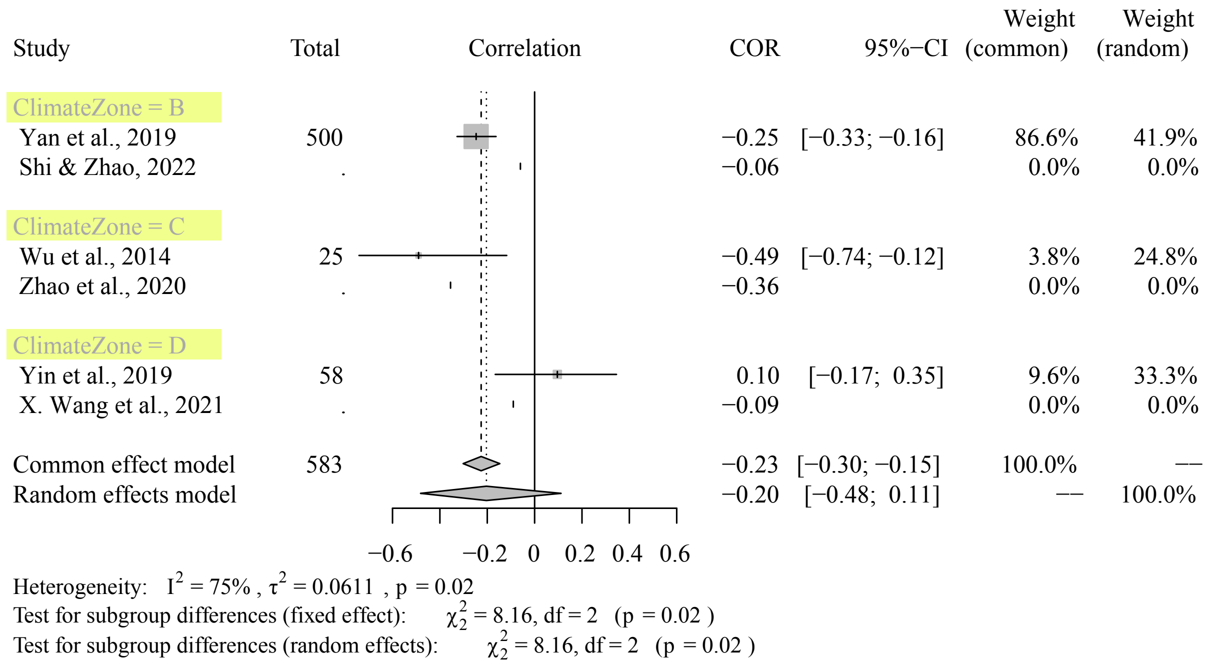

Fig. D21 Forest plot of Pearson correlation between class-level LSI of grassland coverage and mean LST

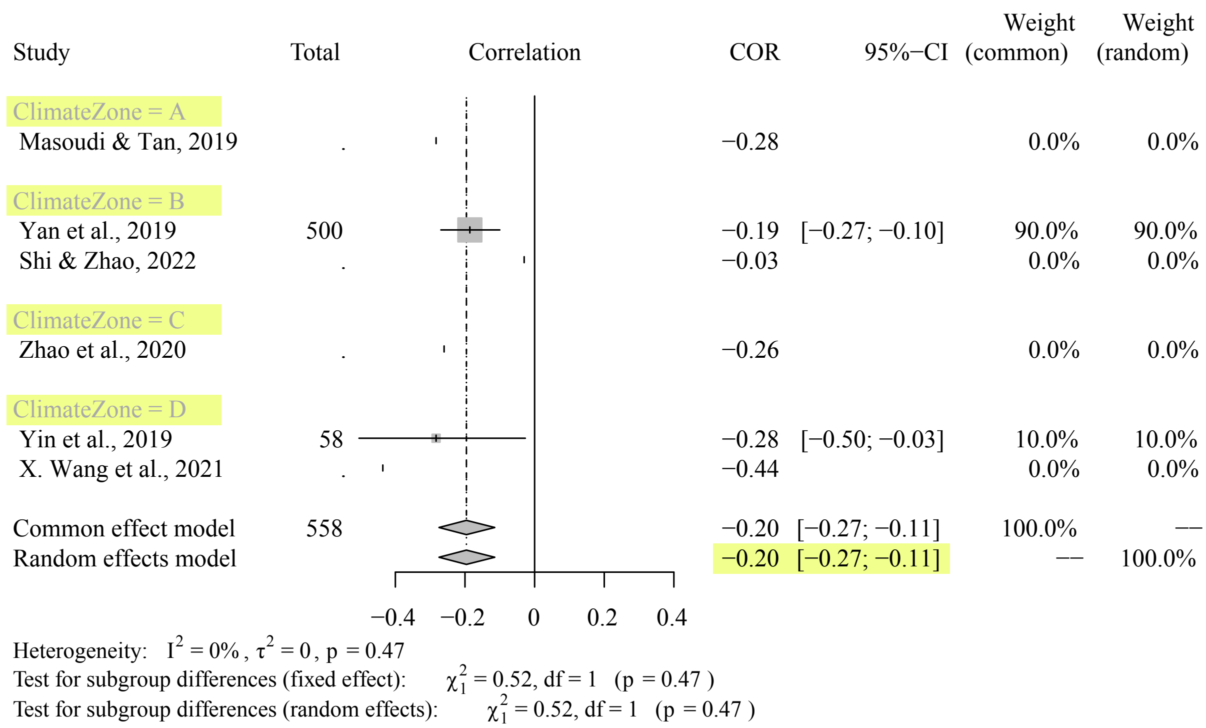

Fig. D22 Forest plot of Pearson correlation between class-level AI of urban vegetation coverage and mean LST

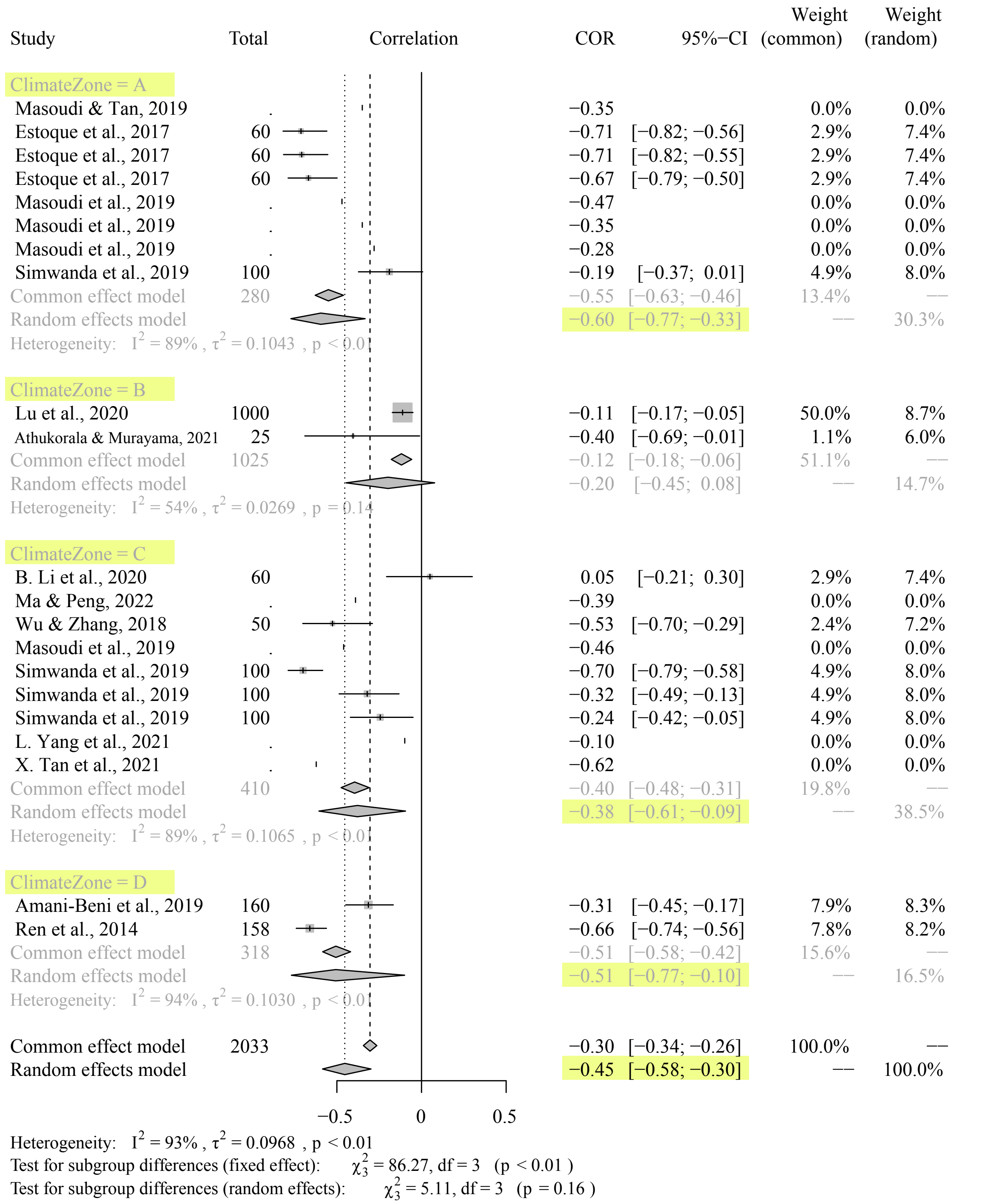

Fig. D23 Forest plot of Pearson correlation between class-level AI of tree canopy coverage and mean LST

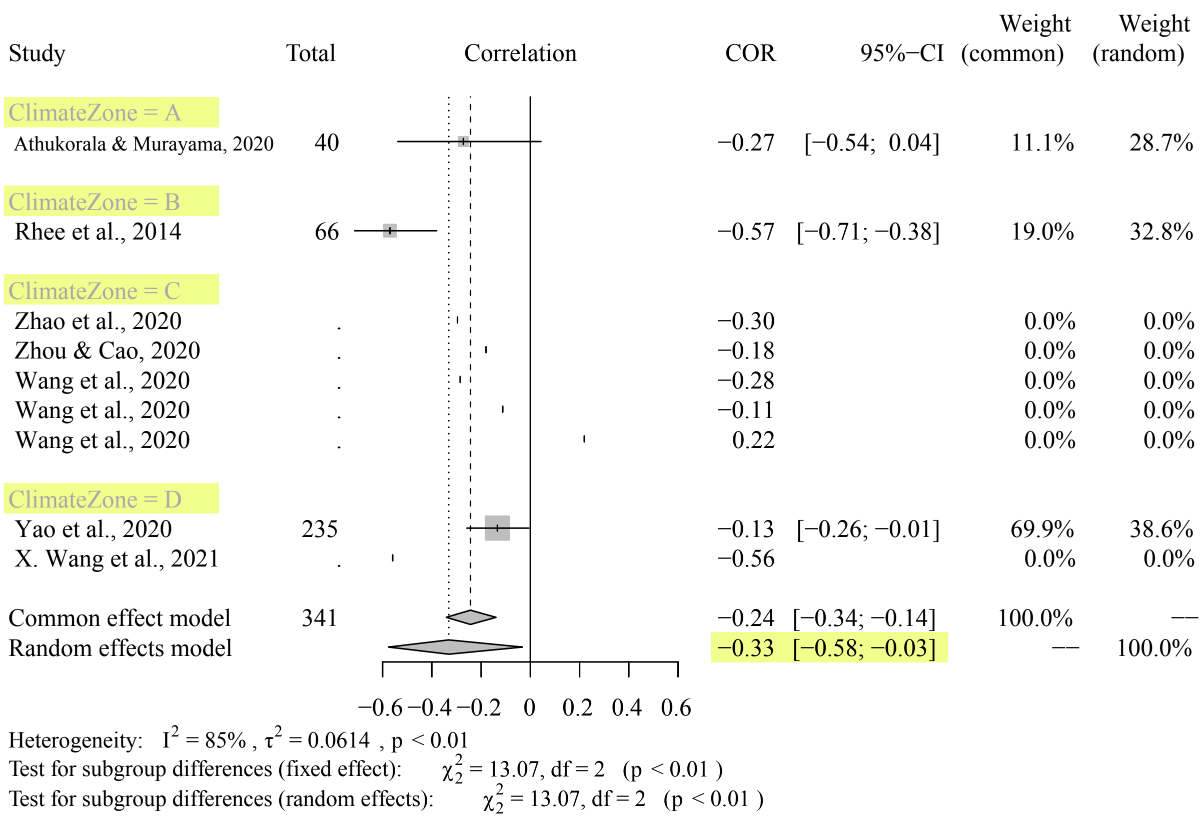

Fig. D24 Forest plot of Pearson correlation between class-level AI of grassland coverage and mean LST

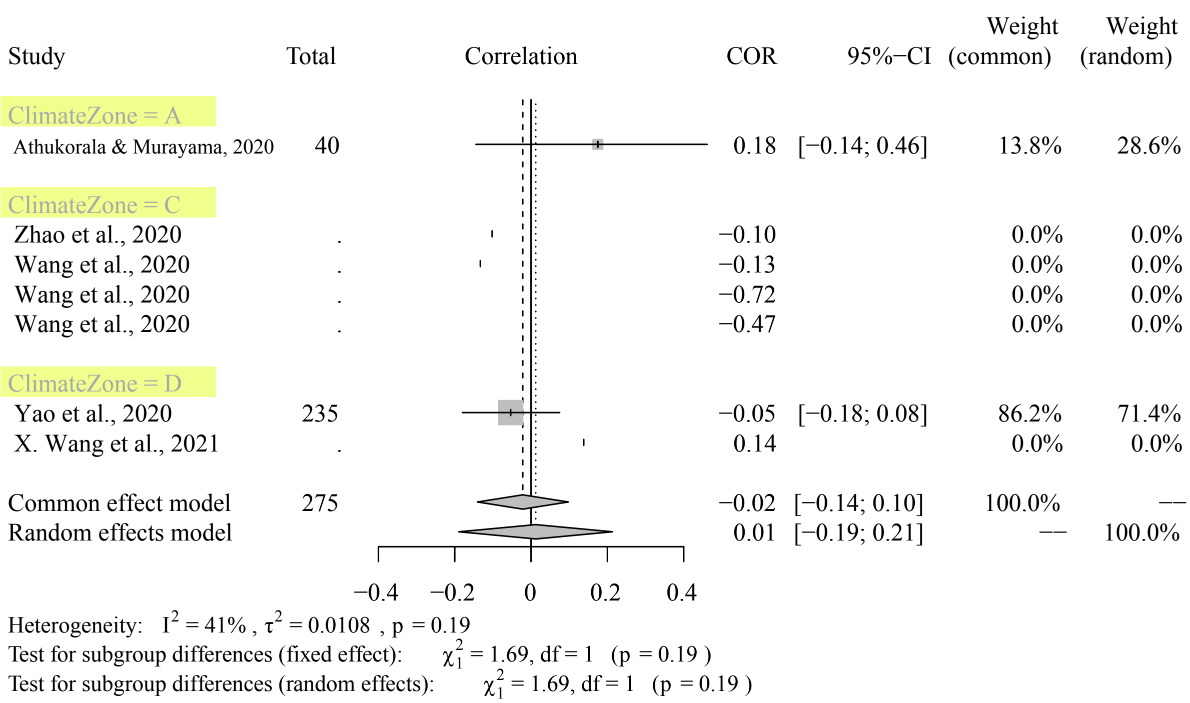

Fig. D25 Forest plot of Pearson correlation between class-level COHESION of urban vegetation coverage and mean LST

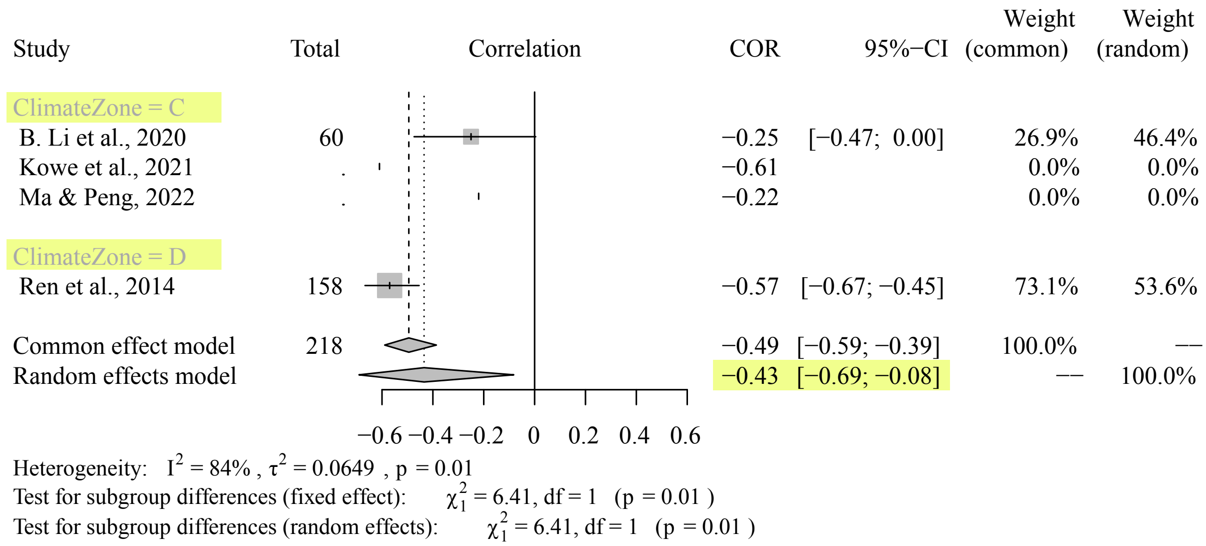

Fig. D26 Forest plot of Pearson correlation between class-level COHESION of tree canopy coverage and mean LST

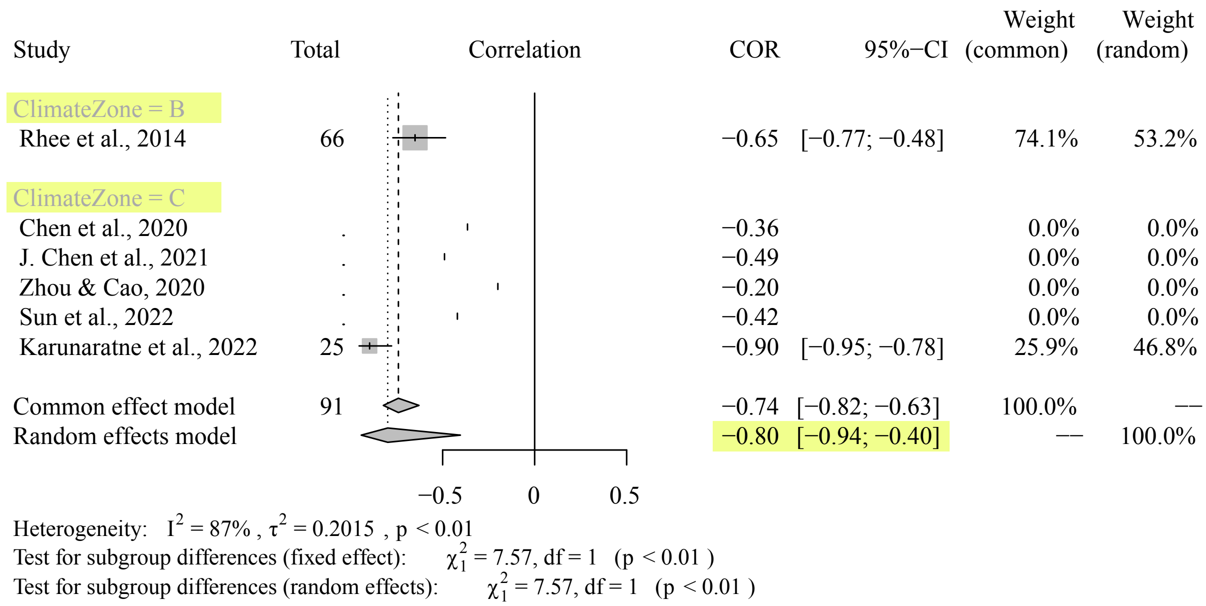

Fig. D27 Forest plot of Pearson correlation between class-level PD of urban vegetation coverage and mean LST

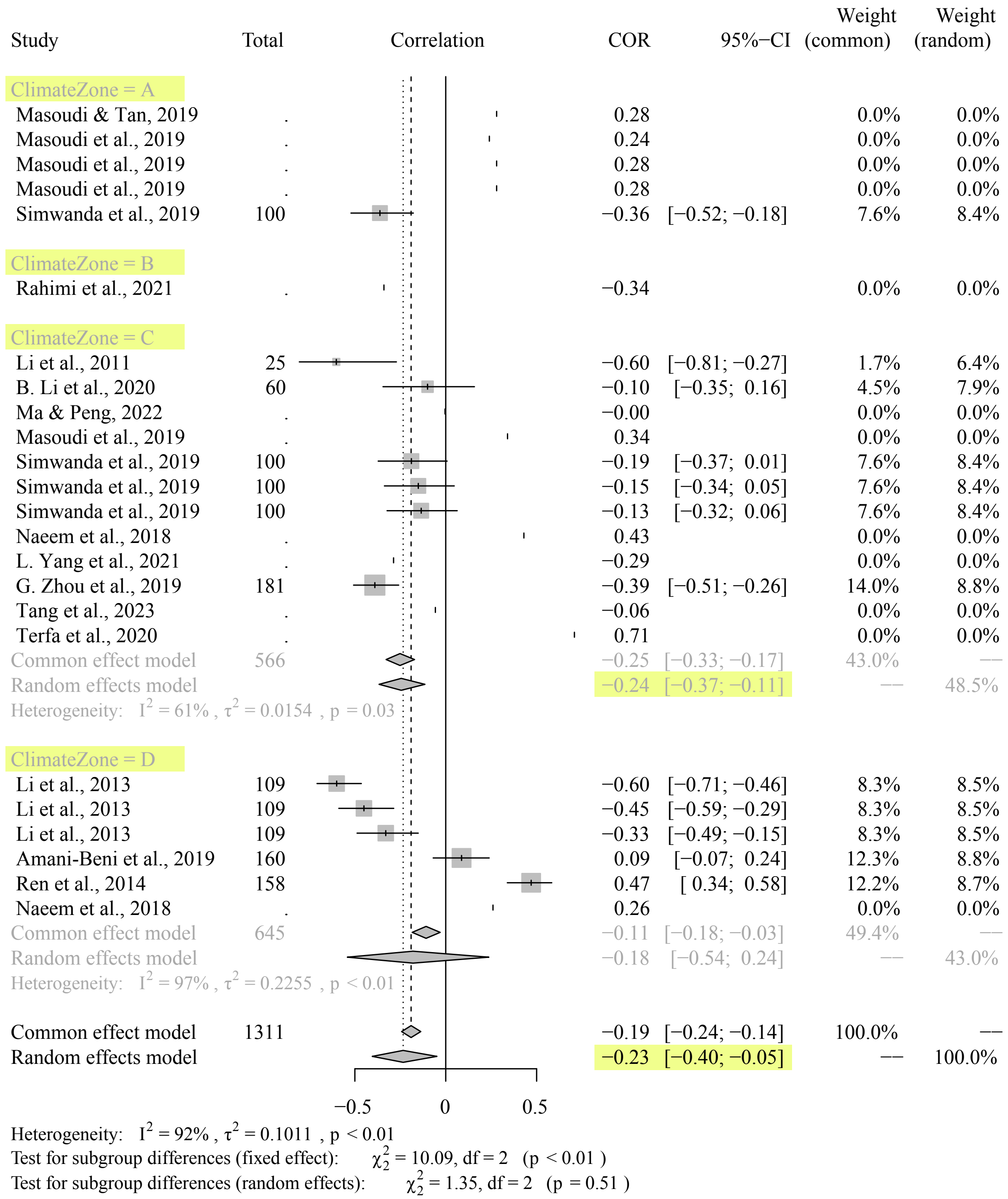

Fig. D28 Forest plot of Pearson correlation between class-level PD of tree canopy coverage and mean LST

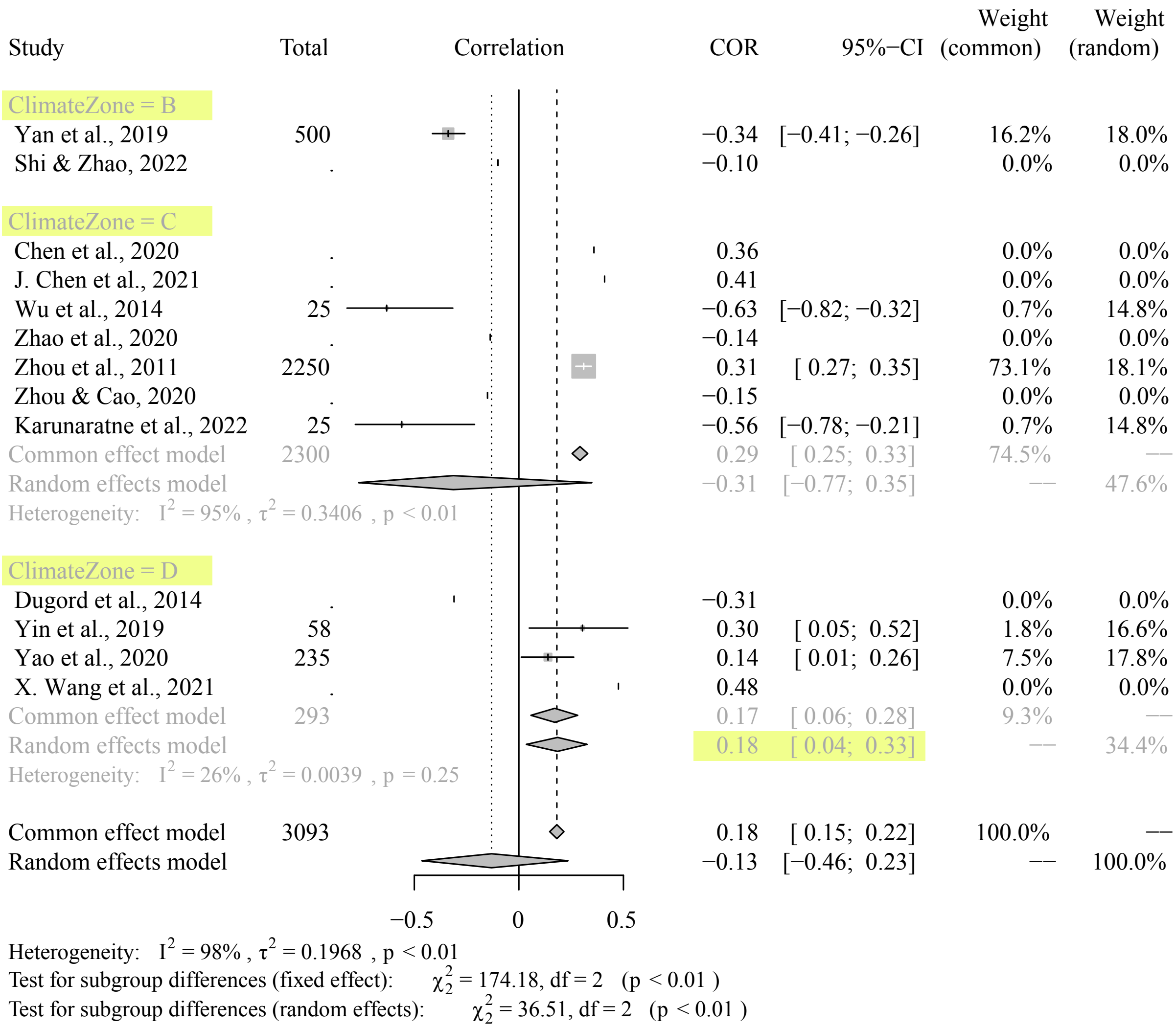

Fig. D29 Forest plot of Pearson correlation between class-level PD of grassland coverage and mean LST

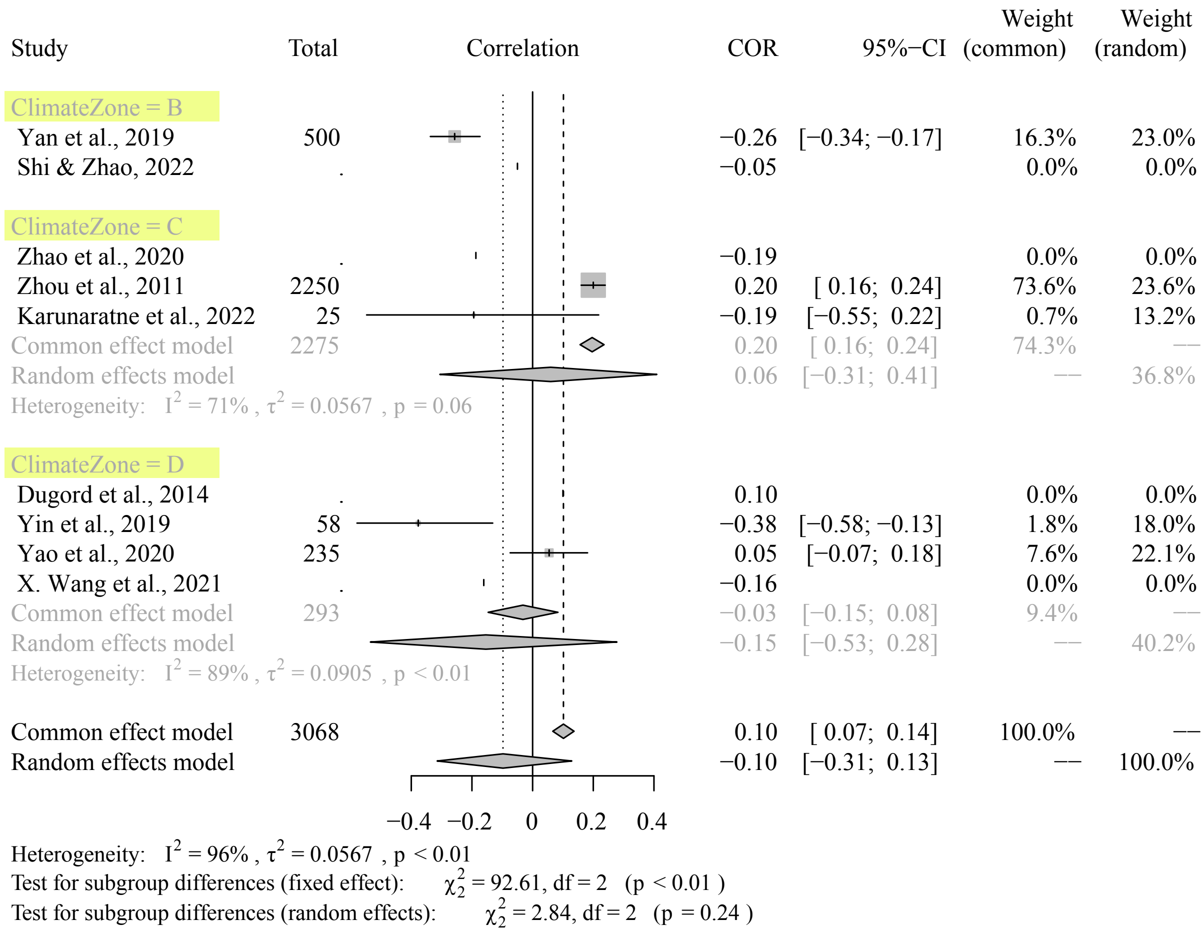

References

Amani-Beni, M., Zhang, B., Xie, G.-D., & Shi, Y. (2019). Impacts of Urban Green Landscape Patterns on Land Surface Temperature: Evidence from the Adjacent Area of Olympic Forest Park of Beijing, China. *Sustainability*, *11*(2). https://doi.org/10.3390/su11020513

An, H., Cai, H., Xu, X., Qiao, Z., & Han, D. (2022). Impacts of Urban Green Space on Land Surface Temperature from Urban Block Perspectives. *Remote Sensing*, *14*(18). https://doi.org/10.3390/rs14184580

Asgarian, A., Amiri, B. J., & Sakieh, Y. (2014). Assessing the effect of green cover spatial patterns on urban land surface temperature using landscape metrics approach. *Urban Ecosystems*, *18*(1), 209-222. https://doi.org/10.1007/s11252-014-0387-7

Athukorala, D., & Murayama, Y. (2020). Spatial Variation of Land Use/Cover Composition and Impact on Surface Urban Heat Island in a Tropical Sub-Saharan City of Accra, Ghana. *Sustainability*, *12*(19). https://doi.org/10.3390/su12197953

Athukorala, D., & Murayama, Y. (2021). Urban Heat Island Formation in Greater Cairo: Spatio-Temporal Analysis of Daytime and Nighttime Land Surface Temperatures along the Urban–Rural Gradient. *Remote Sensing*, *13*(7). https://doi.org/10.3390/rs13071396

Bao, T., Li, X., Zhang, J., Zhang, Y., & Tian, S. (2016). Assessing the Distribution of Urban Green Spaces and its Anisotropic Cooling Distance on Urban Heat Island Pattern in Baotou, China. *ISPRS International Journal of Geo-Information*, *5*(2). https://doi.org/10.3390/ijgi5020012

Bartesaghi-Koc, C., Osmond, P., & Peters, A. (2020). Quantifying the seasonal cooling capacity of 'green infrastructure types' (GITs): An approach to assess and mitigate surface urban heat island in Sydney, Australia. *Landscape and Urban Planning*, *203*. https://doi.org/10.1016/j.landurbplan.2020.103893

Bera, D., Das Chatterjee, N., Mumtaz, F., Dinda, S., Ghosh, S., Zhao, N., Bera, S., & Tariq, A. (2022). Integrated Influencing Mechanism of Potential Drivers on Seasonal Variability of LST in Kolkata Municipal Corporation, India. *Land*, *11*(9). https://doi.org/10.3390/land11091461

Cai, Y.-B., Wu, Z.-J., Chen, Y.-H., Wu, L., & Pan, W.-B. (2022). Investigate the Difference of Cooling Effect between Water Bodies and Green Spaces: The Study of Fuzhou, China. *Water*, *14*(9). https://doi.org/10.3390/w14091471

Cao, X., Onishi, A., Chen, J., & Imura, H. (2010). Quantifying the cool island intensity of urban parks using ASTER and IKONOS data. *Landscape and Urban Planning*, *96*(4), 224-231. https://doi.org/10.1016/j.landurbplan.2010.03.008

Chakraborti, S., Banerjee, A., Sannigrahi, S., Pramanik, S., Maiti, A., & Jha, S. (2019). Assessing the dynamic relationship among land use pattern and land surface temperature: A spatial regression approach. *Asian Geographer*, *36*(2), 93-116. https://doi.org/10.1080/10225706.2019.1623054

Chen, A., Yao, L., Sun, R., & Chen, L. (2014a). How many metrics are required to identify the effects of the landscape pattern on land surface temperature? *Ecological Indicators*, *45*, 424-433. https://doi.org/10.1016/j.ecolind.2014.05.002

Chen, A., Yao, X. A., Sun, R., & Chen, L. (2014b). Effect of urban green patterns on surface urban cool islands and its seasonal variations. *Urban Forestry & Urban Greening*, *13*(4), 646-654. https://doi.org/10.1016/j.ufug.2014.07.006

Chen, D., Zhang, F., Zhang, M., Meng, Q., Jim, C. Y., Shi, J., Tan, M. L., & Ma, X. (2022). Landscape and vegetation traits of urban green space can predict local surface temperature. *Sci Total Environ*, *825*, 154006. https://doi.org/10.1016/j.scitotenv.2022.154006

Chen, J., Du, P., Jin, S., Ding, H., Chen, C., Xu, Y., Feng, L., Guo, G., Zheng, H., & Huang, M. (2022). Unravelling the multilevel and multi-dimensional impacts of building and tree on surface urban heat islands. *Energy and Buildings*, *259*. https://doi.org/10.1016/j.enbuild.2022.111843

Chen, J., Jin, S., & Du, P. (2020). Roles of horizontal and vertical tree canopy structure in mitigating daytime and nighttime urban heat island effects. *International Journal of Applied Earth Observation and Geoinformation*, *89*. https://doi.org/10.1016/j.jag.2020.102060

Chen, J., Zhan, W., Du, P., Li, L., Li, J., Liu, Z., Huang, F., Lai, J., & Xia, J. (2022). Seasonally disparate responses of surface thermal environment to 2D/3D urban morphology. *Building and Environment*, *214*. https://doi.org/10.1016/j.buildenv.2022.108928

Chen, J., Zhan, W., Jin, S., Han, W., Du, P., Xia, J., Lai, J., Li, J., Liu, Z., Li, L., Huang, F., & Ding, H. (2021). Separate and combined impacts of building and tree on urban thermal environment from two- and three-dimensional perspectives. *Building and Environment*, *194*. https://doi.org/10.1016/j.buildenv.2021.107650

Chen, X., Wang, Z., & Bao, Y. (2021). Cool island effects of urban remnant natural mountains for cooling communities: A case study of Guiyang, China. *Sustainable Cities and Society*, *71*. https://doi.org/10.1016/j.scs.2021.102983

Chen, X., Wang, Z., Bao, Y., Luo, Q., & Wei, W. (2022). Combined impacts of buildings and urban remnant mountains on thermal environment in multi-mountainous city. *Sustainable Cities and Society*, *87*. https://doi.org/10.1016/j.scs.2022.104247

Cheng, X., Wei, B., Chen, G., Li, J., & Song, C. (2015). Influence of Park Size and Its Surrounding Urban Landscape Patterns on the Park Cooling Effect. *Journal of Urban Planning and Development*, *141*(3). https://doi.org/10.1061/(asce)up.1943-5444.0000256

Connors, J. P., Galletti, C. S., & Chow, W. T. L. (2012). Landscape configuration and urban heat island effects: assessing the relationship between landscape characteristics and land surface temperature in Phoenix, Arizona. *Landscape Ecology*, *28*(2), 271-283. https://doi.org/10.1007/s10980-012-9833-1

Das, D. N., Chakraborti, S., Saha, G., Banerjee, A., & Singh, D. (2020). Analysing the dynamic relationship of land surface temperature and landuse pattern: A city level analysis of two climatic regions in India. *City and Environment Interactions*, *8*. https://doi.org/10.1016/j.cacint.2020.100046

Du, C., Jia, W., Chen, M., Yan, L., & Wang, K. (2022). How can urban parks be planned to maximize cooling effect in hot extremes? Linking maximum and accumulative perspectives. *J Environ Manage*, *317*, 115346. https://doi.org/10.1016/j.jenvman.2022.115346

Du, H., Cai, W., Xu, Y., Wang, Z., Wang, Y., & Cai, Y. (2017). Quantifying the cool island effects of urban green spaces using remote sensing Data. *Urban Forestry & Urban Greening*, *27*, 24-31. https://doi.org/10.1016/j.ufug.2017.06.008

Du, H., Zhou, F., Cai, W., Cai, Y., & Xu, Y. (2021). Thermal and Humidity Effect of Urban Green Spaces with Different Shapes: A Case Study of Shanghai, China. *Int J Environ Res Public Health*, *18*(11). https://doi.org/10.3390/ijerph18115941

Du, S., Xiong, Z., Wang, Y.-C., & Guo, L. (2016). Quantifying the multilevel effects of landscape composition and configuration on land surface temperature. *Remote Sensing of Environment*, *178*, 84-92. https://doi.org/10.1016/j.rse.2016.02.063

Dugord, P.-A., Lauf, S., Schuster, C., & Kleinschmit, B. (2014). Land use patterns, temperature distribution, and potential heat stress risk – The case study Berlin, Germany. *Computers, Environment and Urban Systems*, *48*, 86-98. https://doi.org/10.1016/j.compenvurbsys.2014.07.005

Ekwe, M. C., Adamu, F., Gana, J., Nwafor, G. C., Usman, R., Nom, J., Onu, O. D., Adedeji, O. I., Halilu, S. A., & Aderoju, O. M. (2020). The effect of green spaces on the urban thermal environment during a hot-dry season: a case study of Port Harcourt, Nigeria. *Environment, Development and Sustainability*, *23*(7), 10056-10079. https://doi.org/10.1007/s10668-020-01046-9

Estoque, R. C., Murayama, Y., & Myint, S. W. (2017). Effects of landscape composition and pattern on land surface temperature: An urban heat island study in the megacities of Southeast Asia. *Sci Total Environ*, *577*, 349-359. https://doi.org/10.1016/j.scitotenv.2016.10.195

Fan, H., Yu, Z., Yang, G., Liu, T. Y., Liu, T. Y., Hung, C. H., & Vejre, H. (2019). How to cool hot-humid (Asian) cities with urban trees? An optimal landscape size perspective. *Agricultural and Forest Meteorology*, *265*, 338-348. https://doi.org/10.1016/j.agrformet.2018.11.027

Feng, L., Zhao, M., Zhou, Y., Zhu, L., & Tian, H. (2020). The seasonal and annual impacts of landscape patterns on the urban thermal comfort using Landsat. *Ecological Indicators*, *110*. https://doi.org/10.1016/j.ecolind.2019.105798

Feng, X., & Myint, S. W. (2016). Exploring the effect of neighboring land cover pattern on land surface temperature of central building objects. *Building and Environment*, *95*, 346-354. https://doi.org/10.1016/j.buildenv.2015.09.019

Feyisa, G. L., Dons, K., & Meilby, H. (2014). Efficiency of parks in mitigating urban heat island effect: An example from Addis Ababa. *Landscape and Urban Planning*, *123*, 87-95. https://doi.org/10.1016/j.landurbplan.2013.12.008

Gage, E. A., & Cooper, D. J. (2017). Relationships between landscape pattern metrics, vertical structure and surface urban Heat Island formation in a Colorado suburb. *Urban Ecosystems*, *20*(6), 1229-1238. https://doi.org/10.1007/s11252-017-0675-0

Galletti, C. S., Li, X., & Connors, J. P. (2019). Establishing the relationship between urban land-cover configuration and night time land-surface temperature using spatial regression. *International Journal of Remote Sensing*, *40*(17), 6752-6774. https://doi.org/10.1080/01431161.2019.1594432

Gao, Z., Zaitchik, B. F., Hou, Y., & Chen, W. (2022). Toward park design optimization to mitigate the urban heat Island: Assessment of the cooling effect in five U.S. cities. *Sustainable Cities and Society*, *81*. https://doi.org/10.1016/j.scs.2022.103870

Greene, C. S., & Kedron, P. J. (2018). Beyond fractional coverage: A multilevel approach to analyzing the impact of urban tree canopy structure on surface urban heat islands. *Applied Geography*, *95*, 45-53. https://doi.org/10.1016/j.apgeog.2018.04.004

Guo, A., Yang, J., Sun, W., Xiao, X., Xia Cecilia, J., Jin, C., & Li, X. (2020). Impact of urban morphology and landscape characteristics on spatiotemporal heterogeneity of land surface temperature. *Sustainable Cities and Society*, *63*. https://doi.org/10.1016/j.scs.2020.102443

Guo, G., Wu, Z., Cao, Z., Chen, Y., & Yang, Z. (2020). A multilevel statistical technique to identify the dominant landscape metrics of greenspace for determining land surface temperature. *Sustainable Cities and Society*, *61*. https://doi.org/10.1016/j.scs.2020.102263

Guo, G., Wu, Z., Cao, Z., Chen, Y., & Zheng, Z. (2021). Location of greenspace matters: a new approach to investigating the effect of the greenspace spatial pattern on urban heat environment. *Landscape Ecology*, *36*(5), 1533-1548. https://doi.org/10.1007/s10980-021-01230-w

Guo, G., Wu, Z., & Chen, Y. (2019). Complex mechanisms linking land surface temperature to greenspace spatial patterns: Evidence from four southeastern Chinese cities. *Sci Total Environ*, *674*, 77-87. https://doi.org/10.1016/j.scitotenv.2019.03.402

He, C., Zhou, L., Yao, Y., Ma, W., & Kinney, P. L. (2021). Cooling effect of urban trees and its spatiotemporal characteristics: A comparative study. *Building and Environment*, *204*. https://doi.org/10.1016/j.buildenv.2021.108103

Hou, H., & Estoque, R. C. (2020). Detecting Cooling Effect of Landscape from Composition and Configuration: An Urban Heat Island Study on Hangzhou. *Urban Forestry & Urban Greening*, *53*. https://doi.org/10.1016/j.ufug.2020.126719

Hu, Y., Dai, Z., & Guldmann, J. M. (2021). Greenspace configuration impact on the urban heat island in the Olympic Area of Beijing. *Environ Sci Pollut Res Int*. https://doi.org/10.1007/s11356-020-12086-z

Huang, M., Cui, P., & He, X. (2018). Study of the Cooling Effects of Urban Green Space in Harbin in Terms of Reducing the Heat Island Effect. *Sustainability*, *10*(4). https://doi.org/10.3390/su10041101

Huang, R., Yang, M., Lin, G., Ma, X., Wang, X., Huang, Q., & Zhang, T. (2022). Cooling Effect of Green Space and Water on Urban Heat Island and the Perception of Residents: A Case Study of Xi'an City. *Int J Environ Res Public Health*, *19*(22). https://doi.org/10.3390/ijerph192214880

Huang, X., & Wang, Y. (2019). Investigating the effects of 3D urban morphology on the surface urban heat island effect in urban functional zones by using high-resolution remote sensing data: A case study of Wuhan, Central China. *ISPRS Journal of Photogrammetry and Remote Sensing*, *152*, 119-131. https://doi.org/10.1016/j.isprsjprs.2019.04.010

Jaganmohan, M., Knapp, S., Buchmann, C. M., & Schwarz, N. (2016). The Bigger, the Better? The Influence of Urban Green Space Design on Cooling Effects for Residential Areas. *J Environ Qual*, *45*(1), 134-145. https://doi.org/10.2134/jeq2015.01.0062

Kamarianakis, Y., Li, X., Turner, B. L., & Brazel, A. J. (2017). On the effects of landscape configuration on summer diurnal temperatures in urban residential areas: application in Phoenix, AZ. *Frontiers of Earth Science*, *13*(3), 445-463. https://doi.org/10.1007/s11707-017-0678-4

Karunaratne, S., Athukorala, D., Murayama, Y., & Morimoto, T. (2022). Assessing Surface Urban Heat Island Related to Land Use/Land Cover Composition and Pattern in the Temperate Mountain Valley City of Kathmandu, Nepal. *Remote Sensing*, *14*(16). https://doi.org/10.3390/rs14164047

Ke, X., Men, H., Zhou, T., Li, Z., & Zhu, F. (2021). Variance of the impact of urban green space on the urban heat island effect among different urban functional zones: A case study in Wuhan. *Urban Forestry & Urban Greening*, *62*. https://doi.org/10.1016/j.ufug.2021.127159

Kim, J. H., Gu, D., Sohn, W., Kil, S. H., Kim, H., & Lee, D. K. (2016). Neighborhood Landscape Spatial Patterns and Land Surface Temperature: An Empirical Study on Single-Family Residential Areas in Austin, Texas. *Int J Environ Res Public Health*, *13*(9). https://doi.org/10.3390/ijerph13090880

Kong, F., Yin, H., James, P., Hutyra, L. R., & He, H. S. (2014). Effects of spatial pattern of greenspace on urban cooling in a large metropolitan area of eastern China. *Landscape and Urban Planning*, *128*, 35-47. https://doi.org/10.1016/j.landurbplan.2014.04.018

Kong, F., Yin, H., Wang, C., Cavan, G., & James, P. (2014). A satellite image-based analysis of factors contributing to the green-space cool island intensity on a city scale. *Urban Forestry & Urban Greening*, *13*(4), 846-853. https://doi.org/10.1016/j.ufug.2014.09.009

Kowe, P., Mutanga, O., Odindi, J., & Dube, T. (2021). Effect of landscape pattern and spatial configuration of vegetation patches on urban warming and cooling in Harare metropolitan city, Zimbabwe. *GIScience & Remote Sensing*, *58*(2), 261-280. https://doi.org/10.1080/15481603.2021.1877008

Lemoine-Rodríguez, R., Inostroza, L., Falfán, I., & MacGregor-Fors, I. (2022). Too hot to handle? On the cooling capacity of urban green spaces in a Neotropical Mexican city. *Urban Forestry & Urban Greening*, *74*. https://doi.org/10.1016/j.ufug.2022.127633

Li, B., Shi, X., Wang, H., & Qin, M. (2020). Analysis of the relationship between urban landscape patterns and thermal environment: a case study of Zhengzhou City, China. *Environ Monit Assess*, *192*(8), 540. https://doi.org/10.1007/s10661-020-08505-w

Li, B., Wang, W., Bai, L., Wang, W., & Chen, N. (2018). Effects of spatio-temporal landscape patterns on land surface temperature: a case study of Xi'an city, China. *Environ Monit Assess*, *190*(7), 419. https://doi.org/10.1007/s10661-018-6787-z

Li, C., Lu, L., Fu, Z., Sun, R., Pan, L., Han, L., Guo, H., & Li, Q. (2022). Diverse cooling effects of green space on urban heat island in tropical megacities. *Frontiers in Environmental Science*, *10*. https://doi.org/10.3389/fenvs.2022.1073914

Li, J., Song, C., Cao, L., Zhu, F., Meng, X., & Wu, J. (2011). Impacts of landscape structure on surface urban heat islands: A case study of Shanghai, China. *Remote Sensing of Environment*, *115*(12), 3249-3263. https://doi.org/10.1016/j.rse.2011.07.008

Li, T., Cao, J., Xu, M., Wu, Q., & Yao, L. (2020). The influence of urban spatial pattern on land surface temperature for different functional zones. *Landscape and Ecological Engineering*, *16*(3), 249-262. https://doi.org/10.1007/s11355-020-00417-8

Li, T., Xu, Y., & Yao, L. (2021). Detecting urban landscape factors controlling seasonal land surface temperature: from the perspective of urban function zones. *Environ Sci Pollut Res Int*, *28*(30), 41191-41206. https://doi.org/10.1007/s11356-021-13695-y

Li, X., Kamarianakis, Y., Ouyang, Y., Turner Ii, B. L., & Brazel, A. (2017). On the association between land system architecture and land surface temperatures: Evidence from a Desert Metropolis—Phoenix, Arizona, U.S.A. *Landscape and Urban Planning*, *163*, 107-120. https://doi.org/10.1016/j.landurbplan.2017.02.009

Li, X., Zhou, W., & Ouyang, Z. (2013). Relationship between land surface temperature and spatial pattern of greenspace: What are the effects of spatial resolution? *Landscape and Urban Planning*, *114*, 1-8. https://doi.org/10.1016/j.landurbplan.2013.02.005

Li, X., Zhou, W., Ouyang, Z., Xu, W., & Zheng, H. (2012). Spatial pattern of greenspace affects land surface temperature: evidence from the heavily urbanized Beijing metropolitan area, China. *Landscape Ecology*, *27*(6), 887-898. https://doi.org/10.1007/s10980-012-9731-6

Li, Y., Fan, S., Li, K., Zhang, Y., & Dong, L. (2020). Microclimate in an urban park and its influencing factors: a case study of Tiantan Park in Beijing, China. *Urban Ecosystems*, *24*(4), 767-778. https://doi.org/10.1007/s11252-020-01073-4

Li, Y., Fan, S., Li, K., Zhang, Y., Kong, L., Xie, Y., & Dong, L. (2021). Large urban parks summertime cool and wet island intensity and its influencing factors in Beijing, China. *Urban Forestry & Urban Greening*, *65*. https://doi.org/10.1016/j.ufug.2021.127375

Li, Z., Xie, C., Chen, D., Lu, H., & Che, S. (2019). Effects of Land Cover Patterns on Land Surface Temperatures Associated with Land Use Types along Urbanization Gradients in Shanghai, China. *Polish Journal of Environmental Studies*, *29*(1), 713-725. https://doi.org/10.15244/pjoes/99974

Liu, H., & Weng, Q. (2009). Scaling Effect on the Relationship between Landscape Pattern and Land Surface Temperature. *Photogrammetric Engineering & Remote Sensing*, *75*(3), 291-304. https://doi.org/10.14358/pers.75.3.291

Liu, H., & Weng, Q. H. (2009). Scaling Effect on the Relationship between Landscape Pattern and Land Surface Temperature: A Case Study of Indianapolis, United States. *Photogrammetric Engineering and Remote Sensing*, *75*(3), 291-304. https://doi.org/Doi 10.14358/Pers.75.3.291

Liu, J., Zhang, L., Zhang, Q., Zhang, G., & Teng, J. (2021). Predicting the surface urban heat island intensity of future urban green space development using a multi-scenario simulation. *Sustainable Cities and Society*, *66*. https://doi.org/10.1016/j.scs.2020.102698

Liu, K., Li, X., Wang, S., & Gao, X. (2022). Assessing the effects of urban green landscape on urban thermal environment dynamic in a semiarid city by integrated use of airborne data, satellite imagery and land surface model. *International Journal of Applied Earth Observation and Geoinformation*, *107*. https://doi.org/10.1016/j.jag.2021.102674

Liu, K., Su, H., Li, X., Wang, W., Yang, L., & Liang, H. (2016). Quantifying Spatial–Temporal Pattern of Urban Heat Island in Beijing: An Improved Assessment Using Land Surface Temperature (LST) Time Series Observations From LANDSAT, MODIS, and Chinese New Satellite GaoFen-1. *IEEE Journal of Selected Topics in Applied Earth Observations and Remote Sensing*, *9*(5), 2028-2042. https://doi.org/10.1109/jstars.2015.2513598

Liu, S., Li, X., Chen, L., Zhao, Q., Zhao, C., Hu, X., & Li, J. (2022). A New Approach to Investigate the Spatially Heterogeneous in the Cooling Effects of Landscape Pattern. *Land*, *11*(2). https://doi.org/10.3390/land11020239

Liu, W., Jia, B., Li, T., Zhang, Q., & Ma, J. (2022). Correlation Analysis between Urban Green Space and Land Surface Temperature from the Perspective of Spatial Heterogeneity: A Case Study within the Sixth Ring Road of Beijing. *Sustainability*, *14*(20). https://doi.org/10.3390/su142013492

Liu, W., Zhao, H., Sun, S., Xu, X., Huang, T., & Zhu, J. (2022). Green Space Cooling Effect and Contribution to Mitigate Heat Island Effect of Surrounding Communities in Beijing Metropolitan Area. *Front Public Health*, *10*, 870403. https://doi.org/10.3389/fpubh.2022.870403

Liu, Y., Peng, J., & Wang, Y. (2018a). Application of partial least squares regression in detecting the important landscape indicators determining urban land surface temperature variation. *Landscape Ecology*, *33*(7), 1133-1145. https://doi.org/10.1007/s10980-018-0663-7

Liu, Y., Peng, J., & Wang, Y. (2018b). Efficiency of landscape metrics characterizing urban land surface temperature. *Landscape and Urban Planning*, *180*, 36-53. https://doi.org/10.1016/j.landurbplan.2018.08.006

Lu, J., Li, C.-d., Yang, Y.-c., Zhang, X.-h., & Jin, M. (2012). Quantitative evaluation of urban park cool island factors in mountain city. *Journal of Central South University*, *19*(6), 1657-1662. https://doi.org/10.1007/s11771-012-1189-9

Lu, L., Weng, Q., Xiao, D., Guo, H., Li, Q., & Hui, W. (2020). Spatiotemporal Variation of Surface Urban Heat Islands in Relation to Land Cover Composition and Configuration: A Multi-Scale Case Study of Xi’an, China. *Remote Sensing*, *12*(17). https://doi.org/10.3390/rs12172713

Lyu, R., Pang, J., Tian, X., Zhao, W., & Zhang, J. (2023). How to optimize the 2D/3D urban thermal environment: Insights derived from UAV LiDAR/multispectral data and multi-source remote sensing data. *Sustainable Cities and Society*, *88*. https://doi.org/10.1016/j.scs.2022.104287

Ma, X., & Peng, S. (2022). Research on the spatiotemporal coupling relationships between land use/land cover compositions or patterns and the surface urban heat island effect. *Environ Sci Pollut Res Int*, *29*(26), 39723-39742. https://doi.org/10.1007/s11356-022-18838-3

Ma, Y., Zhao, M., Li, J., Wang, J., & Hu, L. (2021). Cooling Effect of Different Land Cover Types: A Case Study in Xi'an and Xianyang, China. *Sustainability*, *13*(3). https://doi.org/10.3390/su13031099

Maimaitiyiming, M., Ghulam, A., Tiyip, T., Pla, F., Latorre-Carmona, P., Halik, Ü., Sawut, M., & Caetano, M. (2014). Effects of green space spatial pattern on land surface temperature: Implications for sustainable urban planning and climate change adaptation. *ISPRS Journal of Photogrammetry and Remote Sensing*, *89*, 59-66. https://doi.org/10.1016/j.isprsjprs.2013.12.010

Masoudi, M., & Tan, P. Y. (2019). Multi-year comparison of the effects of spatial pattern of urban green spaces on urban land surface temperature. *Landscape and Urban Planning*, *184*, 44-58. https://doi.org/10.1016/j.landurbplan.2018.10.023

Masoudi, M., Tan, P. Y., & Fadaei, M. (2021). The effects of land use on spatial pattern of urban green spaces and their cooling ability. *Urban Climate*, *35*. https://doi.org/10.1016/j.uclim.2020.100743

Masoudi, M., Tan, P. Y., & Liew, S. C. (2019). Multi-city comparison of the relationships between spatial pattern and cooling effect of urban green spaces in four major Asian cities. *Ecological Indicators*, *98*, 200-213. https://doi.org/10.1016/j.ecolind.2018.09.058

Naeem, S., Cao, C., Qazi, W., Zamani, M., Wei, C., Acharya, B., & Rehman, A. (2018). Studying the Association between Green Space Characteristics and Land Surface Temperature for Sustainable Urban Environments: An Analysis of Beijing and Islamabad. *ISPRS International Journal of Geo-Information*, *7*(2). https://doi.org/10.3390/ijgi7020038

Pang, B., Zhao, J., Zhang, J., & Yang, L. (2022). How to plan urban green space in cold regions of China to achieve the best cooling efficiency. *Urban Ecosystems*. https://doi.org/10.1007/s11252-022-01202-1

Park, J.-H., & Cho, G.-H. (2016). Examining the Association between Physical Characteristics of Green Space and Land Surface Temperature: A Case Study of Ulsan, Korea. *Sustainability*, *8*(8). https://doi.org/10.3390/su8080777

Peng, J., Dan, Y., Qiao, R., Liu, Y., Dong, J., & Wu, J. (2021). How to quantify the cooling effect of urban parks? Linking maximum and accumulation perspectives. *Remote Sensing of Environment*, *252*. https://doi.org/10.1016/j.rse.2020.112135

Peng, J., Jia, J., Liu, Y., Li, H., & Wu, J. (2018). Seasonal contrast of the dominant factors for spatial distribution of land surface temperature in urban areas. *Remote Sensing of Environment*, *215*, 255-267. https://doi.org/10.1016/j.rse.2018.06.010

Peng, J., Xie, P., Liu, Y., & Ma, J. (2016). Urban thermal environment dynamics and associated landscape pattern factors: A case study in the Beijing metropolitan region. *Remote Sensing of Environment*, *173*, 145-155. https://doi.org/10.1016/j.rse.2015.11.027

Pramanik, S., & Punia, M. (2019). Assessment of green space cooling effects in dense urban landscape: a case study of Delhi, India. *Modeling Earth Systems and Environment*, *5*(3), 867-884. https://doi.org/10.1007/s40808-019-00573-3

Qian, Y., Zhou, W., Hu, X., & Fu, F. (2018). The Heterogeneity of Air Temperature in Urban Residential Neighborhoods and Its Relationship with the Surrounding Greenspace. *Remote Sensing*, *10*(6). https://doi.org/10.3390/rs10060965

Qiu, K., & Jia, B. (2020). The roles of landscape both inside the park and the surroundings in park cooling effect. *Sustainable Cities and Society*, *52*. https://doi.org/10.1016/j.scs.2019.101864

Rahimi, E., Barghjelveh, S., & Dong, P. (2021). Quantifying how urban landscape heterogeneity affects land surface temperature at multiple scales. *Journal of Ecology and Environment*, *45*(1). https://doi.org/10.1186/s41610-021-00203-z

Rakoto, P. Y., Deilami, K., Hurley, J., Amati, M., & Sun, Q. (2021). Revisiting the cooling effects of urban greening: Planning implications of vegetation types and spatial configuration. *Urban Forestry & Urban Greening*, *64*. https://doi.org/10.1016/j.ufug.2021.127266

Ren, Z., He, X., Zheng, H., Zhang, D., Yu, X., Shen, G., & Guo, R. (2013). Estimation of the Relationship between Urban Park Characteristics and Park Cool Island Intensity by Remote Sensing Data and Field Measurement. *Forests*, *4*(4), 868-886. https://doi.org/10.3390/f4040868

Ren, Z., Zheng, H., He, X., Dan, Z., & Xingyang, Y. (2014). Estimation of the Relationship Between Urban Vegetation Configuration and Land Surface Temperature with Remote Sensing. *Journal of the Indian Society of Remote Sensing*, *43*(1), 89-100. https://doi.org/10.1007/s12524-014-0373-9

Rhee, J., Park, S., & Lu, Z. (2014). Relationship between land cover patterns and surface temperature in urban areas. *GIScience & Remote Sensing*, *51*(5), 521-536. https://doi.org/10.1080/15481603.2014.964455

Rouhi, H., Chamani, N., Jafarnezhad, J., & Asgarian, A. (2018). Spatial assessment of the effects of in situ and neighbourhood factors on urban land surface temperature mitigation in a rapidly developing region. *International Journal of Urban Sustainable Development*, *10*(3), 292-304. https://doi.org/10.1080/19463138.2018.1522320

Shah, A., Garg, A., & Mishra, V. (2021). Quantifying the local cooling effects of urban green spaces: Evidence from Bengaluru, India. *Landscape and Urban Planning*, *209*. https://doi.org/10.1016/j.landurbplan.2021.104043

Shaker, R. R., Altman, Y., Deng, C., Vaz, E., & Forsythe, K. W. (2019). Investigating urban heat island through spatial analysis of New York City streetscapes. *Journal of Cleaner Production*, *233*, 972-992. https://doi.org/10.1016/j.jclepro.2019.05.389

Shi, Y., & Zhao, S. (2022). Discover the desirable landscape structure for mitigating urban heat: The urban-rural gradient approach for an ancient Chinese city. *Cities*, *127*. https://doi.org/10.1016/j.cities.2022.103737

Shih, W.-y. (2016). The cooling effect of green infrastructure on surrounding built environments in a sub-tropical climate: a case study in Taipei metropolis. *Landscape Research*, *42*(5), 558-573. https://doi.org/10.1080/01426397.2016.1235684

Shih, W. Y. (2017). Greenspace patterns and the mitigation of land surface temperature in Taipei metropolis. *Habitat International*, *60*, 69-80. https://doi.org/10.1016/j.habitatint.2016.12.006

Simwanda, M., Ranagalage, M., Estoque, R. C., & Murayama, Y. (2019). Spatial Analysis of Surface Urban Heat Islands in Four Rapidly Growing African Cities. *Remote Sensing*, *11*(14). https://doi.org/10.3390/rs11141645

Song, Y., Song, X., & Shao, G. (2020). Effects of Green Space Patterns on Urban Thermal Environment at Multiple Spatial–Temporal Scales. *Sustainability*, *12*(17). https://doi.org/10.3390/su12176850

Sun, X., Tan, X., Chen, K., Song, S., Zhu, X., & Hou, D. (2020). Quantifying landscape-metrics impacts on urban green-spaces and water-bodies cooling effect: The study of Nanjing, China. *Urban Forestry & Urban*

Greening, *55*. https://doi.org/10.1016/j.ufug.2020.126838

Sun, Y., Gao, C., Li, J., Gao, M., & Ma, R. (2021). Assessing the cooling efficiency of urban parks using data envelopment analysis and remote sensing data. *Theoretical and Applied Climatology*, *145*(3-4), 903-916. https://doi.org/10.1007/s00704-021-03665-2

Sun, Z., Li, Z., & Zhong, J. (2022). Analysis of the Impact of Landscape Patterns on Urban Heat Islands: A Case Study of Chengdu, China. *Int J Environ Res Public Health*, *19*(20). https://doi.org/10.3390/ijerph192013297

Tan, M., & Li, X. (2013). Integrated assessment of the cool island intensity of green spaces in the mega city of Beijing. *International Journal of Remote Sensing*, *34*(8), 3028-3043. https://doi.org/10.1080/01431161.2012.757377

Tan, X., Sun, X., Huang, C., Yuan, Y., & Hou, D. (2021). Comparison of cooling effect between green space and water body. *Sustainable Cities and Society*, *67*. https://doi.org/10.1016/j.scs.2021.102711

Tang, L., Zhan, Q., Fan, Y., Liu, H., & Fan, Z. (2023). Exploring the impacts of greenspace spatial patterns on land surface temperature across different urban functional zones: A case study in Wuhan metropolitan area, China. *Ecological Indicators*, *146*. https://doi.org/10.1016/j.ecolind.2022.109787

Terfa, B. K., Chen, N., Zhang, X., & Niyogi, D. (2020). Spatial Configuration and Extent Explains the Urban Heat Mitigation Potential due to Green Spaces: Analysis over Addis Ababa, Ethiopia. *Remote Sensing*, *12*(18). https://doi.org/10.3390/rs12182876

Vaz Monteiro, M., Doick, K. J., Handley, P., & Peace, A. (2016). The impact of greenspace size on the extent of local nocturnal air temperature cooling in London. *Urban Forestry & Urban Greening*, *16*, 160-169. https://doi.org/10.1016/j.ufug.2016.02.008

Wang, J., & Zhou, W. (2022). More urban greenspace, lower temperature? Moving beyond net change in greenspace. *Agricultural and Forest Meteorology*, *322*. https://doi.org/10.1016/j.agrformet.2022.109021

Wang, J., Zhou, W., Zheng, Z., Jiao, M., & Qian, Y. (2023). Interactions among spatial configuration aspects of urban tree canopy significantly affect its cooling effects. *Sci Total Environ*, *864*, 160929. https://doi.org/10.1016/j.scitotenv.2022.160929

Wang, L., Hou, H., & Weng, J. (2020). Ordinary least squares modelling of urban heat island intensity based on landscape composition and configuration: A comparative study among three megacities along the Yangtze River. *Sustainable Cities and Society*, *62*. https://doi.org/10.1016/j.scs.2020.102381

Wang, T., Tu, H., Min, B., Li, Z., Li, X., & You, Q. (2022). The Mitigation Effect of Park Landscape on Thermal Environment in Shanghai City Based on Remote Sensing Retrieval Method. *Int J Environ Res Public Health*, *19*(5). https://doi.org/10.3390/ijerph19052949

Wang, X., Cheng, H., Xi, J., Yang, G., & Zhao, Y. (2018). Relationship between Park Composition, Vegetation Characteristics and Cool Island Effect. *Sustainability*, *10*(3). https://doi.org/10.3390/su10030587

Wang, X., Meng, Q., Zhang, L., & Hu, D. (2021). Evaluation of urban green space in terms of thermal environmental benefits using geographical detector analysis. *International Journal of Applied Earth Observation and Geoinformation*, *105*. https://doi.org/10.1016/j.jag.2021.102610

Wang, Y., Huang, J., Chen, C., Shen, J., & Sheng, S. (2021). The Cooling Intensity Dependent on Landscape Complexity of Green Infrastructure in the Metropolitan Area. *Journal of Environmental Engineering and Landscape Management*, *29*(3), 318-336. https://doi.org/10.3846/jeelm.2021.15573

Weber, N., Haase, D., & Franck, U. (2014). Zooming into temperature conditions in the city of Leipzig: how do urban built and green structures influence earth surface temperatures in the city? *Sci Total Environ*, *496*, 289-298. https://doi.org/10.1016/j.scitotenv.2014.06.144

Wen, X., Yang, X., & Hu, G. (2011). Relationship Between Land Cover Ratio and Urban Heat Island from Remote Sensing and Automatic Weather Stations Data. *Journal of the Indian Society of Remote Sensing*, *39*(2), 193-201. https://doi.org/10.1007/s12524-011-0076-4

Wesley, E. J., & A. Brunsell, N. A. (2019). Greenspace Pattern and the Surface Urban Heat Island: A Biophysically-Based Approach to Investigating the Effects of Urban Landscape Configuration. *Remote Sensing*, *11*(19). https://doi.org/10.3390/rs11192322

Wu, C., Li, J., Wang, C., Song, C., Haase, D., Breuste, J., & Finka, M. (2021). Estimating the Cooling Effect of Pocket Green Space in High Density Urban Areas in Shanghai, China. *Frontiers in Environmental Science*, *9*. https://doi.org/10.3389/fenvs.2021.657969

Wu, H., Ye, L.-P., Shi, W.-Z., & Clarke, K. C. (2014). Assessing the effects of land use spatial structure on urban heat islands using HJ-1B remote sensing imagery in Wuhan, China. *International Journal of Applied Earth Observation and Geoinformation*, *32*, 67-78. https://doi.org/10.1016/j.jag.2014.03.019

Wu, Q., Li, Z., Yang, C., Li, H., Gong, L., & Guo, F. (2022). On the Scale Effect of Relationship Identification between Land Surface Temperature and 3D Landscape Pattern: The Application of Random Forest. *Remote Sensing*, *14*(2). https://doi.org/10.3390/rs14020279

Wu, Q., Tan, J., Guo, F., Li, H., & Chen, S. (2019). Multi-Scale Relationship between Land Surface Temperature and Landscape Pattern Based on Wavelet Coherence: The Case of Metropolitan Beijing, China. *Remote Sensing*, *11*(24). https://doi.org/10.3390/rs11243021

Wu, W.-B., Yu, Z.-W., Ma, J., & Zhao, B. (2022). Quantifying the influence of 2D and 3D urban morphology on the thermal environment across climatic zones. *Landscape and Urban Planning*, *226*. https://doi.org/10.1016/j.landurbplan.2022.104499

Wu, Y., Hou, H., Wang, R., Murayama, Y., Wang, L., & Hu, T. (2022). Effects of landscape patterns on the morphological evolution of surface urban heat island in Hangzhou during 2000 – 2020. *Sustainable Cities and Society*, *79*. https://doi.org/10.1016/j.scs.2022.103717

Wu, Z., & Zhang, Y. (2018). Spatial Variation of Urban Thermal Environment and Its Relation to Green Space Patterns: Implication to Sustainable Landscape Planning. *Sustainability*, *10*(7). https://doi.org/10.3390/su10072249

Xie, M., Chen, J., Zhang, Q., Li, H., Fu, M., & Breuste, J. (2020). Dominant landscape indicators and their dominant areas influencing urban thermal environment based on structural equation model. *Ecological Indicators*, *111*. https://doi.org/10.1016/j.ecolind.2019.105992

Xie, M., Wang, Y., Chang, Q., Fu, M., & Ye, M. (2013). Assessment of landscape patterns affecting land surface temperature in different biophysical gradients in Shenzhen, China. *Urban Ecosystems*, *16*(4), 871-886. https://doi.org/10.1007/s11252-013-0325-0

Xu, X., Cai, H., Qiao, Z., Wang, L., Jin, C., Ge, Y., Wang, L., & Xu, F. (2017). Impacts of park landscape structure on thermal environment using QuickBird and Landsat images. *Chinese Geographical Science*, *27*(5), 818-826. https://doi.org/10.1007/s11769-017-0910-x

Yan, J., Zhou, W., & Jenerette, G. D. (2019). Testing an energy exchange and microclimate cooling hypothesis for the effect of vegetation configuration on urban heat. *Agricultural and Forest Meteorology*, *279*. https://doi.org/10.1016/j.agrformet.2019.107666

Yan, L., Jia, W., & Zhao, S. (2021). The Cooling Effect of Urban Green Spaces in Metacities: A Case Study of Beijing, China's Capital. *Remote Sensing*, *13*(22). https://doi.org/10.3390/rs13224601

Yang, C., He, X., Wang, R., Yan, F., Yu, L., Bu, K., Yang, J., Chang, L., & Zhang, S. (2017). The Effect of Urban

Green Spaces on the Urban Thermal Environment and Its Seasonal Variations. *Forests*, *8*(5). https://doi.org/10.3390/f8050153

Yang, C., He, X., Yu, L., Yang, J., Yan, F., Bu, K., Chang, L., & Zhang, S. (2017). The Cooling Effect of Urban Parks and Its Monthly Variations in a Snow Climate City. *Remote Sensing*, *9*(10). https://doi.org/10.3390/rs9101066

Yang, C., Zhu, W., Sun, J., Xu, X., Wang, R., Lu, Y., Zhang, S., & Zhou, W. (2021). Assessing the effects of 2D/3D urban morphology on the 3D urban thermal environment by using multi-source remote sensing data and UAV measurements: A case study of the snow-climate city of Changchun, China. *Journal of Cleaner Production*, *321*. https://doi.org/10.1016/j.jclepro.2021.128956

Yang, G., Yu, Z., Jørgensen, G., & Vejre, H. (2020). How can urban blue-green space be planned for climate adaption in high-latitude cities? A seasonal perspective. *Sustainable Cities and Society*, *53*. https://doi.org/10.1016/j.scs.2019.101932

Yang, L., Yu, K., Ai, J., Liu, Y., Lin, L., Lin, L., & Liu, J. (2021). The Influence of Green Space Patterns on Land Surface Temperature in Different Seasons: A Case Study of Fuzhou City, China. *Remote Sensing*, *13*(24). https://doi.org/10.3390/rs13245114

Yang, L., Yu, K., Ai, J., Liu, Y., Yang, W., & Liu, J. (2022). Dominant Factors and Spatial Heterogeneity of Land Surface Temperatures in Urban Areas: A Case Study in Fuzhou, China. *Remote Sensing*, *14*(5). https://doi.org/10.3390/rs14051266

Yao, L., Li, T., Xu, M., & Xu, Y. (2020). How the landscape features of urban green space impact seasonal land surface temperatures at a city-block-scale: An urban heat island study in Beijing, China. *Urban Forestry & Urban Greening*, *52*. https://doi.org/10.1016/j.ufug.2020.126704

Ye, H., Li, Z., Zhang, N., Leng, X., Meng, D., Zheng, J., & Li, Y. (2021). Variations in the Effects of Landscape Patterns on the Urban Thermal Environment during Rapid Urbanization (1990–2020) in Megacities. *Remote Sensing*, *13*(17). https://doi.org/10.3390/rs13173415

Yin, J., Wu, X., Shen, M., Zhang, X., Zhu, C., Xiang, H., Shi, C., Guo, Z., & Li, C. (2019). Impact of urban greenspace spatial pattern on land surface temperature: a case study in Beijing metropolitan area, China. *Landscape Ecology*, *34*(12), 2949-2961. https://doi.org/10.1007/s10980-019-00932-6

Yu, S., Chen, Z., Yu, B., Wang, L., Wu, B., Wu, J., & Zhao, F. (2020). Exploring the relationship between 2D/3D landscape pattern and land surface temperature based on explainable eXtreme Gradient Boosting tree: A case study of Shanghai, China. *Sci Total Environ*, *725*, 138229. https://doi.org/10.1016/j.scitotenv.2020.138229

Yu, Z., Guo, X., Jørgensen, G., & Vejre, H. (2017). How can urban green spaces be planned for climate adaptation in subtropical cities? *Ecological Indicators*, *82*, 152-162. https://doi.org/10.1016/j.ecolind.2017.07.002

Yuan, B., Zhou, L., Dang, X., Sun, D., Hu, F., & Mu, H. (2021). Separate and combined effects of 3D building features and urban green space on land surface temperature. *J Environ Manage*, *295*, 113116. https://doi.org/10.1016/j.jenvman.2021.113116

Zawadzka, J. E., Harris, J. A., & Corstanje, R. (2020). A simple method for determination of fine resolution urban form patterns with distinct thermal properties using class-level landscape metrics. *Landscape Ecology*, *36*(7), 1863-1876. https://doi.org/10.1007/s10980-020-01156-9

Zawadzka, J. E., Harris, J. A., & Corstanje, R. (2021). The importance of spatial configuration of neighbouring land cover for explanation of surface temperature of individual patches in urban landscapes. *Landscape Ecology*, *36*(11), 3117-3136. https://doi.org/10.1007/s10980-021-01302-x

Zeng, P., Sun, F., Liu, Y., Tian, T., Wu, J., Dong, Q., Peng, S., & Che, Y. (2022). The influence of the landscape pattern on the urban land surface temperature varies with the ratio of land components: Insights from 2D/3D building/vegetation metrics. *Sustainable Cities and Society*, *78*. https://doi.org/10.1016/j.scs.2021.103599

Zhang, H., Zhao, X., Kang, M.-y., & Han, J.-j. (2022). Contrasting changes in fine-scale land use structure and summertime thermal environment in downtown Shanghai. *Sustainable Cities and Society*, *83*. https://doi.org/10.1016/j.scs.2022.103965

Zhang, L., Shi, X., & Chang, Q. (2022). Exploring Adaptive UHI Mitigation Solutions by Spatial Heterogeneity of Land Surface Temperature and Its Relationship to Urban Morphology in Historical Downtown Blocks, Beijing. *Land*, *11*(4). https://doi.org/10.3390/land11040544

Zhang, M., Zhang, F., Chen, D., Tan, M. L., & Chan, N. W. (2022). Urban local surface temperature prediction using the urban gray-green space landscape and vegetation indices. *Building and Environment*, *226*. https://doi.org/10.1016/j.buildenv.2022.109723

Zhang, X., Zhong, T., Feng, X., & Wang, K. (2009). Estimation of the relationship between vegetation patches and urban land surface temperature with remote sensing. *International Journal of Remote Sensing*, *30*(8), 2105-2118. https://doi.org/10.1080/01431160802549252

Zhang, Y., Wang, Y., & Ding, N. (2022). Spatial Effects of Landscape Patterns of Urban Patches with Different Vegetation Fractions on Urban Thermal Environment. *Remote Sensing*, *14*(22). https://doi.org/10.3390/rs14225684

Zhao, H., Tan, J., Ren, Z., & Wang, Z. (2020). Spatiotemporal Characteristics of Urban Surface Temperature and Its Relationship with Landscape Metrics and Vegetation Cover in Rapid Urbanization Region. *Complexity*, *2020*, 1-12. https://doi.org/10.1155/2020/7892362

Zhou, G., Wang, H., Chen, W., Zhang, G., Luo, Q., & Jia, B. (2019). Impacts of Urban land surface temperature on tract landscape pattern, physical and social variables. *International Journal of Remote Sensing*, *41*(2), 683-703. https://doi.org/10.1080/01431161.2019.1646939

Zhou, L., Hu, F., Wang, B., Wei, C., Sun, D., & Wang, S. (2022). Relationship between urban landscape structure and land surface temperature: Spatial hierarchy and interaction effects. *Sustainable Cities and Society*, *80*. https://doi.org/10.1016/j.scs.2022.103795

Zhou, W., & Cao, F. (2020). Effects of changing spatial extent on the relationship between urban forest patterns and land surface temperature. *Ecological Indicators*, *109*. https://doi.org/10.1016/j.ecolind.2019.105778

Zhou, W., Cao, F., & Wang, G. (2019). Effects of Spatial Pattern of Forest Vegetation on Urban Cooling in a Compact Megacity. *Forests*, *10*(3). https://doi.org/10.3390/f10030282

Zhou, W., Huang, G., & Cadenasso, M. L. (2011). Does spatial configuration matter? Understanding the effects of land cover pattern on land surface temperature in urban landscapes. *Landscape and Urban Planning*, *102*(1), 54-63. https://doi.org/10.1016/j.landurbplan.2011.03.009

Zhou, W., Shen, X., Cao, F., & Sun, Y. (2019). Effects of Area and Shape of Greenspace on Urban Cooling in Nanjing, China. *Journal of Urban Planning and Development*, *145*(4). https://doi.org/10.1061/(asce)up.1943-5444.0000520

Zhou, W., Wang, J., & Cadenasso, M. L. (2017). Effects of the spatial configuration of trees on urban heat mitigation: A comparative study. *Remote Sensing of Environment*, *195*, 1-12. https://doi.org/10.1016/j.rse.2017.03.043

Zhou, W., Yu, W., & Wu, T. (2022). An alternative method of developing landscape strategies for urban cooling: A threshold-based perspective. *Landscape and Urban Planning*, *225*. https://doi.org/10.1016/j.landurbplan.2022.104449

Zhu, W., Sun, J., Yang, C., Liu, M., Xu, X., & Ji, C. (2021). How to Measure the Urban Park Cooling Island? A Perspective of Absolute and Relative Indicators Using Remote Sensing and Buffer Analysis. *Remote Sensing*, *13*(16). https://doi.org/10.3390/rs13163154